MODELLING OF LOSSES IN MULTI-STAGE AXIAL COMPRESSORS WITH SUBSONIC CONDITIONS

William James Swift
B. Eng (Mechanical)

Thesis submitted in partial fulfilment of the requirements for the degree
Master of Engineering
School of Mechanical and Materials Engineering
at the
Potchefstroom University for Christian Higher Education

Promoter: Dr. B.W. Botha
Potchefstroom
2003

ABSTRACT

Name: W.J. Swift

Title: Modelling of losses in multi-stage axial compressors with subsonic conditions

Date: October 2003

The need was identified to develop an analytical performance prediction code for subsonic multi-stage axial compressors that can be included in network analysis software. It was found that performance calculations based on an elementary one-dimensional meanline prediction method could achieve remarkable accuracy, provided that sound models are used for the losses, deviation and the onset of rotating stall. Consequently, this study focuses on gaining more expertise on the modelling of losses in such compressors through investigating the mechanisms responsible, the methods of predicting them, their implementation and possible usage.

Internal losses are seen as mechanisms that increase the entropy of the working fluid through the compressor and it was found that, at a fundamental level, all internal losses are a direct result of viscous shearing that occurs wherever there are velocity gradients. Usually the methodology employed to predict the magnitudes of these mechanisms uses theoretically separable loss components, ignoring the mechanisms with negligible velocity gradients. For this study these components were presented as: Blade profile losses, endwall losses including tip leakage and secondary losses, part span shroud losses, other losses, losses due to high subsonic Mach numbers and incidence loss. A preliminary performance prediction code, with the capability of interchanging of the different loss models, is presented. Verification was done by comparing the results with those predicted by a commercial software package and the loss models were evaluated according to their ease of implementation and deviation from the predictions of the commercial package. Conclusions were made about the sensitivity of performance prediction to using the different loss models.

Furthermore, the combination of loss models that include the most parameters and gave the best comparison to the commercial software predictions was selected in the code to perform parametric studies of the loss parameters on stage efficiency. This was done to illustrate the ability of the code for performing such studies to be used as an aid in understanding compressor design and performance or for basic optimization problems.

It can therefore be recommended that the preliminary code can be implemented in an engineering tool or network analysis software. This may however require further verification, with a broader

spectrum of test cases, for increased confidence as well as further study regarding aspects like multi-stage annulus blockage and deviation.

Keywords:

Loss, axial, compressor, modelling, performance, prediction, subsonic, meanline, mechanisms

UITTREKSEL

Naam: W.J. Swift

Titel: Modellering van verliese in multi-stadium aksiale kompressors met subsoniese kondisies

Datum: Oktober 2003

Die behoefte is geïdentifiseer om 'n analitiese kode te ontwikkel wat die werkverrigting van 'n subsoniese multi-stadium aksiale kompressor kan voorspel en ingesluit kan word in netwerk analise sagteware. Daar is gevind dat werkverrigtingsberekeninge gebaseer op elementêre eendimensionele voorspellings, by die gemiddelde radius, merkwaardige akkuraatheid kan oplewer, mits geskikte modelle vir die verliese, deviasie en roterende stol gebruik word. Gevolglik fokus hierdie studie daarop om kundigheid aangaande die verliese in sulke kompressors te verbeter deur die verantwoordelike meganismes, die metodes om hulle te voorspel, die implementering en moontlike gebruike daarvan te ondersoek.

Interne verliese word beskou as enige meganisme wat die entropie van die vloeier deur die kompressor verhoog en daar is gevind dat, op 'n fundamentele vlak, alle interne verliese 'n direkte resultaat van viskeuse skuifspanning is. Dit kom voor waar daar snelheidsgradiënte teenwoordig is. Gewoonlik maak die metodologie om hierdie meganismes te voorspel gebruik van teoreties skeibare verlieskomponente. Die komponente wat in hierdie studie gebruik word is: Lemprofiel verliese, annulus verliese insluitende tiplekkasie en sekondêre verliese, deelspanmantel verliese, ander verliese, verliese a.g.v hoë subsoniese Mach getalle en invalshoek verliese. 'n Voorlopige kode, vir die voorspelling van kompressor werkverrigting, is voorgestel en het die vermoë om tussen verskillende verliesmodelle te ruil. Die verifikasie van hierdie kode is gedoen deur die resultate te vergelyk met die van 'n kommersiële sagteware pakket en die verliesmodelle is geëvalueer volgens hulle eenvoud en afwyking van die kommersiële pakket se voorspellings. Gevolgtrekkings is daarna gemaak oor die sensitiwiteit van werkverrigting t.o.v. die gebruik van die verskillende verliesmodelle.

Verder is die kombinasie van die verliesmodelle, wat die meeste parameters bevat en die beste vergelyk het met die voorspellings van die kommersiële sagteware, geselekteer vir gebruik in die kode om parametries studies te doen van die uitwerking van die verliesparameters op die stadium effektiwiteit. Dit is gedoen om die vermoë van die kode om as hulpmiddel in kompressor ontwerp en basiese optimeringsprobleme te illustreer.

Na aanleiding van bogenoemde kan dit dus voorgestel word dat die voorlopige kode geïmplementeer kan word in 'n ingenieursnutspakket of netwerk analise sagteware. Daar word egter verder voorgestel dat verdere verifikasie, met meer toetsgevalle, gedoen word om die vertroue in akkuraatheid van die voorlopige kode te versterk en dat verdere studie op aspekte soos multi-stadium annulus blokkasie en deviasie aandag moet geniet.

Sleutelwoorde:
Verlies, aksiaal, kompressor, modellering, werkverrigting, voorspelling, subsonies, meganismes

ACKNOWLEDGEMENTS

I thank my Heavenly Father for his guidance throughout this study as well as the opportunities and talents he has given me.

I would also like to thank my parents for their understanding and support through some of the difficult and frustrating times.

Furthermore, a special thanks to Petro for her love and companionship throughout the past two years. Her strength and support contributed greatly to the successful completion of this study. I also thank her family for their love and support.

Thanks Gareth for your blatant wit and optimism and your gift for seeing the lighter side of life.

Thank you to Dr. Barend Botha, my promoter, for his guidance on a professional and personal level as well as his special ability to uplift and motivate in even the worst of times. His contribution to my growth as a researcher and person is greatly appreciated.

Finally, I thank my friends and colleagues for making the past two years more pleasurable and the university for the working environment and financial support.

TABLE OF CONTENTS

LIST OF FIGURES

LIST OF TABLES

NOMENCLATURE

a	Velocity of sound
A, B	Gap loss coefficients
A_a	Annulus area
A_p	Blade passage area
A_{sh}	Shroud frontal area
AR	Aspect ratio
AS	Blade axial spacing
c	Blade chord
C	Absolute velocity
C_{bp}	Base pressure coefficient
C_d	Discharge coefficient
C_{D_A}	Annulus drag coefficient
C_{D_S}	Secondary loss drag coefficient
C_{Dsh}	Shroud drag coefficient
C_f	Skin friction coefficient
C_L	Blade lift coefficient
C_m	Moment coefficient
C_P	Static pressure rise coefficient
C_s	Blade surface length
D	Diffusion ratio, diameter
D_{eq}	Equivalent diffusion ratio
F_D	Drag force
g	Blade staggered spacing
h	Specific enthalpy, blade height
H	Boundary layer form factor
h_a	Annulus height
i	Blade incidence angle
K	Constant value
k_{CLA}	Centreline average of roughness particles

k_s	Equivalent sand roughness
k_{sec}	Endwall loss fraction
M	Mach number
N_B	Number of blades
P	Pressure
PR	Pressure ratio
q	Dynamic head
r	Distance in radial direction, radius
R	Gas constant
R_t	Reference tip radius
Re	Reynolds number
Re_θ	Reynolds number based on momentum thickness
s	Blade pitch, specific entropy
t	Blade or part span shroud thickness
T	Temperature
U	Tangential blade speed
V	Arbitrary velocity
V_{bs}	Blade surface velocity
V_{jet}	Leakage jet velocity
$V_{\max}$	Maximum suction surface velocity
V_p	Velocity in blade passage
W	Relative velocity, Work
W_τ	Flow velocity inside tip gap
W_{njet}	Normal jet velocity in tip gap
$W_{usefull}$	Useful power
$\Delta W_{windage}$	Windage power loss

Greek symbols

α	Absolute flow angle
β	Relative flow angle
η	Efficiency
ϕ	Dimensionless axial component of absolute velocity, flow coefficient

γ	Ratio of specific heats
$\overline{\delta}$	Boundary layer displacement thickness
ε	Throat width
ζ	Dimensionless radius
ζ_s	Entropy loss coefficient
θ	Boundary layer momentum thickness
θ_{camber}	Blade camber angle
ξ	Blade stagger angle
ν	Kinematic viscosity, $\frac{\mu}{\rho}$
ν_t	Tangential force thickness
ρ	Fluid density
ρ_p	Fluid density in blade passage
ς	Energy loss coefficient
η	Efficiency
φ	Stage loading coefficient
σ	Blade solidity
ω	Pressure loss coefficient, rotor angular velocity
Γ	Blade circulation
τ	Tip clearance
χ	Blade metal angle

Sub - and superscripts

a	In the absolute frame
ex	Wake
fs	Freestream
hb	Hub
i	Isentropic
m	Vector mean value
max	Maximum condition or value
min	Minimum condition or value
p	Pressure surface
rms	Root mean square

r	In the relative frame
s	Suction surface
sh	Shroud
t	Tip
T	Based on rothalpy
te	Trailing edge
θ	Tangential direction, momentum thickness
x, y, z	Cartesian coordinates with z in the axial direction
$\bar{}$	Averaged value, average
∞	Vector mean condition
0	Stagnation condition
1	Inlet into blade rotor or stage
2	Outlet from rotor and inlet to stator
3	Outlet from stator and stage

Chapter 1

INTRODUCTION

Chapter 1 aims at providing the reader with an introduction to the thesis. This is done by describing the background leading to the study as well as giving the reader a short overview of the main concepts contained in the study. Further aspects that receive attention are the primary restrictions, contributions and outline of the study as given in the thesis.

1.1 Background

Flownex (M-Tech Industrial (Pty) Ltd., 2003) is a general network analysis code that solves the flow, pressure and temperature distribution in arbitrary-structured thermal-fluid networks. One of the components that may be included in such a network is the axial compressor. Flownex currently uses turbomachine performance maps obtained from the manufacturer to predict the performance of an axial compressor. These maps are a graphical representation of the machine performance over a range of ambient temperatures, rotational speeds and mass flow rates.

This method is, however, not always satisfactory because turbomachine manufacturers are often reluctant to supply detail performance information about their products and the required maps might therefore not always be available. Another drawback is the fact that performance maps are characteristic to a specific machine. This severely limits their use as optimization or preliminary design tools because new maps have to be obtained each time geometrical changes are made.

One possibility to resolve these issues is to develop a performance prediction model and integrate it into the Flownex source code. Geometrical changes to the turbo machine can be made directly in Flownex and the influence of these changes can be seen immediately, not only on the compressor performance, but also on the performance of the network as a whole. Song *et al.* (2001:90) pointed out some of the advantages of integrating multi-stage axial compressor performance prediction with network analysis.

It must be clearly stated that the author is aware of the extreme complexity involved in accurately predicting the performance of multi-stage axial compressors. Sophisticated axial compressor performance prediction models are routinely used within the gas turbine industry; however, there are very few models published in the open literature. Casey (1987:273), however, demonstrated that performance calculations based on an elementary one-dimensional meanline prediction method could achieve remarkable accuracy, provided that sound models are used for the losses, deviation and the onset of rotating stall.

1.2 Outcomes of this study

It was concluded that detail studies of loss, deviation and stall are necessary to gain confidence in attempting performance prediction for axial compressors. A primary and secondary outcome was subsequently identified.

The primary outcome of the study is the comprehensive understanding of the sources and mechanisms that cause loss, and the investigation of the available models that describes them. The secondary outcome can be defined as the generation of a meanline performance prediction code, with emphasis on the modelling of the losses from the knowledge gained while satisfying the primary outcome. This code can possibly be used for predicting and investigating axial compressor losses and the relative influence of parameter changes on these losses. A sound methodology for loss modelling can then be deducted from, for instance, parametric studies of the influence of the loss variables on compressor performance. This methodology can then be adapted and incorporated, through further studies, into a more complex performance prediction model for use in applications like Flownex.

1.3 The axial compressor

Modern axial flow compressors are normally built up of a number of stages. Each stage consists of a row of rotating blades (rotor blades) and a row of fixed blades (stator blades). The rotating blades are attached to a number of disks mounted on a central shaft forming the rotor. The stator blades are fastened to the inside of the compressor casing. Usually, there is a gradual decrease in the cross-sectional flow area from the compressor inlet to outlet. Figure 1.1 shows a typical axial compressor.

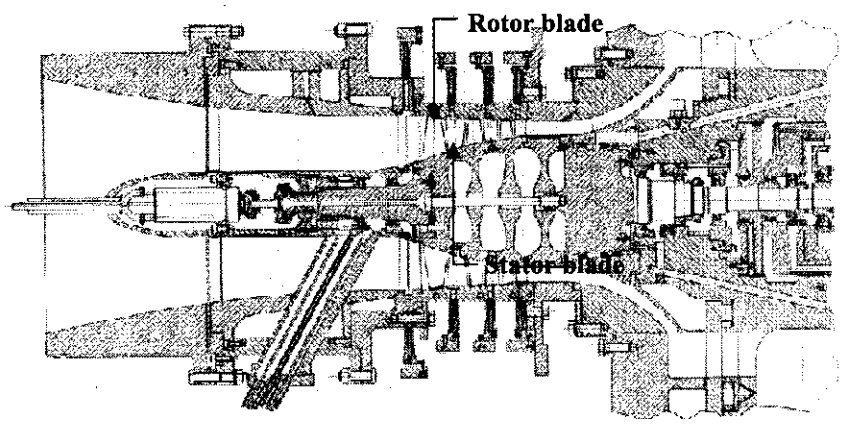

Fig. 1.1 Illustration of a typical multi-stage axial compressor.

Work is transferred from the moving blades to the fluid by means of the changing swirl, or tangential velocity, through the stage. In multi-stage industrial compressors, the first stage is often preceded by a row of stationary inlet guide vanes, which set an appropriate level of swirl into the first stage of the compressor (Japikse and Bianes, 1997:5-1).

1.4 Loss and compressor performance

An axial compressor is designed according to certain requirements. During operation at the design point it delivers the required pressure ratio at a specified rotational speed and mass flow rate at maximum compressor efficiency.

Several conflicting definitions exist for the 'correct' inlet flow angle chosen during the design phase of axial compressor bladerows. Cumpsty (1989:164) gives a detail summary of these, but states that the differences in the definitions are relatively unimportant because of the similarity in results. Due to the difficulty arising from such a wide array of definitions etc. and the fact that the prediction of the losses are dependent on these values (see Chapter 4), this study will assume the definition proposed by Cumpsty and given by Lieblein (1956). It gives the design point inlet angle in terms of the angle at which the absolute minimum blade profile loss will occur.

Figure 1.2 illustrates the operating line at a constant rotational speed for an axial compressor stage designed according to the aforementioned criteria.

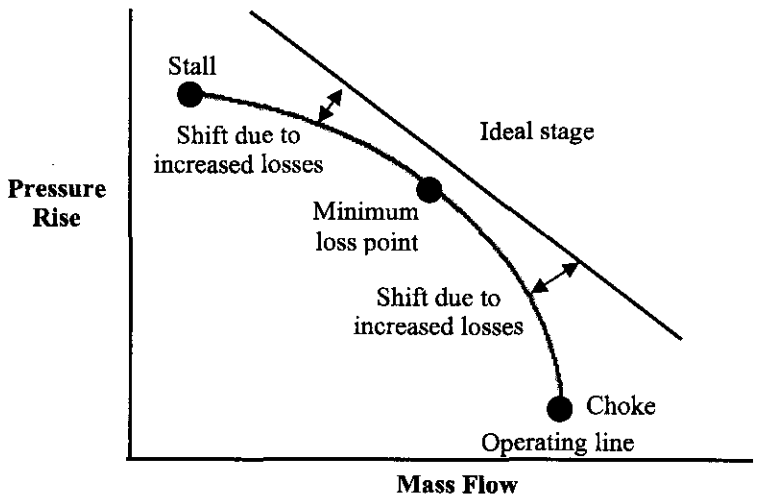

Fig. 1.2 Operating line at constant rotational speed for an axial compressor stage

The axial velocity is a function of the mass flow and reduces proportional to a mass flow reduction. As the axial velocity decreases, the angle at which the fluid enters the blade row increases. This increases the blade losses and the pressure ratio over the stage decreases accordingly in a progressive manner. This continues to the extent that the flow separates from the blade profile and a sudden decrease in the pressure ratio is experienced. This separation point is known as the stall point (Botha, 2002:80).

As the mass flow increases, the axial velocity is increased leading to a smaller fluid entry angle. This continues with a proportional increase in losses until a critical mass flow is reached and a further mass flow increase through the blades is not possible. At this point the blades start to choke and a sharp increase in loss and decrease in pressure ratio is experienced.

1.5 The concept of loss

According to Wilson and Korakianitis (1998:358) a real compressor can be thought of as an ideal machine taking in a gas at $p_{0_{in}}, h_{0_{in}}$ (Figure 1.3), and delivering it at $p'_{0_{out}}, h'_{0_{out}}$ (point 1) with added losses, which make the actual delivery conditions $p_{0_{out}}, h_{0_{out}}$ (point 2). Point 2 could be arrived at in two conceptual ways: a pressure decrease, $\sum' \Delta p_0$, and an energy increase, $\sum' \Delta h_0$; or an isentropic enthalpy rise followed by a pure entropy increase, which represents the entropy generated by the internal losses. The dotted line represents a typical adiabatic compression process.

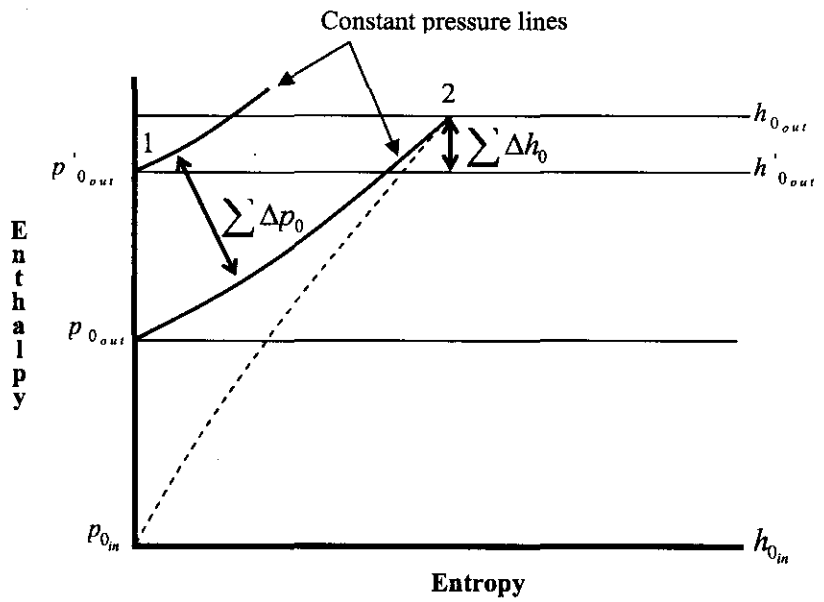

Fig. 1.3 Loss representation in adiabatic compression.

Following the article by Denton (1993), this study will concentrate on the conceptualism that internal losses manifest as an entropy increase. This is motivated by the fact that it leads to more consistent reasoning and that entropy is a particularly convenient loss measure because, unlike stagnation pressure, stagnation enthalpy, or kinetic energy, its value does not depend on whether it is viewed from a rotating or stationary blade row and simple summation of entropy increases throughout the machine is now possible.

According to Denton (1993:625), entropy creation or internal losses is a direct result of the following fluid dynamic processes:

1. Viscous friction (shearing), e.g., boundary layers and mixing,
2. Heat transfer across finite temperature differences, e.g., from mainstream flow to flow of coolant gas, and
3. Non-equilibrium processes such as very rapid expansion or shock waves.

For an adiabatic, subsonic axial compressor, only viscous shearing is responsible for entropy increase.

Another source of loss can be mechanical friction losses in external bearings or seals. These losses increase the compressor's power requirements and are also called mechanical losses or external losses. They do not contribute to the entropy increase of the fluid.

1.6 Introduction to loss modelling

In an attempt to quantify the internal loss generation in axial compressors, various authors defined certain loss components and modelled their influence separately. The classifications are not always precise, and at times different authors present different groupings. In any case, it is physically impossible to separate the effects of an individual loss type from those of its interaction with other dissipative phenomena.

The common loss components are profile loss, endwall loss and shock loss. In a fully subsonic compressor, shock losses do not occur. Profile loss is usually taken to be the loss generated in the blade boundary layers well away from the endwalls. It is often assumed that the loss here is two-dimensional. This is done to make use of two-dimensional cascade tests or boundary layer calculations for modelling purposes. The extra mixing loss at the blade trailing edge is usually included in the profile loss. Sometimes, endwall loss is further broken down into more theoretically separable components called tip leakage or clearance loss, annulus boundary layer loss and secondary loss. Secondary loss arises partly from the secondary flows generated from interaction between the annulus boundary layers and the blade rows. Profile loss, endwall loss and tip leakage loss are in many compressors comparable in magnitude, accounting for about one third of the total loss.

Denton (1993:621) stated that some purely analytical models of the loss components were formulated from basic principles, but these were usually highly idealized. Another method would be to use numerical solutions for the loss prediction. Unfortunately, they are computationally very intensive and are consequently not suitable for the preliminary design phase.

Because of the aforementioned reasons, loss prediction methods remain very dependent on correlations from test data. The NACA-65 series, C-series and double-circular-arc (DCA) blade profile families were used extensively in cascades for obtaining data for correlation purposes. Cumpsty (1989:140) presents a detail discussion on the blade profile families and clearly points out the geometrical and performance differences between various profiles. He concluded that blade shape has a quite small effect on the deviation, pressure rise and loss as long as the flow remains subsonic over the whole blade section.

1.7 Primary restrictions

For this study it is assumed that the flow through an axial compressor is adiabatic, thus the compressor is isolated from its surroundings and no heat is supplied to or rejected from the system.

It is also assumed that the conditions throughout the compressor are fully subsonic. The reason for this restriction is that, although the losses could relatively easily be included to accommodate transonic Mach numbers, the performance prediction and the non-loss correlations involved change dramatically due to the use of other blade profiles etc. Separate studies are therefore recommended for including transonic and supersonic loss modelling. Consequently, it is assumed that the compressor or stage absolute inlet axial Mach number will, in this study, not exceed 0.8 to stay clear of supersonic patches forming on the blades with high relative velocity. This assumption is based on the discussion given in Section 3.6 regarding losses due to high subsonic Mach numbers.

The present study is not concerned with predicting mechanical or external losses and it is treated as a constant input if necessary. The manufacturers of the bearings or seals usually provide values for these losses.

Further constraints are that it does not attempt to deal with losses due to, for example, mismatching between stages at part speed operation or improper selection of blade shapes for the aerodynamic environment. Only losses in the stable operating range are modelled, therefore, no blade rows are stalled. These constraints were partly adopted from Koch and Smith (1976:411) in order not to stray too much from the most common loss correlation restrictions.

Losses due to inlet ducting, inlet guide vanes or discharge diffusers are also excluded from the investigation because it is thought that these components are not essentially part of all compressors and the literature for modelling them is abundant.

1.8 Contributions of this study

The study will aim at improving axial compressor expertise through investigating and serving as a reference on loss mechanisms, methods of predicting their magnitudes, their implementation and their possible use. The possibility of developing performance prediction software, with general applicability to subsonic multi-stage compressors with different geometries and working fluids will be investigated. Further investigations will also include the evaluation of different loss models and parametric studies reflecting the influence of input variable changes on particularly the loss magnitudes and this relation to other performance variables.

1.9 Study Outline

Chapter 1 aimed at providing the reader with the background to this study as well as a short introduction and overview of the basics regarding axial compressors and their losses. Chapter 2 describes the loss mechanisms found in an axial compressor. In Chapter 3 the loss models published in the open literature for predicting the losses produced by the various loss mechanisms are reviewed and some are discussed in detail. Chapter 4 presents the reader with a method of performance prediction and indicates where and how the loss models fit in. In Chapter 5 some issues regarding the implementation of the concepts and equations given in Chapters 3 and 4 are discussed. Chapter 6 verifies the validity and accuracy of the code by comparing its results to those from a commercial software package and evaluation of the different loss models are done. In Chapter 7 parametric studies are conducted and some conclusions are made about the role that each model and other relevant parameters play in loss and performance. Chapter 8 contains conclusions and recommendations for future work on improving the loss prediction models, and our understanding of it, as well as some remarks on compressor performance prediction as a whole.

Chapter 2

LOSS MECHANISMS

The mechanisms mainly responsible for the losses in subsonic axial compressors are presented in Chapter 2. The mechanisms that are commonly used in loss modelling are then described in more detail.

2.1 Introduction

Chapter 1 gave a brief overview of multi-stage axial compressors, the losses that occur in them, the influence on performance and how these losses are currently conceptualized and modelled. It was seen that at the fundamental level for an adiabatic, subsonic axial compressor, all the loss mechanisms could be related to viscous shearing. Viscous shearing occurs wherever there are velocity gradients, but its magnitude is only of concern in regions where these gradients are very steep (Cumpsty, 1989:28).

In this chapter the mechanisms responsible for entropy increases and equivalently internal losses through an axial compressor are discussed. Figure 2.1 shows the entropy contours between blade rows for a $3\frac{1}{2}$ stage axial compressor.

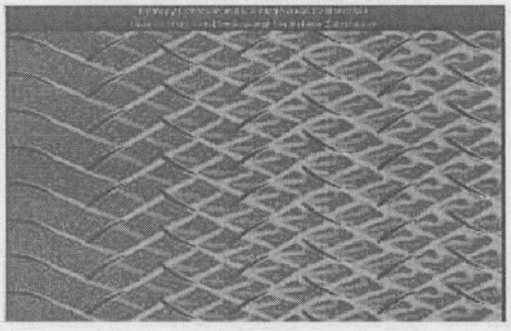

Fig. 2.1 Entropy contours between blade rows in a $3\frac{1}{2}$ stage axial compressor

In axial compressors, steep velocity gradients particularly occur in the following instances: The boundary layers that form on the blades and endwalls, the mixing processes in which non-uniformities in flows are mixed out to a uniform condition. These non-uniformities occur are in the wakes behind blades, at the edges of separated flow (flow not attached to a solid body) regions, in vortices and in leakage jets. Figure 2.2 gives a graphical illustration of the aforementioned concepts.

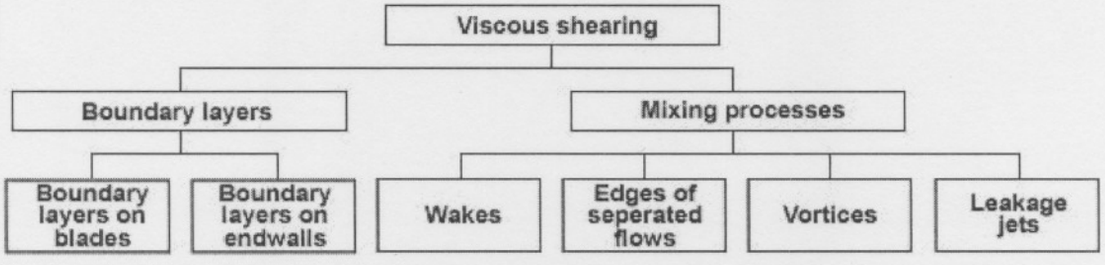

Fig. 2.2 Diagram to indicate divisions of loss mechanisms

2.2 Entropy production in boundary layers

Figure 2.3 represents a blade section moving through initially undisturbed fluid.

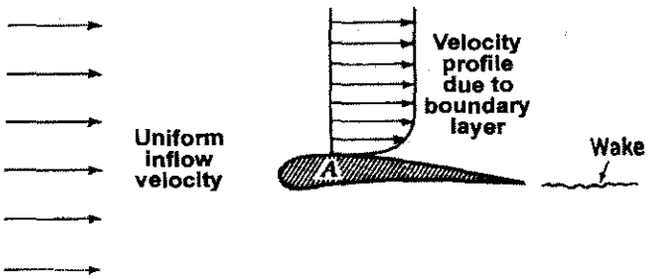

Fig. 2.3 Velocity profile on blade section due to endwall

According to Shames (1992:131) real fluids "stick" to the surface of a solid body. At Point A on the blade section the fluid velocity must be equal to zero relative to the blade and at a comparatively short distance away, it is almost equal to the initial fluid velocity. This is illustrated in the velocity profile of the diagram. It can be seen that there is a thin region, called the boundary layer, adjacent to the boundary, where sizable velocity gradients must be present. Consequently, high shear stresses, which oppose the motion of the fluid, occur, resulting in a rise in the internal energy and entropy of the fluid. At some point the shear stresses become too big and there is a transition from laminar to turbulent flow. Boundary layers grow progressively along a solid body.

When the flow angle, of the fluid relative to the blade, becomes too large the flow will separate from the boundary causing added entropy production due to mixing. During this condition the entropy increases rapidly, with respect to the separation, and the blade section stalls. Similarly, boundary layers form on the endwalls of the compressor. Figure 2.4 illustrates axial compressor boundary layers in which entropy is generated.

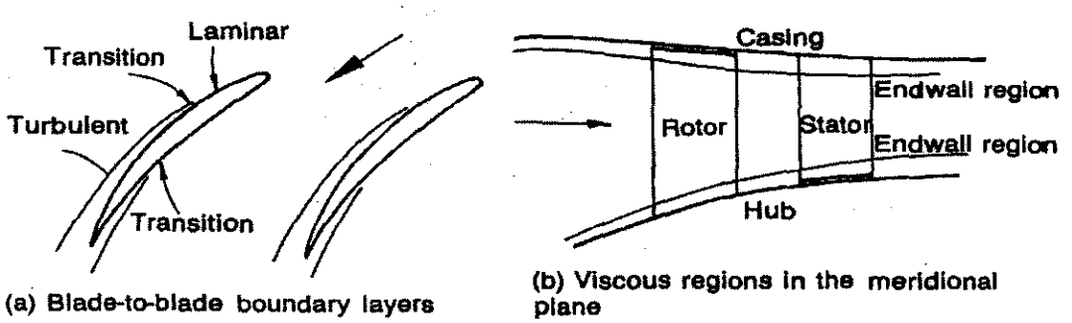

Fig. 2.4 Schematic of boundary layers in axial compressor on a (a) blade and (b) endwall

Compared with other viscous regions in compressors the understanding and prediction of axial blade boundary layers away from the endwalls is good although also influenced by the magnitude of the other loss mechanisms in the compressor. A thorough description thereof can be found in Cumpsty (1989:331). Unfortunately, this is not the case for the endwall region due to the extreme complexity of the flow and its interaction with the mixing processes and the blade boundary layer.

2.3 Entropy production in the mixing processes

Relatively high rates of shearing occur in wakes, at the edges of separated regions, in vortices and in leakage jets. Such phenomena are usually associated with turbulent flow and therefore the local entropy creation rates may be considerable.

The flow processes involved are extremely complex and often unsteady. A thorough understanding and an accurate analytical means of predicting them in axial compressors are therefore not yet available, especially in the endwall regions. Consequently, this study will not attempt to give a detail discussion on all the different mixing mechanisms and more attention will be given to the methods of predicting them macroscopically by correlation in the next chapter. Two special cases that are, however, presented are wake mixing behind a blade trailing edge and tip clearance.

For a blade in subsonic flow, about one third of the total two-dimensional entropy generation is due to the mixing of the blade boundary layers behind the trailing edge in the wake. Denton (1993:653) gives the basic theory of entropy creation due to the mixing out of a wake and employs the conservation of mass and momentum over a control volume at the trailing edge in incompressible flow. This analysis includes detail about the blade boundary layers and also the base pressure acting on the trailing edge.

The flow and entropy creation mechanisms through a tip clearance are well understood for unshrouded compressor blades. In this case, the axial velocity of the flow leaking over the tips is certain to be less than that of the mainstream and may even be directed upstream. There is a vortex sheet at their interface and this rolls up into a concentrated vortex as the flow moves downstream. The total entropy production depends on the leakage flow rate and the difference between the velocity of the mainstream flow and the leakage flow. Figure 2.5 shows a two-dimensional illustration of the flow over an unshrouded blade.

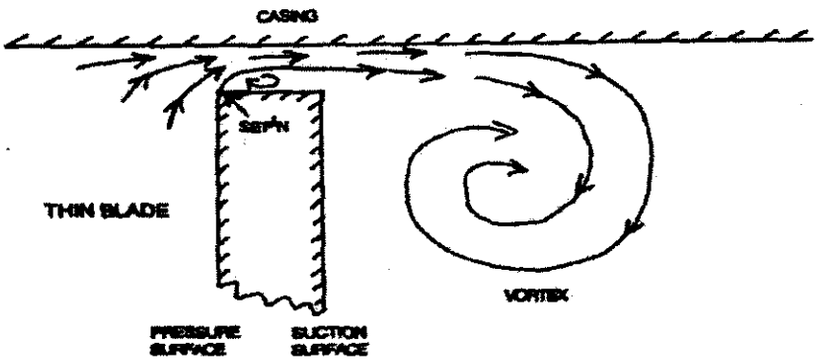

Fig. 2.5 Leakage flow over compressor rotor tip

2.4 Summary and conclusions

Internal losses, and therefore entropy increases, at a fundamental level, are a direct result of viscous shearing that occurs wherever there are velocity gradients. Steep velocity gradients particularly occur in the boundary layers that form on the blades and endwalls and the mixing processes in which non-uniformities in flows are mixed out to a uniform condition.

As an aid to understanding and modelling entropy production, it was subdivided into physical mechanisms, which are easier to conceptualize, ignoring mechanisms with negligible velocity gradients. The mechanisms that are commonly used are: Boundary layers on the endwalls, boundary layers on the blades, entropy production in wakes, edges of separated flows, vortices and leakage jets. Methods were devised to quantify these mechanisms and some of those available in the open literature are discussed in detail in Chapter 3.

Chapter 3

LOSS PREDICTION METHODS

Chapter 3 presents the reader with a comprehensive literature survey regarding loss prediction methods for subsonic axial compressors. The loss mechanisms are interactive and complex by nature and methods of predicting them rely greatly on empirical correlations. Also, the open literature is rather diffused and the main groupings used in this chapter are: Blade profile losses, endwall losses including literature on tip leakage and secondary losses, part span shroud losses, other losses, losses due to high subsonic mach numbers and off-minimum losses.

3.1 Introduction

The mechanisms mainly responsible for the losses in subsonic axial compressors were presented in Chapter 2. They are interactive and complex by nature and methods of predicting them rely greatly on empirical correlations. A thorough knowledge about the origin of these models is crucial due to the high degree of empirical reliance and therefore, limited general applicability.

The literature on loss prediction methods for axial compressors is rather diffused and many of the models used in the industry are propriety information and not available in the open literature for evaluation. Several authors furthermore also used different nomenclature, units, and sign conventions.

The cascade nomenclature used throughout this thesis is based on Figure 3.1. The nomenclature for a stationary cascade (stator) is shown, but applies equally well to a rotor if the positive α angles are replaced with negative β angles and W are used instead of C.

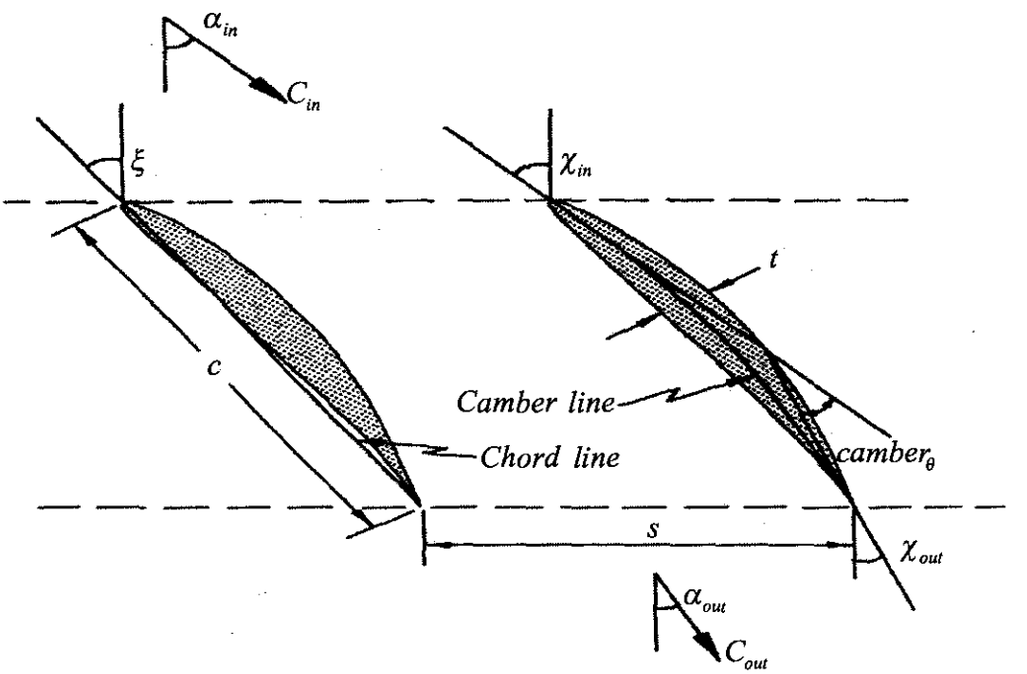

Fig. 3.1 Cascade nomenclature

Incidence is taken as the angle between the mean flow direction into the blade and the blade angle at the leading edge, $i = \alpha_{in} - \chi_{in}$.

In most instances the methodology employed to predict the minimum total losses uses a superposition of theoretically separable loss components. More specifically, for this study they will be presented under the following headings:

- Blade profile losses
- Endwall losses including literature on tip leakage and secondary losses
- Part span shroud losses
- Other losses
- Losses due to high subsonic mach numbers

The prediction of the off-minimum losses are presented in a separate section and are mostly modelled with the use of a correlation that is, among others, a function of the minimum profile loss or variables contained in the minimum blade profile loss. Sometimes, this loss is called an incidence loss. The available literature, on these categories, is discussed chronologically in the following sections and the work of some of the contributing authors is presented in detail.

3.2 Blade profile losses

Howell (1945) attempted to estimate this loss in terms of the familiar drag and lift coefficients used for aircraft analysis. In calculating the blade profile loss, most correlations, however, use a technique developed by Lieblein (1959) using a diffusion factor that is a function of the maximum relative flow velocity in the blade passage, and relative inlet and exit flow velocities.

Koch and Smith (1976), who presented the most comprehensive model, performed operations similar to Lieblein, but accounted for compressibility, Reynolds number and streamtube contraction effects found in real compressors. Starke (1980) adapted the purely two-dimensional Lieblein correlations to account for quasi-two-dimensional flow often found across compressor blade sections. Denton (1993) emphasized the importance of understanding the physical origins of loss rather than to rely on conventional correlations. He defined loss in terms of entropy increase and derived the relationship of this to the more familiar loss coefficients. Swan (1961), Cetin et al. (1989), König et al. (1993) and Roy and Kumar (1999) used the same basic principles as Lieblein, but obtained correlations for transonic compressor blades and are therefore not considered for this study. These articles did, however, make a valuable contribution to the author's insight into compressor losses.

Denton's (1993:633-636) model support the conceptualism of loss being equivalent to entropy production, and this study would seem incomplete without giving it the necessary attention. However, his model is not directly used in the study and the discussion of his work follows in

Appendix A. The models of Lieblein and Koch and Smith are discussed in more detail in the following sections.

3.2.1 Lieblein

Lieblein (1959) derived a method from cascade tests, which satisfactorily describes the low-speed relationship between blade-element loading and losses at any flow conditions (Swan, 1961:322). Some of his work and comments from other authors are presented here and the restrictions of his results are stated clearly. Hirsch and Denton showed in 1981 that Lieblein's model is as reliable as more modern correlations (Casey, 1987:275).

Lieblein showed that the losses around the blade profile appeared as a boundary layer momentum thickness, θ_{ex}, in the wake behind the blade. He also showed that as the aerodynamic loading on a compressor blade increased, the diffusion on the suction-surface increased, but that on the pressure-surface stayed approximately constant.

Therefore the suction-surface velocity distribution becomes the main factor in determining the total pressure loss. Figure 3.2(a) shows a typical velocity distribution derived from surface pressure measurements on a compressor cascade blade in the region of minimum loss. The diffusion in velocity may be expressed as the ratio of maximum suction-surface velocity to outlet velocity, $W_{max,s}/W_2$. Figure 3.2(b) illustrates the wake development in flow across cascade blades as reported by Lieblein (1959:389).

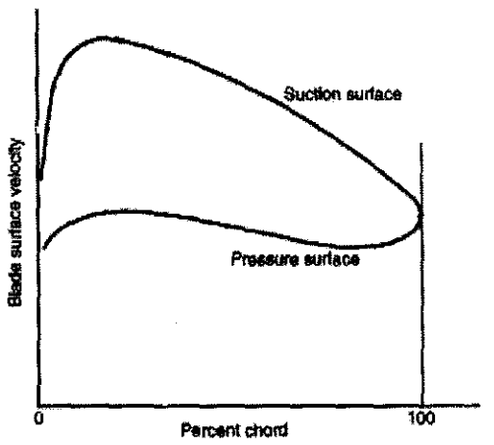

Fig. 3.2(a) Cascade blade surface velocity distribution

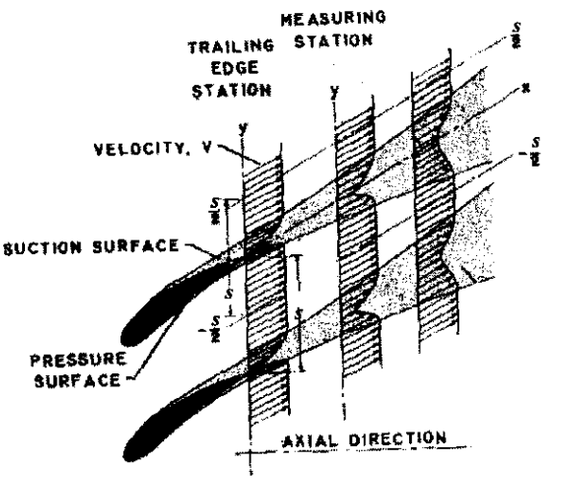

Fig. 3.2(b) Wake development in flow across cascade blades

Lieblein used a power law velocity profile to represent the wake and was then able to derive the loss in terms of the blade boundary layer momentum thickness, θ_{ex}, and the blade boundary layer form factor, H_{ex}:

$$\bar{\omega} = 2\frac{\theta_{ex}}{c}\frac{\sigma}{\cos\beta_2}\left(\frac{\cos\beta_1}{\cos\beta_2}\right)^2\left[\frac{2}{3-1/H_{ex}}\right]\left[1-\left(\frac{\theta_{ex}}{c}\right)\frac{\sigma H_{ex}}{\cos\beta_2}\right]^{-3} \tag{3.1}$$

The correlations are applicable to both rotors and stators, where W denotes the velocity relative to either a rotor or stator and β the relative angle measured from the axial direction. The subscripts 1 and 2 represent the leading and trailing edge of the blade respectively. The pressure loss coefficient (see Chapter 4 for more information), $\bar{\omega}$, gives the averaged pressure loss over a blade row due to profile losses of each blade, made non-dimensional by the inlet dynamic head of the blade row. A measure of the degree to which the wake has mixed out is the form parameter H defined by $H = \frac{\bar{\delta}}{\theta}$, where $\bar{\delta}$ is the boundary layer displacement thickness and θ the momentum thickness. Full definitions of these boundary layer parameters can be found in Lieblein (1959:389).

For blades with "healthy" boundary layers, the mixing takes place rapidly after the trailing edge and the difference between measurements of the boundary layer parameters in the wake or at the trailing edge is usually small (Cumpsty, 1989:172). A constant value for H_{ex} of 1.08 was used. Lieblein found a correlation between the diffusion ratio and the wake momentum thickness to chord ratio, θ_{ex}/c at the reference incidence (minimum loss incidence) for American NACA 65-(A_{10}) and British C.4 circular arc blades. Several authors provide correlations for Lieblein's data, but Starke showed in 1981 that the original constants given by Lieblein lead to values of momentum thickness that are too large and gave the following correlation (Casey, 1987:275):

$$\frac{\theta_{ex}}{c} = \frac{0.0045}{1-0.95\ln D_{eq}} \tag{3.2}$$

Casey also suggests an addition of 0.0025 to the momentum thickness to chord ratio as proposed by Koch and Smith (1976:419) for better predictions of efficiency. This suggestion was, however not included in the work of Starke and excluded in Japikse and Baines (1997:5-14) and is therefore not included in this study. It can be seen that knowledge of suction-surface velocities

are assumed in the above equations. This data is not always available and can be obtained from a correlation given by Lieblein:

$$D_{eq} = \frac{W_{max,s}}{W_2} = \frac{\cos\beta_2}{\cos\beta_1}\left[1.12 + 0.61\frac{\cos^2\beta_1}{\sigma}\left(\tan\beta_2 - \tan\beta_1\right)\right] \tag{3.3}$$

Because the form parameter is so close to unity, Lieblein has demonstrated the simplified relationship between the wake momentum thickness ratio and the stagnation pressure loss, valid for unstalled blades as:

$$\varpi = 2\frac{\theta_{ex}}{c}\frac{\sigma}{\cos\beta_2}\left[\frac{\cos\beta_1}{\cos\beta_2}\right]^2 \tag{3.4}$$

Lieblein's model limits element losses to those caused by surface friction, flow separation and wake mixing. The correlations and expressions were obtained from studies done on purely two-dimensional, low speed cascades with NACA 65-(A_{10}) and British C.4 circular arc blade profiles. Cumpsty (1989:175) states that the loss from different profile sections is very nearly the same at subsonic Mach numbers and that Mach number does not have a large influence on total profile losses until shock losses start to form as a result of supersonic patches. Lieblein's correlations are still very widely used as a means of estimating total pressure loss in the unstalled range of operation of blades commonly employed in subsonic axial compressors (Dixon, 1998:74).

3.2.2 Koch and Smith

Compressible boundary layer theory has been employed as a rational means to extend the two-dimensional, low speed correlation of Lieblein into the Mach and Reynolds numbers that are of interest to compressor designers.

The effects of blade surface curvature were neglected for simplicity. In their study, Koch and Smith assumed the boundary layers to be turbulent everywhere and that an adiabatic wall condition existed. They calculated the blade surface boundary layers over ranges of Mach number, Reynolds number and streamtube contraction for diffusion ratios, $W_{max,s}/W_2$ of 1.3 up to the value at which the turbulent boundary layer was predicted to separate (Koch and Smith, 1976:413).

From this it was possible to arrive at functional relationships at the trailing edge of the form:

$$\left.\begin{matrix}\theta_{te}/c \\ H_{te}\end{matrix}\right\} = f\left(W_{\max,s}/W_2, M_1, \mathrm{Re}, h_1/h_2\right) \tag{3.5}$$

with h_1 and h_2 being the blade height at inlet and outlet respectively.

The results of the boundary layer calculation were then compared to the correlation presented by Lieblein. This was done by converting the calculated trailing-edge momentum thickness to a wake momentum thickness with a form factor of 1.08.

It was found that for diffusion ratios below 1.7 the calculated wake and trailing edge momentum thickness are virtually the same. For higher diffusion ratios the wake momentum thickness is greater than the trailing-edge momentum thickness by a significant amount. Koch and Smith (1976:413) reported higher values than Lieblein for diffusion ratios below 1.7. This is probably due to the considerable amount of laminar flow that existed in the cascades studied by Lieblein.

To account for blade surface roughness, Koch and Smith defined a roughness Reynolds number below which the airfoils can be considered hydraulically smooth. This criterion is taken as:

$$\frac{W_1 k_s}{\nu} \leq 90 \tag{3.6}$$

In fluid mechanics, roughness is usually specified in terms of an equivalent sand grain size, k_s. To relate this equivalent sand roughness to compressor blade surface finish, the following equation can be used:

$$k_s = 6.2 k_{CLA} \tag{3.7}$$

where k_{CLA} is the centreline average of the roughness particles and is defined as the arithmetical average deviation expressed in microns measured normal to the centreline.

The methodology suggested by Koch and Smith (1976:412-415) to predict blade profile losses due to the results obtained from their calculations is summarized below. Where appropriate, contributions were taken from Wilson and Korakianitis (1998:361).

The suction surface diffusion ratio, $W_{max,s}/W_2$, is calculated from the cascade geometry and the vector diagrams, accounting for blade thickness, annulus contraction and compressibility effects. To simplify matters, a semi-empirical formulation is provided in Equation 3.8. This formulation is similar to Equation 3.3 derived by Lieblein, but is somewhat more representative of the conditions in a compressor as opposed to two dimensional test cascades. A detail derivation of Equation 3.8 can be found in Koch and Smith (1976:423). The equivalent diffusion ratio, D_{eq}, at minimum loss incidence is

$$D_{eq} = \frac{W_1}{W_2}\frac{V_{max}}{V_p}\frac{V_p}{W_1} \tag{3.8}$$

where V_p is the relative velocity in the passage throat and V_{max} is the maximum possible relative velocity in the blade passage throat region.

They can respectively be given by:

$$V_p/W_1 = \left[\left(\sin\beta_1 - 0.2445\sigma\Gamma\right)^2 + \left(\frac{\cos\beta_1}{A_p\,\rho_p/\rho_1}\right)^2\right]^{1/2} \tag{3.9}$$

$$V_{max}/V_p = \left(1 + 0.7688\frac{t_{max}}{c} + 0.6024\Gamma\right) \tag{3.10}$$

The area contraction ratio from blade inlet to throat is given by

$$A_p = \left(1 - 0.4458\sigma\left(\frac{t_{max}}{c}\right)/\cos\left(\frac{(\beta_1+\beta_2)}{2}\right)\right)\left(1 - \frac{A_1 - A_2}{3A_1}\right) \tag{3.11}$$

and the density in the passage throat by

$$\rho_p/\rho_1 = 1 - \frac{M_z^{\,2}}{1 - M_z^{\,2}}\left(1 - A_p - 0.2445\frac{\tan\beta_1}{\cos\beta_1}\sigma\Gamma\right). \tag{3.12}$$

The circulation, Γ, for a two-dimensional, incompressible cascade is given by

$$\Gamma = \frac{r_{rms_1} C_{\theta_1} - r_{rms_2} C_{\theta_2}}{r_{rms} \sigma W_1} \tag{3.13}$$

The ratio of trailing edge momentum thickness to chord length, θ_{te}/c, and trailing edge form factor, H_{te} can found from Figure A.2.1 and Figure A.2.2 in Appendix A.2. These correlations given are for nominal conditions for a Reynolds number of 1×10^6, hydraulically smooth blades, a streamtube height ratio, h_1/h_2, of 1, and a Mach number of 0.05. Corrections have to be applied for conditions other than nominal and the correctional multiplier correlation figures are also given in Appendix A.2.

With the new values for trailing-edge momentum thickness to chord ratio, θ_{te}/c, and form factor, H_{te}, known, a new trailing-edge freestream velocity can be determined from iteration and therefore changes to the initial estimate for the diffusion ratio. This continues until all the trailing-edge parameters converge.

It is now possible to estimate the total pressure loss by calculating the mixing of the freestream and the boundary layers in a control volume analysis. According to Wilson and Korakianitis (1998:362), the use of Equation 3.1, derived by Lieblein, is satisfactory to calculate the total pressure loss, but with, θ_{te}/c, instead of θ_{ex}/c.

3.3 Endwall losses

The endwall loss is the most difficult loss component to understand and predict and virtually all prediction methods rely on very little underlying physics. Much effort and many papers have been directed to endwall flows in cascades. Unfortunately, these flows are not representative of the flow in compressor blade rows and the correlations derived from them should be used with the greatest caution. (Cumpsty, 1989:355)

Hübner and Fottner (1996:2) also states that: "...the flow in the endwall region is not well understood in spite of the research over a period of more than two human generations. However the process of loss generation still remains not very clear up to now and thus the losses cannot be predicted with reasonable accuracy."

Classic denominations of endwall losses are: annulus boundary layer loss, tip clearance loss and secondary loss. The term secondary loss is also sometimes used to describe all the losses in the endwall region. The effects of tip clearance are overwhelming on the endwall flow development and on the blade-to-blade flow near the tip and it would be somewhat artificial to treat it in a separate section as is done in many instances in the literature.

The first modelling of tip clearance losses in compressor cascades seems to be that done by Betz in 1926. Chauvin, Cyrus and Senoo published reviews in the 1980's on improved correlations (Hübner and Fottner, 1996:8).

Early methods by Betz, Vavra, and Lakshminarayana, referenced by Hübner and Fottner (1996:9) tended to work in terms of the induced drag on the blades, analogous to the drag on an aircraft wing. This is, however an inviscid effect. Rains assumed the kinetic energy of the leakage flow driven by the pressure difference between the pressure and suction side as lost. Another method is to consider the pressure rise of the cascade in terms of the blade loading and authors following this approach are: Bauermeister, Scholz, Baljé, Grieb, Hultsch and Sauer and Cyrus (Hübner and Fottner (1996:9).

More recent studies, for example by Storer in 1991 and Papailiou in 1995, measured the tip leakage flow in great detail and modelled it in terms of the mixing loss between the tip leakage and the main flow. Denton (1993:638) states that there is no known work on the flow processes over shrouded compressor blades and the current study confirms this.

Several methods that calculate the annulus boundary layer displacement thickness via a two-dimensional boundary layer calculation along the whole endwall of a compressor has been published e.g. De Ruyck and Hirsh (1983). Denton (1993:640) states that such methods that use conventional boundary layer theory must be regarded as dubious, because during their interaction with the blade rows, the boundary layers cannot be considered as conventional boundary layers. Their reasonable predictions are a result of considerable empiricism.

The models of the following authors are discussed in detail and are thought to be a good representation of a lump of the work done: Howell assumed the endwall loss to be made up of friction at the annulus walls and a secondary loss that was greatly influenced by the tip clearance (Cohen et al, 1996:210). Koch and Smith (1976:416) relate the loss of efficiency due to the presence of endwall effects to two properties of an endwall boundary layer, i.e. the averaged displacement thickness and the tangential-force thickness. Denton (1993:640) presents models

for the tip clearance losses and endwall losses separately and defines them in terms of entropy generation. His models were again included in this study (Appendix A.3) due to their effort to find models that are based less on empirical results and calculate the loss as an entropy increase. Hübner and Fottner (1996:8-11) give a short overview of the available tip clearance loss correlations and propose an improved approach for the calculation of these losses. Roy and Kumar (1999) modelled some secondary losses by lumping them with the blade profile losses. A hub endwall loss model and a tip clearance loss model accounted for the remaining losses.

3.3.1 Howell

Howell (1945:115-131) realized as early as 1945 the importance of loss at the annulus walls and provided a rough estimate for the axial compressors of the time. Several assumptions were made for simplification. He further assumed the endwall losses to be made up of a so-called annulus loss and a secondary loss. Figure 3.3 gives a graphical representation of this reasoning.

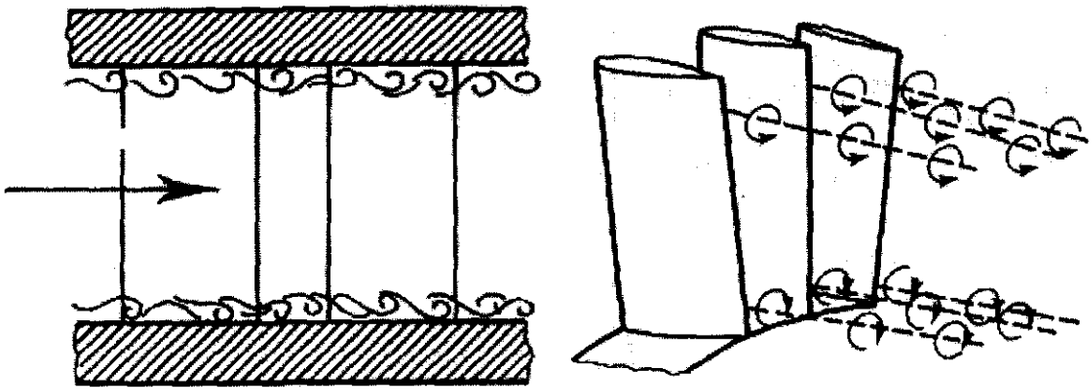

(a) Annulus Loss (b) Secondary Losses

Fig. 3.3 Three Dimensional Flow Effects according to Howell

From Figure 3.3 it can be seen that the annulus loss is the loss due to friction on the annulus walls or annulus drag and a drag coefficient was assigned a constant value:

$$C_{D_A} = 0.02\frac{s}{h} \tag{3.14}$$

In turn, the secondary loss drag coefficient was related to the reduction in blade circulation in the blade end region and was derived by analogy with the trailing vortex loss behind aircraft. With

$$C_{D_s} = 0.018(C_L)^2 \tag{3.15}$$

and C_L the blade lift coefficient outside the endwall region calculated from:

$$C_L = 2\sigma^{-1}(\tan\beta_1 - \tan\beta_2)\cos\beta_m \tag{3.16}$$

with the value of the vector mean angle, β_m, calculated from:

$$\tan\beta_m = \frac{1}{2}(\tan\beta_1 + \tan\beta_2) \tag{3.17}$$

The mean pressure loss coefficient over a blade row due to the endwall losses can now be calculated from:

$$\varpi = \frac{(C_{D_A} + C_{D_s})\sigma\cos^2\beta_1}{\cos^3\beta_m} \tag{3.18}$$

Cumpsty (1989:337) stated that, although there are no grounds on which the model for the secondary losses can be proven accurate, nor to believe the separation of loss into two components, this did provide a way of introducing the loss of approximately the right magnitude. He also states that later work confirmed that the secondary losses were actually proportional to the square of the lift coefficient as shown in Equation 3.15.

3.3.2 Koch and Smith

The influence of the endwall boundary layer is modelled in terms of its averaged displacement thickness, $\overline{\delta}$, which contributes directly to an efficiency decrease, but is partly offset by the reduction in the tangential blade force in the boundary layer (Japikse and Baines, 1997:5-27).

The displacement thickness is a measure of the mass flow reduction caused by the presence of the endwall boundary layer, compared to the mass flow if the free-stream flow profiles (flow without endwall losses) were extended to the wall. Another variable, the tangential-force thickness, ν_t, is

introduced and represents the reduction of the tangential component of blade force from its free-stream value due to the presence of an endwall boundary layer.

Koch and Smith (1976:416) made detailed measurements of the flow profiles in several low-speed multistage compressors for the hub and casing boundary layers behind both rotors and stators. Values for $\overline{\delta}$ and v_t were deduced from these measurements. The thickness of the hub and casing boundary layers were added and represented by $2\overline{\delta}$, and the rotor and stator exit values were averaged and normalized by the averaged staggered spacing, $\overline{g} = s\cos\xi$, at the mean diameter. They found that by assuming v_t to be a fixed fraction of $\overline{\delta}$, it was possible, with the help of a representative profile model, to construct fairly accurate pressure rise and efficiency characteristic curves for a series of stages with aspect ratios, $\frac{h}{c}$, varying from 2 to 5 and tip clearances varying from 0.8-3.6 percent annulus height. Their resulting correlations are given in Appendix A.4. It shows $\frac{2\overline{\delta}}{\overline{g}}$ and $\frac{2\overline{v_t}}{\overline{g}}$ plotted against the stage static pressure rise coefficient relative to the maximum static pressure rise coefficient which the stage is capable of as well as a correction for the axial spacing of the blade rows.

The stage stagnation-to-stagnation efficiency can now be calculated from

$$\eta = \eta_{fs}\frac{1-\left(2\overline{\delta}/\overline{g}\right)\left(\overline{g/h_a}\right)}{1-\left(2\overline{v_t}/2\overline{\delta}\right)\left(2\overline{\delta}/\overline{g}\right)\left(\overline{g/h_a}\right)} \tag{3.19}$$

where η is the stage efficiency and η_{fs} is the free-stream efficiency, i.e. the efficiency if there were no endwall losses, and $\overline{g/h_a}$ is the weighted average rotor and stator mean diameter staggered spacing to annulus height ratio. The weighting function is again the blade row inlet dynamic heads.

Koch and Smith (1976:318) realize that their model is of limited scope and questionable general applicability. They suggest that the model should not be used for aspect ratios less than unity. For calculating the free stream axial velocity, due to blockage from the boundary layer, for use in other models like the profile loss model, $\frac{2\delta}{\overline{h}}$ is taken as 0.17 if the value deduced from the figures is greater than 0.17.

3.3.3 Hübner and Fottner

Hübner and Fottner (1996:8) classified some loss correlations for the endwall losses into two groups. They state that the one group (Vavra in reference to Mehldahl - 1960, Vavra in reference to Rains - 1960, Scholz - 1965, Baljé - 1968, Lakshminaraya - 1970, Grieb - 1975, Storer and Cumpsty - 1993) considers the loss as a linear superposition of the secondary and the tip clearance losses:

$$\varpi_{endwall} = \varpi_{secondary} + \varpi_{tip-clearance} \tag{3.20}$$

In this case the secondary losses are the endwall without a tip gap.

The second group (Bauermeister - 1963, Hultsch and Sauer - 1979, Cyrus - 1992) looks at the hub and the tip region separately and defines the mean value as the total endwall loss:

$$\varpi_{endwall} = \frac{1}{2}\left(\varpi_{secondary,hb} + \varpi_{secondary,t}\right). \tag{3.21}$$

They compared the correlations of Equation 3.20 and Equation 3.21 with experimental measurements from a highly loaded, linear cascade with high speed flow and NACA 65-K48 profiles. It was noted that the definition, as presented by Equation 3.20, was physically not well founded and suggested the use of the definition given by Equation 3.21. The reason is that the endwall losses are a strong function of the tip clearance.

The correlation of Bauermeister was identified as the best to start from for an improvement. Hübner and Fottner (1996:10,11) changed Bauermeister's correlating parameters for the secondary losses of the tip region according to their experimental data and experience. Thus, the endwall loss is given by Equation 3.21 where:

$$\varpi_{secondary,t} = \frac{0.165}{h/c}\left[\cot^2(\beta_1 - 90) - \cot^2(\beta_2 - 90)\right]\sin^2(\beta_1 - 90)\tanh\left(35\frac{\tau}{c}\right) + 0.0288 \tag{3.22}$$

and

$$\varpi_{secondary,hb} = 2\frac{c}{h}\left[0.0505\left(\cot^2(\beta_1 - 90) - \cot^2(\beta_2 - 90)\right) - 0.01313\right]\sin^2(\beta_2 - 90) \tag{3.23}$$

The subtraction of the 90 degrees is necessary because their angles were measured with respect to the tangential direction. For this study, the relative flow angles for the rotor are negative, therefore absolute values are used.

3.3.4 Roy and Kumar

The profile model used by Roy and Kumar was based on the model proposed by Leiblein with different values for $\frac{\theta}{c}$ applicable to transonic blades. It is, however, fundamentally based on models obtained from subsonic tests. It is also the only model included in this study that explicitly gives a magnitude to the loss due to tip clearance. It must be stated that every effort was made to follow the literature carefully, but that some error might have slipped in due to limited detail and unclear nomenclature supplied by the authors. A boundary layer loss model (from the hub), transposed to the midspan section, and a tip clearance loss model accounted for the endwall losses.

The boundary layer endwall loss model is based on a model presented by Vavra in 1960. The effect of aspect ratio has been included and then the loss was transposed to the midspan section to give:

$$\varpi_{ew} = 0.04 C_L^2 \frac{\sigma c}{h} \frac{\cos^2 \beta_1}{\cos^3 \beta_m} \tag{3.24}$$

It is suggested that Equation 3.24 be used only for $AR < 2.0$ and that for high aspect ratio blades a different model may be necessary.

The tip clearance loss model is based on an assumption that the kinetic energy in the gap flow normal to the blade chord is lost due to the interaction between the tip leakage flow and the main flow. The most important factors in the model are the prediction of the mass flow through the clearance and the magnitude of the velocity component of the leakage jet normal to the tip clearance. The high velocity leakage jet mixes with the main flow to result in high shearing losses and ultimately flow separation (Roy and Kumar, 1999:2).

The total pressure loss is modelled as the sum of the pressure loss inside the tip gap and the pressure loss due to the leakage jet mixing with the main flow. Thus:

$$\varpi_{\tau} = \frac{\Delta P_{total}}{q_1} \tag{3.25}$$

$$\Delta P_{total} = \Delta P_{gap} + \Delta P_{mixing} \tag{3.26}$$

$$\Delta P_{gap} = 0.5 c \rho \tau W_1^3 B\left(C_p\right)^{1.5} \tag{3.27}$$

$$\Delta P_{mixing} = 0.5 c \rho \tau V_{jet}^3 \tag{3.28}$$

In the above equations, W_1 is the entry flow velocity to the tip gap, V_{jet} is the leakage jet velocity and these values can be approximated from simultaneous calculation of:

$$\frac{V_{njet}}{W_1} = C_d \sqrt{C_p} \tag{3.29}$$

$$\frac{V_{njet\max}}{W_1} = A \sqrt{C_p} \tag{3.30}$$

$$V_{jet} = 1.05 V_{njet} + 0.5\sigma\left(U\cos\theta_{camber} - V_{njet\max}\right) \; for \; U\cos\theta_{camber} > V_{njet\max} \tag{3.31}$$

$$V_{jet} = 1.05 V_{njet} \; for \; U\cos\theta_{camber} < V_{njet\max} \tag{3.32}$$

In the above equations, $V_{njet\max}$ is the maximum normal jet velocity in the tip gap, C_p is the static pressure coefficient across the tip gap, C_d is the discharge coefficient across the tip gap, A and B are gap loss coefficients, U is the average relative wall speed, and θ_{camber} is the camber angle of the blade at the tip.

The static pressure coefficient, C_p, across the tip gap is the static differential between the pressure surface and the suction surface divided by the inlet dynamic head of the blade row. The tip gap loss coefficients and the discharge coefficient were determined for four tip gap geometries and are given in Table 3.1.

Table 3.1: Tip gap loss coefficients and discharge coefficients

Geometry	A	B	C_d
Uniform	1	0.24	0.84
Parabolic	0.87	0.19	0.87
Inverse Parabolic	0.74	0.11	0.72
Triangular	0.8	0.15	0.76

The geometries are considered for their shape across the thickness of the blade. Since the blade thickness changes along the chord the shape of the gap may change. Also, if the blade tip section is at a stagger, the gap between the blade tip section and the casing, which has a circular curvature, is decided by the stagger angle.

For example if the tip section is flat, then the tip gap will increase up to mid-chord and decrease thereafter towards the trailing edge. This is corrected by curving the tip section appropriately. Hence there are a number of possibilities of the gap geometry across the tip and only a few have been properly considered in the model.

The endwall loss can now be given by:

$$\varpi_{total} = \varpi_{ew} + \varpi_{\tau} \tag{3.33}$$

3.4 Part span shroud losses

Part span shrouds are often found in compressor stages. Their main purpose is the damping of possible damaging resonance and improving strength characteristics. Denton (1993:649) and Koch and Smith (1976:418) established an appropriate loss model based on the drag coefficient of the shroud member.

The components of the drag force are the shroud profile drag and an interference drag due to the interaction of the shroud and the blades. The shroud profile drag is modelled as a simple airfoil or a curved section, whereas the interference drag was determined purely empirically (Japikse and Baines, 1997:5-28).

The model presented by Koch and Smith (1976:418) gives the shroud drag coefficient based on shroud frontal area, $C_{D_{sh}}$, as

$$C_{D_{sh}} = \frac{F_D}{\frac{1}{2}\rho_\infty V_\infty^2 A_{sh}\cos\beta_\infty} \tag{3.34}$$

where F_D is the drag force, V_∞ is the vector mean of the upstream and downstream velocities, ρ_∞ is the density at the vector mean velocity, β_∞ is the vector mean flow angle and

$$A_{sh} = 2\pi r_{sh} t_{sh}\,. \tag{3.35}$$

In Equation 3.35, A_{sh} is the shroud frontal area and r_{sh} and t_{sh} is the shroud radius and thickness respectively. To estimate the magnitude of $C_{D_{sh}}$, Koch and Smith gives the following expression

$$C_{D_{sh}} = K_{sh}\left\{0.012\left[\frac{c_{sh}/t_{sh}}{\cos\beta_\infty} + 2 + 60P_M^3\left(\frac{t_{sh}}{c_{sh}}\right)^2\right] + 3P_M^3\left(\frac{t_{sh}}{b}\right)\left(\frac{t_{sh}}{c_{sh}}\right)\right\} \tag{3.36}$$

where K_{sh} is an empirical constant that must be determined from experience or empirically. Koch and Smith used the value of 1.8. Also, c_{sh} is the shroud chord in the axial direction and:

$$P_M = (1 - M_\infty^2\cos^2\beta_\infty)^{-1/2}, \tag{3.37}$$

$$b = \frac{2\pi r_s}{N_B} \quad \textit{with} \quad N_B \ \textit{the number of blades} \tag{3.38}$$

$$M_\infty = \frac{V_\infty}{\sqrt{\gamma R T_\infty}} \tag{3.39}$$

The entropy increase, thus a quantification of the loss produced due to the shroud addition is given by:

$$\Delta s = \left(C_{D_{sh}}\frac{\gamma}{2}M_\infty^2\frac{A_{sh}}{A_{a\infty}}\right)R \tag{3.40}$$

3.5 Other losses

In Chapter 2, it was seen that only the mechanisms producing a steep velocity gradient are usually taken into account when it comes to predicting the losses.

There are, however, numerous other mechanisms of loss, which are mostly small, but can become significant in special cases (Denton, 1993:647). Denton advises further reading of Chapter 8 of literature published by Glassman in 1973 for more details about these other loss mechanisms. The most important of these are briefly discussed in the following sections.

3.5.1 Losses due to unsteady flow

Wakes, vortices and separations often mix out in the downstream blade row. This leads to mixing in an unsteady environment and is a lot different from that which is modelled or observed in cascade tests.

For wakes, the mixing loss is usually relatively small and normally takes place close to the trailing edge. Therefore, the added loss of this effect is mostly insignificant. A flow separation can be thought of as a large wake, but in this case the added mixing loss can be large and might have a noticeable affect on the entropy generation. The magnitude of such a process is, however, difficult to quantify.

The vortex from one blade row will be convected through the downstream blade row in much the same manner as a wake, but with different effects on the loss generation. If a vortex is stretched longitudinally, from moving through the downstream blade row, it can be shown that its secondary kinetic energy varies as the square of its length. When viscous effects then dissipate this increased kinetic energy, it will increase the loss. Again the magnitude of such an increase is not known, but it could have important implications in certain cases.

Other means in which unsteady flow can affect entropy generation are through dissipation of the spanwise vorticity shed from a trailing edge as a result of changes in blade circulation, the presence of unsteady velocity profiles due to wake passage and unsteady boundary layer transition (Denton, 1993:648).

It is assumed that the aforementioned losses are usually small enough to justify their elimination in loss modelling. Nevertheless, it is important that the reader is aware that such losses do contribute to the total loss and might, in special cases, be larger in magnitude than anticipated.

3.5.2 Windage loss

According to Denton (1993:648), windage loss is the loss caused by viscous shearing on all parts of the machine other than the annulus boundaries and the blades, where it has already been accounted for.

Denton describes this loss in terms of the entropy increase experienced wherever fluid is moving relative to a solid boundary layer. This entropy finds its way into the flow and is present at the exit of the machine. He observes that loss does not only occur on rotating surfaces, but on any surface exposed to the flow and that some reheat effects are noticeable. The reheat effect is thought of as frictional heat production, which increases the work input of downstream stages.

Roelke presented a simple estimate of the ratio of the power lost by windage to useful power in 1973. He applies a skin friction factor, which is a function of the Reynolds number, to all rotating surfaces for estimating these windage losses. This ratio, assuming an axial flow machine with a two-sided disk, is given by

$$\frac{\Delta W_{windage}}{W_{useful}} = 0.1 \frac{C_f}{\psi\phi} \frac{D_{hb}}{h_b} \frac{1}{1+4h_b/D_{hb}} \tag{3.41}$$

where C_f is the skin friction factor, D_{hb} is the hub diameter of the disc and:

$$\psi = \frac{C_z}{U} \tag{3.42}$$

$$\phi = \left(\frac{\Delta h_0}{U^2} \right)_{stage} \tag{3.43}$$

$$C_f = 0.398 C_m \tag{3.44}$$

The value of C_m can be determined from Figure 3.4.

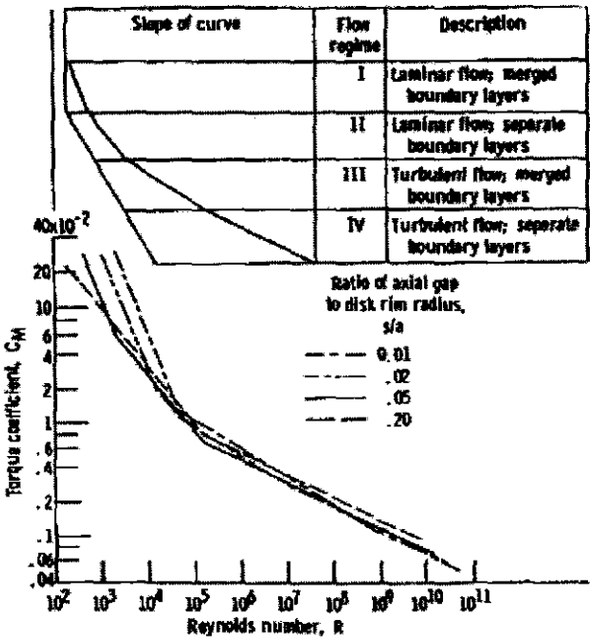

Fig. 3.4 Moment coefficient for frictional torque on smooth rotating disks

The fraction of lost power for most machines is very small with C_f in the order of 0.002. It is most significant for compressors with short blades and low flow and loading coefficients. Of course, the loss can be much greater for disks that are not smooth.

3.6 Losses due to High Subsonic Mach Numbers

This study does not present a detail review on shock loss models as it only deals with purely subsonic compressors. However, a short discussion on this subject follows for the sake of completeness and to increase this thesis's value as a reference.

The conditions where the maximum velocity on the suction surface reaches sonic velocity, is called the critical Mach number. The critical Mach number depends on many variables like the overall blade thickness, mean camber, distribution of thickness and camber along the blade chord and most importantly the angle of incidence (Cumpsty, 1989:181). Cumpsty also states that the achievement of critical conditions does not in itself have a major influence on the cascade performance, even if the sonic patches are terminated by a shock at slightly higher Mach numbers.

According to Denton (1993:636) the maximum suction surface velocity for conventional axial compressors is well above the inlet velocity and will reach sonic conditions at an inlet Mach

number of about 0.7. Cohen et al. (1996:217) also states figures from 0.7 to 0.85 for typical subsonic cascades at zero incidence. The real performance penalties result from shocks that are so strong that they cause the blade boundary layers to separate and not reattach again. This is most likely when the inlet Mach number is greater than 1.4. Consequently, this study will assume shock losses to be crucial only when the inlet Mach number increases beyond 0.8 and therefore it is recommended that further reading of Cumpsty (1989:132-194) and Koch and Smith (1976:415) must be pursued if transonic conditions need to be modelled.

3.7 Off-minimum loss prediction

Almost all off-minimum loss predictions are done with primarily two types of off-minimum loss prediction methods. The first of these methods use correlations to calculate the off-minimum loss as a function of the minimum total profile loss and the difference between the local incidence and the minimum loss incidence, with incidence being the difference between the inlet flow angle and the blade 'metal' angle:

$$\varpi = f\left(\varpi_{\min}, i - i_{\min}\right) \tag{3.45}$$

Cohen et al. (1996:217) presents the effect that Mach number has on the off-minimum losses for a typical subsonic cascade as shown in Figure 3.5

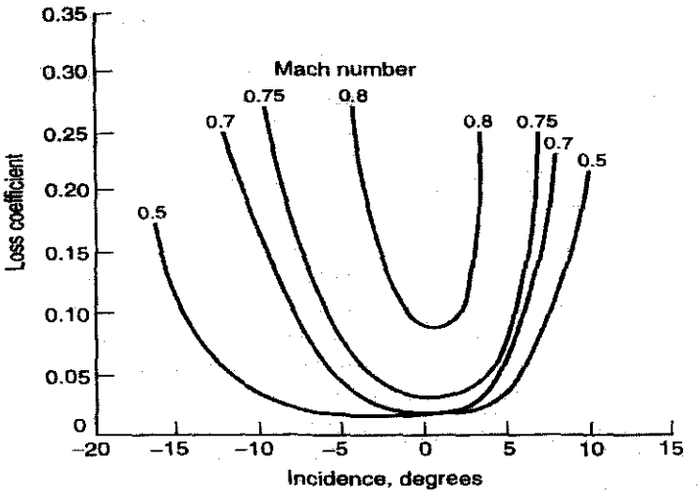

Fig. 3.5 Loss coefficient presentation at minimum and off-minimum loss condition, showing the effect of Mach number

Casey (1987:276) uses a correlation given by Jansen and Moffatt in 1967 which correlates a graph similar to Figure 3.5. This correlation is given as

$$\frac{\varpi}{\varpi_{min}} = 1 + 0.1667\kappa + 0.833\kappa^2 \tag{3.46}$$

where κ is an off-minimum loss factor related to incidence and operating range. Chapter 4 gives a more detailed discussion on predicting the operating range, $\delta\beta$. The off-minimum loss factor can be calculated as follows:

$$\kappa = \frac{|i - i_{min}|}{\delta\beta/2} \tag{3.47}$$

The second method is very similar to the prediction of the minimum profile loss by Lieblein (1959), but the diffusion ratio, D_{eq} is corrected away from minimum loss incidence. This value is then used in the calculation of the off-minimum momentum thickness to chord ratio. Lieblein (1959) suggested a correlation for the off-minimum loss equivalent diffusion ratio by using his minimum loss correlation, but applying a shift to account for the incidence angle.

$$D_{eq} \equiv \frac{\cos\beta_2}{\cos\beta_1}\left[1.12 + k\left(|i - i_{min}|\right)^{1.43} + 0.61\frac{\cos^2\beta_1}{\sigma}\left(\tan\beta_2 - \tan\beta_1\right)\right] \tag{3.48}$$

In the above equation $k = 0.0117$ and $k = 0.007$ for the NACA 65-(A_{10}) blades and C.4 circular arc blades respectively (Dixon, 1998:74). Starke (1980:7) suggested a value of 0.013 for their experimental setup which consisted of 9C7/32, 5C50 blades with a circular camber line. Wilson and Korakianitis accept $k = 0.0117$ as a satisfactory approximation for all blade shapes. The momentum thickness to chord ratio can now again be calculated by the correlations, Equations 3.2, used for the minimum loss case.

3.8 Summary and conclusions

The main groupings for predicting minimum total loss in this chapter were: Blade profile losses, endwall losses including literature on tip leakage and secondary losses, part span shroud losses, other losses and losses due to high subsonic mach numbers.

For the blade profile losses, most authors use a technique developed by Lieblein using a diffusion factor. Koch and Smith's correlations seem to be the most complete, accounting for compressibility, Reynolds number and streamtube contraction effects. This is also the only model available that takes blade passage blockage into account. The loss from different profile sections is very nearly equal at low to moderate subsonic Mach numbers. If necessary, the correlations by Lieblein can be used for simplification purposes.

The literature on endwall losses consists of many different groupings of components. The model of Koch and Smith appears to be the most complete and comprehensive as it does not distinguish between loss components and models the endwall loss as a function of tip clearance and annulus boundary layer parameters. It is further advantageous due to the fact that it gives a value for endwall blockage resulting from the boundary layer and additional correlations are not needed to calculate this quantity for performance prediction. Unfortunately, it requires a great amount of iteration during performance prediction, and correlations from other authors can be used where less complexity is desired.

Part span shroud losses should be included when applicable. Losses due to unsteady flow are usually negligible, but can become important in special circumstances. There is, however, no present way of predicting their magnitude. Windage loss is small in most cases, except if large solid areas other than the annulus or blades are present in the flow path and especially if these surfaces are not smooth.

Off-minimum loss predictions are done with primarily two types of prediction methods. The first method calculates the off-minimum loss as a function of the minimum total profile loss and the difference between the local incidence and the minimum loss incidence. The second method corrects the diffusion ratio away from minimum loss incidence. This value is then used in the calculation of the off-minimum momentum thickness to chord ratio that is used in calculating the off-minimum loss.

It would seem rather pointless to do parametrical studies of the influence of loss parameter changes based purely on the loss models, because these effects can almost be seen directly from the correlations from which the models were constructed. The study of these models can therefore not be viewed in isolation from the concepts involved in axial compressor performance and its prediction. Chapter 4 presents the concepts involved in performance prediction.

Chapter 4

PERFORMANCE PREDICTION

The study of the models that predict subsonic axial compressor losses cannot be viewed in isolation from the concepts involved in axial compressor performance prediction. This chapter therefore attempts to provide the reader with a framework into which the loss models can be integrated through presenting the theory required for a meanline compressor analysis.

4.1 Introduction

Chapter 3 discussed several loss models that can be used to quantify the internal losses in axial compressors. These models cannot be used in isolation, because their input variables are dependent on other performance prediction calculations and in turn, the other performance prediction models need values for losses in order to give realistic predictions. The loss models, therefore, need to be solved implicitly with other performance prediction models in order to obtain realistic predictions.

This chapter attempts to provide the reader with a framework into which the loss models can be integrated as well as the non-loss models and theory involved.

4.2 Method of performance prediction

Three-dimensional calculation methods are relatively new and extremely complex. It is therefore still common to consider the flow in two separate, but interrelated two-dimensional surfaces. The meridional plane, also known as throughflow, connects the flow in the radial direction and the flow at various sections is required to be compatible and to satisfy the momentum equation. The intersecting two-dimensional surface is usually a surface of revolution and is normally referred to as the blade-to-blade flow and calculations are made in relation to the passage between adjacent blades. Figure 4.1 represents these surfaces (Cumpsty, 1989:96).

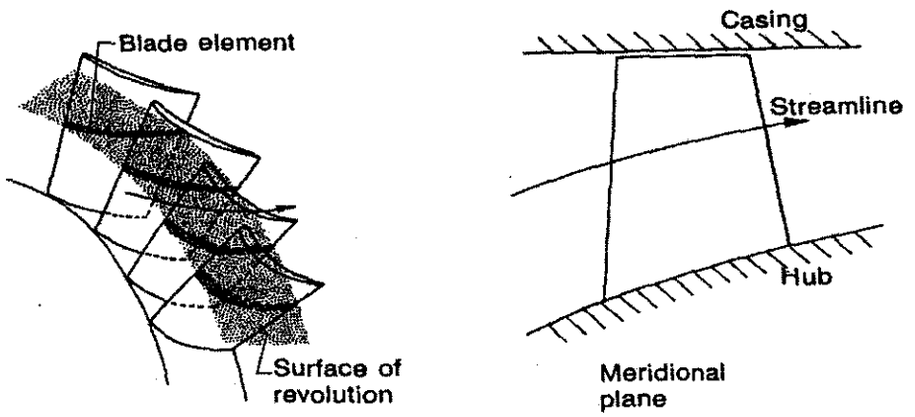

Fig. 4.1 Conventional description of flow on surface of revolution and on meridional plane

For this study, the relative influence and magnitude of the losses and their parameters on axial compressor performance need to be analyzed. The performance prediction is therefore not aimed at calculating the fine details of the flow pattern, but rather at generating a simple method of estimating the stage performance from knowledge of the compressor geometry. This, together

with the fact that the radial entropy or loss gradient is commonly assumed negligible; the throughflow calculation will be excluded altogether. Dixon (1998:138) states that this simplification can be justified if the blade height is small compared to the mean radius and suggests that radial velocities should be incorporated for hub to tip ratios less than 0.8. For simplicity it is also assumed that the mean streamlines intersect the blades with right angles.

Analysis at only one radial station at the root mean square radius (RMS) is performed. Values of quantities at these radii are taken to represent the whole stage annulus and such methods are commonly known as one-dimensional or mean-line analysis. The RMS radius divides the annulus into two equal annular areas and is the mass averaged mean radius for a uniform flow. This radius is also more or less independent of the axial velocity profile for stages with gradients of axial velocity with radius. It is defined as:

$$r_{rms} = \sqrt{\frac{r_t^2 + r_{hb}^2}{2}} \tag{4.1}$$

Usually, the stages are modelled individually. They are then stacked sequentially for modelling of the whole compressor with the outlet conditions of the one stage taken as the inlet conditions for the next stage. Song et al. (2001:89), however, suggests that the interstage parameters should be calculated simultaneously rather than sequentially when the compressor is linked with other components in a gas turbine environment.

4.3 Ideal stage analysis

The rotor and stator blades are arranged to diffuse the fluid. Diffusion can be described as a process whereby a moving fluid is decelerated, thus transforming kinetic energy into internal energy. This leads to a rise in static enthalpy and pressure. A point of minimum blade passage area occurs at or near the leading edge after which the passage increases downstream of this point.

The vector relation between velocity components in an axial compressor stage is represented by velocity triangles at a specific radial location as shown in Figure 4.2 taken from Japikse and Baines (1997:5-3). The relative velocities, measured with respect to the rotating system, are denoted by W and the absolute velocities, measured with respect to a fixed system by C. The absolute velocity tangential component is designated by C_θ and the blade speed by U.

The velocity triangles can be completed in all cases by using the vector relation:

$$W + U = C \tag{4.2}$$

The relative flow angles are denoted by β and the absolute flow angles by α and both are measured with respect to the axial direction (direction parallel to the rotating axis). The convention is that flow angles are positive with the direction of rotation. The subscripts *1* to *3* indicate the stations used for analysis, with Station 1 the inlet to the rotor, Station 2 the outlet of the rotor and inlet of the stator and Station 3 the outlet of the stator.

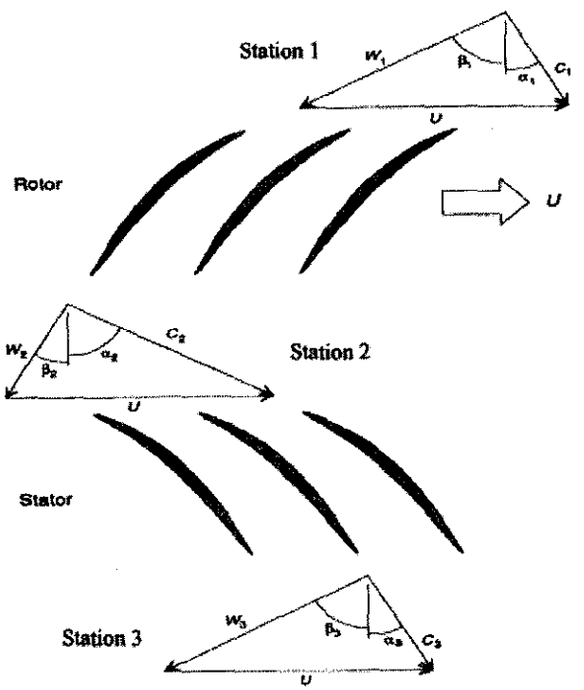

Fig. 4.2 Axial compressor stage velocity triangles

The fluid approaches the rotor with a high level of relative velocity and relative kinetic energy at station one. Thereafter, the fluid is diffused in the rotor passage and the external work input from the rotating blade row increases the total enthalpy. The combined effect of the aforementioned actions leads to a higher fluid static enthalpy and static pressure at station two.

In the stator, the diffusion takes place in the absolute frame of reference with a high absolute velocity approaching the stator. The absolute velocity is reduced and the kinetic energy is again transformed into internal energy, resulting in a higher static pressure at Station 3. The stator, however, is fixed and no external work transfer occurs. The total enthalpy therefore remains

constant over the stator. Japikse and Baines (1997:5-3) give a graphical representation showing changes in fluid properties and velocity through an axial compressor stage. The enthalpy – entropy or Mollier diagram of the compression process is also shown and the relative contribution of the rotor and stator can be seen. These figures are reproduced in Figure 4.3 and Figure 4.4.

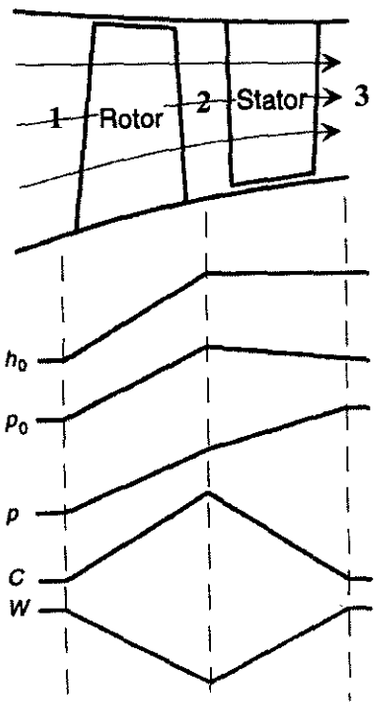

Fig. 4.3 Changes in fluid properties and velocities

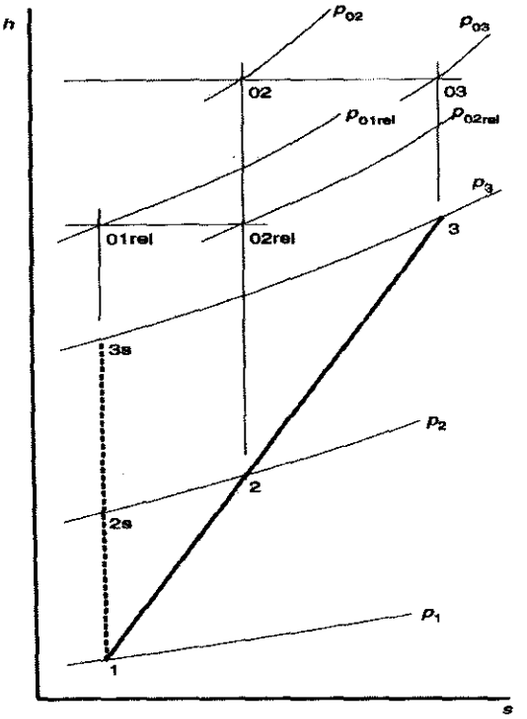

Fig. 4.4 Mollier diagram of compression

In the analysis of a compressor stage, both relative and absolute velocities are considered and therefore it is necessary to define a different absolute and relative stagnation state, but the static state will be the same. Thus, for enthalpy:

$$h_0 = h + \frac{1}{2}C^2 \tag{4.3}$$

$$h_{0r} = h + \frac{1}{2}W^2 \tag{4.4}$$

The subscript h_0 denotes the stagnation enthalpy in the absolute frame and h_{0r} the stagnation enthalpy in the relative frame. The same principle applies to stagnation temperatures in the absolute and relative frame. In an isentropic (no losses) compression process for a semi-perfect or ideal gas in the absolute and relative frame:

$$\frac{P_0}{P_{ref}} = \left(\frac{T_0}{T_{ref}} \right)^{\frac{\gamma}{\gamma-1}} \tag{4.5}$$

The Euler turbomachinery equation stems directly from the energy and momentum equations applied to a blade row. For adiabatic, steady flow through a rotor it follows that the work input per unit mass flow rate is given as the change in total enthalpy between any two points 1 and 2:

$$\Delta h_0 = U_2 C_{\theta 2} - U_1 C_{\theta 1} \tag{4.6}$$

When Equation 4.6 is applied along a streamline, thus a fluid element is only influenced by the blade-to-blade pressure gradient; an invariant thermodynamic property called rothalpy can be deduced as shown in Cumpsty (1989, 6). In rotating blade rows, rothalpy has properties analogues to stagnation enthalpy in stationary passages. Rothalpy is conserved along a streamline through a rotor and is defined by:

$$h_T = h_{01r} - \frac{1}{2}U_1^2 = h_{02r} - \frac{1}{2}U_2^2 \tag{4.7}$$

Equation 4.7 can be written for a perfect gas to give the relative total temperature increase by:

$$C_p \left(T_{02r} - T_{01r} \right) = \frac{U_2^2 - U_1^2}{2} \tag{4.8}$$

It therfore follows that if, no change in radius occurs, $T_{01r} = T_{02r}$ throughout the rotor. In the stator, the work input is zero and the total enthalpy is conserved, $h_{03} = h_{02}$, thus assuming a perfect gas, $T_{03} = T_{02}$. The conservation of rothalpy in a rotor and total enthalpy in a stator is true even in the presence of friction, loss and radius change.

For an inviscid and isentropic process, i.e. an ideal stage, the total pressure based on rothalpy or, if no change in radius occurs, the relative total pressure is constant in the rotor and the absolute total pressure is constant in the stator. The total pressure based on rothalpy might be defined as:

$$P_T = P\left(\frac{h_T}{C_p T}\right)^{\frac{\gamma}{\gamma-1}} \tag{4.9}$$

The aforementioned equations provide the basis for analysis of an ideal stage. In a real stage, the compression is not isentropic and usually an increase in entropy leads to a decrease in the respective total pressure. This is often used as a basis for assessing the loss of an axial compressor stage or element and is included through the use of non-dimensional loss coefficients. Other phenomena, for which estimates should be included in order to obtain a realistic mean line analysis, are blockage at the annulus walls, minimum loss incidence, deviation and estimates for the onset of stall and choke. With the magnitude of these quantities known, the ideal stage analysis can be adapted to represent a real stage and the efficiency and other performance parameters can be computed.

Values for these phenomena are, however, not amenable to confident mathematical models and normally come from correlations constructed from experimental data. This data usually comes from two-dimensional cascades, tested under controlled conditions.

4.4 Real stage parameters

This section discusses the estimation of the performance prediction parameters that are based on correlations obtained from test data and need to be included in order to obtain a realistic meanline analysis of a stage or are needed by some loss models. The parameters that need to be discussed here are: Loss coefficients, blockage at the annulus walls, minimum loss incidence, deviation and estimates for the onset of stall and choke.

4.4.1 Loss coefficients

Loss coefficients are introduced in Chapter 3 and are the dimensionless quantities used to express the loss obtained by some loss models. An in depth discussion and comparison of the different loss coefficients used for axial compressor blade rows are given by Brown (1972). The form of loss coefficient that is most common for compressors and diffusers is the pressure loss coefficient. It describes the drop in available total pressure, in the respective frame, in terms of

the inlet kinetic energy approaching the component. In adiabatic flow, a connection exists between entropy increase and stagnation pressure decrease.

For a rotor the compressible loss coefficient is defined in terms of the relative frame as:

$$\varpi = \frac{P_{T1} - P_{T2}}{P_{01r} - P_1} \frac{P_{01r}}{P_{T1}} \tag{4.10}$$

For a stator, in the absolute frame, the pressure loss coefficient is given by:

$$\varpi = \frac{P_{02} - P_{03}}{P_{02} - P_2} \tag{4.11}$$

4.4.2 Blockage

Frictional shear forces of the flow on the blades or annulus walls cause low momentum fluid to accumulate and form boundary layers. This leads to a reduction in effective flow area and an increase in axial velocity. The blockage is perhaps the most critical quantity in high-speed compressor design, but its creation is not well understood nor is its magnitude accurately predictable (Cumpsty, 1989:311). The endwall blockage in axial compressors has been the subject of several investigations over a period of many years. Horlock (2000:218-224) gives a detailed comparison of the available methods and the attributes of each. The work of Smith and Khalid et al. are discussed in detail in this paper and it is concluded that Smith's method would be the most appropriate for determining the absolute stage blockage through a multi-stage compressor.

For the purpose of this study the effect and magnitude of the endwall blockage will be included through the use of an annulus blockage factor (ABF). This factor, which is a function of the endwall boundary layer displacement thickness, is calculated as:

$$ABF = 1 - \frac{2\bar{\delta}}{\bar{h}} \tag{4.12}$$

The value of the ABF is restricted to 0.83 if the value deduced from the model is greater.

Values for the endwall boundary layer thickness are calculated in the Koch and Smith endwall loss model, or when other endwall loss models are used, assumed a constant value provided by the user. Estimates for this parameter can be obtained while using the Koch and Smith endwall loss model. Taking into account the uncertainty involved in predicting the blockage and its dependence on tip clearance and stage pressure rise, this method provides the best possible solution without including additional correlations and is, in any case, based on the same data used by Smith.

Endwall blockage leads to a reduction in the effective annulus flow area, which in turn leads to an increase in the free stream axial velocity due to the conservation of mass, where $m = (\rho AV)_{old} = (\rho AV)_{new}$. The effective flow area is related to the geometrical flow area according to:

$$A_{effective} = A_{geometrical} ABF \tag{4.13}$$

The ABF grows gradually through the compressor in a multi-stage environment. As stated before, however, the ABF is limited to 0.83 so that the boundary layer increases in the first few stages and then assumes a constant value in later stages where the limit is exceeded. The boundary layer growth is simulated by inputting the exit boundary layer from a previous stage or inlet guide vanes as an inlet boundary layer to the next stage or some form of inlet ABF reduction throughout the stages.

4.4.3 Minimum loss incidence

Lieblein introduced the concept of minimum loss incidence in 1956. It is the incidence at which a cascade will experience an absolute minimum loss. Many authors assume this value to be zero, but as was seen in Chapter 3, it serves as the reference value for predicting the off-minimum loss coefficients, and needs to be calculated for more accurate results.

The correlation assumes an equation of the form

$$i_{\min} = i_0 + n\theta_{camber} \tag{4.14}$$

where i_0 is the minimum incidence angle for a blade with zero camber and n is the slope of the variation in incidence with camber (Lieblein, 1960:578).

The value of n can be found from Figure B.1.1 from Appendix B.1. i_0 can, in turn, be calculated from:

$$i_0 = K_{sh} K_t (i_0)_{10} \tag{4.15}$$

In Equation 4.15, $(i_0)_{10}$ is the minimum loss incidence for a NACA-65 cascade of zero camber and 10 percent thickness to chord ratio. Values for $(i_0)_{10}$ can be found from Figure B.1.2 for a range of inlet air angles. Further, K_{sh} and K_t are correction factors for different shape distributions and thickness to chord ratios as for the $(i_0)_{10}$ correlation respectively. K_t can be obtained from Figure B.1.3 and K_{sh} is assumed 1.1 for C-series blades and 0.7 for DCA blades, with NACA-65 having a value of one (Japikse and Baines, 1997:5-18).

Finally a correction of –1 degree should be applied to the predicted *minimum* loss incidence according to Casey (1987:275). This correction allows for operation at constant stagger angle whereas the measurements of Lieblein were carried out at a constant air angle.

4.4.4 Deviation

Deviation can be described as the difference in the outlet flow angle and the blade angle at the trailing edge of the blade. Predictions of this value are based on empirical correlations as described in the following sections.

The correlation that is still used most often, but with modifications and adaptations by various authors is known as Carter's rule. Another common, but more complete and accurate, correlation is the one provided by Lieblein (1960) and is calculated somewhat similar to his correlation for the *minimum*-loss incidence. This correlation is used rather than Carter's rule due to its direct connection with the definition for minimum-loss incidence.

The deviation at minimum loss incidence is given by

$$\delta_{\min} = \delta_0 + \left(\frac{m}{\sigma^b}\right)\theta_{camber} \tag{4.16}$$

with m the slope factor of the deviation angle variation with camber at a solidity of unity. Values for m can be obtained from Figure B.2.1. b is the solidity exponent variable with air

inlet angle and can be found from Figure B.2.2. δ_0 is the reference minimum-loss deviation angle at zero camber and can be represented as:

$$\delta_0 = K_{sh} K_t (\delta_0)_{10} \tag{4.17}$$

Similar to the minimum loss incidence, $(\delta_0)_{10}$ is the basic variation for the NACA-65 blade profile with a ten percent thickness distribution. Figure B.2.3 gives values for $(\delta_0)_{10}$. K_{sh} is a correction for blade shapes with other thickness distributions than the blades used to obtain the $(\delta_0)_{10}$ correlation and K_t is the correction necessary for blades with a maximum thickness other than 10 percent (Lieblein, 1960:580). Values for K_{sh} are assumed the same as for the minimum-loss incidence and K_t can be obtained from Figure B.2.4.

For off-minimum loss deviation, a correlation that is a function of minimum-loss deviation and incidence is used:

$$\delta = \delta_{\min} + (i - i_{\min}) \left(\frac{d\delta}{di} \right)_{\min} \tag{4.18}$$

In Equation 4.18, $\left(\frac{d\delta}{di} \right)_{\min}$ represents the slope of the deviation angle variation at the minimum-loss incidence angle and can be found from Figure B.2.5.

Lieblein's correlation only gives a correct estimate for axial velocity density ratios of one, however, there is no satisfactory correlation available for predicting the deviation for other axial velocity density ratios. Usually, an addition of one or two degrees to the result is employed to account for this (Cumpsty, 1989:171). This addition will, however, not be implemented in this study due to further lack of support for this statement.

4.4.5 Stall and choke

The stalling incidence of a blade row is usually determined from cascade data, while the choking incidence is a function of the cascade throat area and the inlet Mach number. From Chapter 3, if using loss as a measure, a factor of two times the minimum profile loss for stalling and three times the minimum profile loss for choking (see Figure 3.5) is a common measure for preliminary estimates of the corresponding incidences (Miller, 1987:249-250). Alternatively, some authors

use an off-minimum loss correlation that employs an operating range parameter. The operating range is defined as the range of inlet flow angle within which the loss coefficient is less than twice the minimum loss value and can be calculated from the following correlation

$$\delta\beta = \delta\beta_i K_M \tag{4.19}$$

where $\delta\beta_i$ is the operating range of the NACA-65 series cascades at low Mach number and K_M is a correction for the effect of Mach number. Analysis of NACA data by Hugentobler in 1986 has led to the following correlation for the operating range at low Mach number for $30° \le \beta_{in} \le 70°$:

$$\delta\beta_i = 21 + \frac{0.001(1+\sqrt{\sigma})\left(-40 - 7(\beta_{in} - 45) + 0.25(\beta_{in} - 45)^2 - 0.02(\beta_{in} - 45)^3\right)}{\sigma\theta_{camber}} \tag{4.20}$$

The correction for Mach number is taken into account as proposed by Hoheisel in 1969 (Casey, 1987:275):

$$K_M = 1 \qquad for\ \ Mach\ number < 0.2$$
$$K_M = 10^{-2.5(M-0.2)^{4.4}} \qquad for\ \ Mach\ number > 0.2 \tag{4.21}$$

Casey (1987:277) assumes that stall and choke will occur in terms of incidence at the root mean square radius when:

$$|i - i_{\min}| = 0.8\left(\frac{\delta\beta}{2}\right) \tag{4.22}$$

The aforementioned criterion provides crude estimates for predicting when a blade row will stall or choke. These estimates, however, provide no information on when the stage as a whole stalls or chokes or the maximum static pressure rise that can be obtained in a stage at the stall point. This value needs to be calculated in order to correctly predict the endwall losses as given by Koch and Smith. Casey (1987:277) assumed very roughly the stage to be choked when no pressure rise is being produced.

De Haller recognized in 1955 that the endwall boundary layers limit the pressure rise achievable by any cascade of compressor blades. His work, however, provides only a very preliminary

guideline and cannot really be used with confidence in this study. Koch (1981) found the maximum static pressure rise coefficient to correlate well with a standard two-dimensional diffuser performance when plotted against a passage width to length ratio and this seems to provide a better estimate for predicting the stall point of a stage. According to Koch (1981:646), "It does, however, give the peak pressure rise capability of an individual stage operating in a multi-stage environment, and used in conjunction with a stage stacking off-design performance prediction method, it can indicate when the limiting conditions that de-stabilize the system and lead to surge will occur within a multi-stage compressor."

The geometry parameter used by Koch is the meanline arc length of the cambered airfoil, divided by the cascade trailing edge staggered spacing, $\frac{L}{g}$. The stage average value of the length to width ratio is calculated by using the blade row inlet dynamic head of rotor and stator as the weighting factor. The static pressure rise coefficient is based on the mean effective dynamic head at inlet to the rotor and stator. The effective inlet kinetic energy takes into account the ability of compressor blades with high stagger angles to re-energize low momentum boundary layer fluid leaving an upstream blade row as this fluid impinges on the following blade row in the other frame of reference (Casey, 1987:277).

Casey (1987:277) modified the correlation by Koch to provide an even better fit to the diffuser data and this is given in Figure B.3.1, also showing the De Haller diffusion limit and the fit used by Koch. The maximum value of the effective static pressure rise coefficient is calculated as

$$C_{P_{max}} = C_{P_D} K_{\mathrm{Re}} K_{\tau} K_{AS} \tag{4.23}$$

where C_{P_D} is the maximum static pressure rise coefficient from the diffuser data, K_{Re} is a Reynolds number correction factor form Figure B.3.2, K_{τ} a correction for tip clearance effects given by Figure B.3.3 and K_{AS} a correction for axial spacing between the blade rows from Figure B.3.4.

For a stage, Casey assumes the stage to choke when the stage produces no pressure rise and for simplicity this is also accepted in this study.

4.5 Loss and efficiency

The definition of entropy allows for the easy summation of entropy gains or losses. For a perfect gas,

$$\Delta s = C_p \ln\left(\frac{T}{T_{ref}}\right) - R\ln\left(\frac{P}{P_{ref}}\right), \tag{4.24}$$

where the temperatures and pressures can either have total or static values, as long as it is consistent, and the equation can be used for rotors (relative frame) and stators (absolute frame).

Therefore, in a component, the total entropy increase is equal to the sum of all the entropy increases due to the various losses. For a stage:

$$\Delta s_{stage} = \Delta s_{rotor} + \Delta s_{stator} \tag{4.25}$$

The entropy increase due to all the losses through an axial compressor can then similarly be found from:

$$\Delta s_{compressor} = \sum_{1}^{i} \Delta s_{stage}\ ,\ i = Number\ of\ stages \tag{4.26}$$

The loss of efficiency of a stage or compressor is directly proportional to the increase in specific entropy and also to its exit temperature (Denton, 1993:624). Efficiency is the ratio of work into the ideal compressor or stage to actual work at a given pressure ratio and mass flow rate. In an ideal compressor or stage, which is adiabatic and reversible, no entropy change due to losses occurs and the process is therefore considered isentropic. The corresponding definition of efficiency is isentropic efficiency, with the work input equal to the rise in stagnation enthalpy:

$$\eta_i = \frac{h_{0s_{out}} - h_{0_{in}}}{h_{0_{out}} - h_{0_{in}}} \tag{4.27}$$

This definition is also known as the total-to-total isentropic efficiency. Other variations include static-to-static or total-to-static and represents respective values of enthalpy used.

On a Mollier diagram (Figure 4.4), the local slope of the pressure lines are given by the local value of the respective temperature. If the assumption is made that these pressure lines have a constant slope, the efficiency definition can be given in terms of the entropy increase:

$$\eta_i = 1 - \frac{T_{0_{out}} \sum \Delta s}{\Delta h_0} \tag{4.28}$$

4.6 Summary and conclusions

This chapter presents the performance prediction theory for a meanline analysis at the RMS radius. The rotor and stator blades are arranged to diffuse the fluid by decelerating it, thus transforming kinetic energy into internal energy. This leads to a rise in static enthalpy and pressure. Through an ideal rotor, rothalpy and total pressure based on rothalpy are conserved and through an ideal stator, total enthalpy and total pressure are conserved. Furthermore, the losses manifest itself as entropy increases in the fluid and equivalently reduce the respective outlet total pressure. Losses are usually expressed with the use of dimensionless loss coefficients, with the pressure loss coefficient the most commonly used as can be seen in Chapter 3.

Together with estimates for the losses, estimates for annulus blockage, minimum loss incidence, deviation and the onset of stall and choke also need to be obtained in order to include real fluid effects found in compressors. These quantities are found from correlations obtained from cascade or compressor data. In this study, the correlations from Lieblein are used for the minimum loss and deviation predictions and the correlation provided by Koch will be used for obtaining estimates for the stalling stage pressure rise. For the annulus blockage factor, values will be obtained from the endwall loss model from Koch and Smith and detail regarding the implementation thereof is given in Chapter 5.

It was seen that values for entropy increases due to the different losses can be obtained for each blade row. The sum of all the entropy gains can then be used to estimate the efficiency of single-stage or multi-stage compressors as well as individual stages of multi-stage compressors.

In this stage of the study, enough information is available to generate a preliminary multi-stage performance prediction code. Chapter 5 consequently presents the reader with the methodology employed for implementing the theory and correlations obtained from the literature and given in Chapters 3 and 4.

Chapter 5

IMPLEMENTATION

Chapter 5 presents the methodology employed in this study for the generation of a performance prediction code, with general applicability to subsonic multi-stage compressors with different geometries and working fluids, which allows the interchanging of loss models. It utilizes the theory and models described in Chapters 3 and 4.

5.1 Introduction

Chapters 3 and 4 presented the reader with the available literature regarding loss models and the basic theory for performance prediction. Some models were identified as the most suitable to use in this study and these were described in more detail.

This chapter will focus on the methodology employed to generate a performance prediction code from these chapters, with general applicability to subsonic multi-stage compressors with different geometries and working fluids, which allows the interchanging of loss models. It is further necessary for this code to have the capability to be used for parametric studies, reflecting the influence of input variable changes on particularly the loss magnitudes and this relation to other performance variables.

5.2 Methodology

From the previous chapters, it was seen that an implicit approach is necessary and it was decided to use a software package called Engineering Equation Solver (EES) Academic Version 6.867-3D (F-Chart Software, 2003). The basic function provided by EES is the solution of a set of algebraic equations, but it has the advantage of automatically identifying and grouping equations that must be solved simultaneously.

The EES code can consist of several 'sub-sections' or 'sub-equation groups' employing modules, procedures and functions. Some of the advantages of using a modular approach are that it makes it easy to switch between different loss models and also aids in applying the same equations in both the relative and absolute frames by just calling them with the respective variable inputs. Future users can easily modify or replace certain 'parts' of the code almost independently, as long as the inputs and outputs of the calling argument are satisfied. Modules can be considered to be stand-alone EES programs that can be called from the main EES program or from other modules lower in the equation window. When EES calls a module, it adds the equations in the module into the main equation set, as opposed to conventional procedures and functions, which are solved separate and sequentially, but supports logical control statements like IF-ELSE.

A recommended algorithm to generate the code is presented in Appendix C.1 and was developed in such a way that easy implementation in lower-level programming languages would be possible in future studies. Unfortunately, it was found that EES becomes unstable when trying to solve too large equation sets, especially when employing modules due to the increase in sensitivity to the guess values used. Consequently, for this study, each stage of a multi-stage compressor was

solved in a separate EES program and the required variables from the one stage exported to an ASCII (American standard code for information interchange) file. The next stage then imports the required boundary condition values from the file generated by the previous stage and so on. The entropy and total enthalpy change from each stage is also saved to an ASCII file for each stage and used in the compressor performance calculations. This method is commonly known as 'stage stacking', however, it is recommended, that when a more stable solver has been employed, the compressor as a whole should be solved simultaneously according to Appendix C.1. Some of the advantages of using such an approach are that easier parametrical studies on the whole compressor can be performed and boundary variables can be chosen as required.

Table 5.1 gives the loss models that have been implemented in the code for evaluation in the order in which they were implemented according to their complexity. The next step was to identify the variables that need to be supplied by the user for including the models given in Table 5.1. These variables, and how they are supplied to EES, through the use of lookup tables, are given in Appendix C.2.

Table 5.1: Loss models implemented for evaluation

Profile losses			
Lieblein		Koch and Smith	
Off-minimum loss			
Casey		Lieblein	
Endwall losses			
Howell	Hübner and Fottner	Roy and Kumar	Koch and Smith
Part span shroud loss			
Koch and Smith			
Other losses: Windage loss			
Denton			

Each loss model was implemented in its own sub-section and is then called from the sub-sections containing the equations for the performance prediction variables for the rotor and stator as necessary, providing the input variables from the respective frame.

A logical discussion of the code and practical information covering the generation thereof are given in the following sections. The sub-sections containing the equations for the loss models are discussed first, followed by a discussion of the code as a whole showing where and how the models are called and giving the equations for the performance prediction and the input variables

to the loss models. The complete EES source code is given in Appendix C.6, with the formatted equation sets for the loss models and performance prediction given in Appendix C.3 and Appendix C.4 respectively. The code is essentially generated for the NACA-65 blade profile family, but can be easily adapted to include the other profile families commonly used in subsonic axial compressors.

5.3 The loss models

In this section, a discussion on the implementation of the loss models is presented. The formatted equation sets from the code for the loss models are given in Appendix C.3. The equation numbers from Chapter 3 is also shown and the input variables and outputs from each model can clearly be seen from the sub-section declaration, with the output variables shown to the right of the colon.

5.3.1 Profile loss model implementation

Section C.3.1 shows the formatted equations for the Lieblein profile loss model. The correlations of Casey for the momentum thickness to chord ratio have been implemented for evaluation. Two equations for calculating the pressure loss coefficient have been included, with the one assuming the form factor to be one and excluded the terms containing it. The one not used is commented out when running the code. To satisfy the requirements of the calling argument to this module, it is necessary for this sub-section to return a value for blade blockage and a constant value of zero has been used as this model was not indented to be used with a blockage value.

Section C.3.2 shows the formatted equations for the Koch and Smith profile loss model. Corrections for conditions other than nominal are made to the momentum thickness to chord ratio as well as the boundary layer form factor. Unfortunately, the correction factors are given in the literature in a graphical format as given in Appendix A.2 and curve fits had to be performed in order to obtain equations that could be implemented in the code.

The curve fit equations for the correction factors are contained in separate sub-sections that return the values for the correction factors to the profile loss sub-section. Linear interpolation was necessary in some cases and a sub-section to facilitate this function was also generated. Koch and Smith limit the applicability of their model to equivalent diffusion ratios below 1.7 and a warning mechanism was included in one of the correction factor sub-sections to warn the user when this is not the case. These correction factor sub-sections and the sub-section to do linear interpolation between the desired values are given after the profile loss sub-section in Section C.3.2.

5.3.2 Off-minimum loss model implementation

The formatted equations for the sub-section containing the equations for the off-minimum loss model of Casey are shown in Section C.3.3 and those of Lieblein in Section C.3.4. A value of 0.0117 was used for the constant in Equation 3.48.

5.3.3 Endwall loss model implementation

The formatted equations for the implementation of the Howell, Hübner and Fottner and Roy and Kumar endwall loss models are given in Section C.3.5, C.3.6 and C.3.7 respectively. The sub-section for the Roy and Kumar model also employs a function for calculating the leakage jet velocity. This function is showed below the sub-section containing the Roy and Kumar endwall loss equations in Section C.3.7.

The Koch and Smith endwall loss model, presented in Section 3.3.2, gives predictions for the endwall loss of a complete stage. However, in order to enable the evaluation of the endwall loss in single bladerows and to see the contribution of each bladerow to the total endwall loss, the model needs to be converted to be applicable to single bladerows. It also makes the comparison between the different loss models simpler, because the other models are component-based. Unfortunately, the Koch and Smith endwall loss model requires predictions of parameters like the stalling static pressure rise coefficient from the correlation by Koch and the stage static pressure rise coefficient. The implicit nature of the code can now be clearly seen from the fact that these values are calculated for the whole stage while being input values to the rotor and stator modules. It is further necessary for the stage freestream efficiency to be inputted to the Koch and Smith endwall loss model sub-section. Consequently, the Koch and Smith endwall loss sub-section is called from the stage sub-section, with the inputs for the stage stalling static rise coefficient, stage static pressure rise coefficient and the stage freestream total-to-total efficiency as input parameters. In turn, the entropy generation due to the endwall loss from each bladerow and the endwall boundary layer displacement thickness are returned and given as input parameters when calling the rotor and stator sub-sections. The methodology for adapting the Koch and Smith model to be used in such a manner are explained below.

From Appendix A.4 it was seen that the endwall parameters for a stage was correlated against the static pressure rise coefficient divided by the maximum static pressure rise coefficient of the stage, $\left(\frac{\Delta P_{rotor}+\Delta P_{stator}}{q_{1_{rotor}}+q_{1_{stator}}}\right)\Big/\left(\frac{\Delta P_{rotor}+\Delta P_{stator}}{q_{1_{rotor}}+q_{1_{stator}}}\right)_{max}$. The correlations were again only available in graphical format (Appendix A.4), but curve fittings were done and these equations and how they are used are presented in the formatted equations shown in Section C.3.8. A warning procedure,

halting the calculations if the stage static pressure rise coefficient is bigger than the stage stalling static pressure rise coefficient and thus warning the user that the stage is stalled, is also included.

For the stalling static pressure rise correlation of Koch, the static pressure rise coefficient is based on the mean effective dynamic head at inlet to the rotor and stator. The effective inlet kinetic energy takes into account the ability of compressor blades with high stagger angles to re-energize low momentum boundary layer fluid leaving an upstream blade row as this fluid impinges on the following blade row in the other frame of reference.

An effective inlet dynamic head is therefore calculated for each bladerow according to equations given by Koch (1981:646). This parameter was used to obtain a 'row factor' by dividing it by the sum of the rotor and stator inlet dynamic heads and was also given as an input parameter to the loss model. The entropy generation due to the endwall loss of the whole stage is then multiplied by the row factor for the specific bladerow to obtain an entropy generation value for each bladerow which is then given as an input parameter to the rotor or stator calling arguments.

It was necessary to manipulate Equation 3.19 so that it gives an entropy change instead of a new efficiency value. Consequently, an expression for entropy change due to the endwall loss through the stage was therefore derived as

$$\Delta s = \frac{\left(1-\eta_{fs}\left(\frac{1-\left(2\bar{\delta}/g\right)(g/h)}{1-\left(2\bar{v}_t/2\bar{\delta}\right)\left(2\bar{\delta}/g\right)(g/h)}\right)\right)\Delta h_0}{T_{03}} - \Delta s_{fs} \tag{5.1}$$

where g and h are the weighted stage staggered spacing and blade height respectively and Δs_{fs} is the stage freestream entropy change value. Further detail about the usage of Equation 5.1 and the application of the row factor can be seen in Section C.3.8.

5.3.4 Part span shroud loss – Koch and Smith

Section C.3.9 shows the formatted equation set for the part span shroud loss sub-section.

5.3.5 Windage loss - Denton

The windage loss is given as a fraction of lost power to useful power in the literature. For the purpose of implementing it in the code, it has to return either a pressure loss coefficient or an entropy increase. The windage loss does attribute to an efficiency decrease. An entropy change must, therefore, be returned from this sub-section as shown in Section C.3.10. It is known that the work input to a stage per unit mass is equal to the change of total enthalpy through the stage. The windage loss sub-section is only applied to the rotor and if it is accepted that $\Delta s = \frac{\Delta h_0}{T_{02}}$, the entropy change due to windage loss can be written as:

$$\Delta s = \frac{\Delta W_{windage}}{T_{02}} \tag{5.2}$$

The loss models have now been presented in their specific sub-sections. However, these sub-sections do not function on their own and realistic input variables have to be supplied. This is done, by generating performance prediction sub-sections from which these loss models can be called. The following sections present the generation of the performance prediction code.

5.4 The performance prediction code

5.4.1 The compressor code

A multi-stage axial compressor consists of a number of stages. Ideally, as proposed in Appendix C.1, a single code should represent such a compressor and a sub-section that contains the necessary equations for each stage is called according to the number of stages. As stated previously, however, EES becomes unstable with too large equation sets and each stage has to be solved in a separate EES program. The outputs are then written to an ASCII file for use as inputs to the next stage and for the calculation of efficiency and other performance parameters for the stage as a whole. For this study, the compressor code is therefore defined as an EES program that reads the necessary variables from the ASCII files that were generated sequentially from stage one for each stage. The ASCII files imported as lookup tables are then used to calculate performance parameters like compressor total-to-total adiabatic efficiency, total-to-total pressure ratio and total-to-total temperature ratio. Section C.4.1 shows the formatted equations used in the compressor code.

5.4.2 Stage

Each stage consists of a rotor and a stator and the stage code calls the sub-codes for the rotor and the stator. Values for the stage stalling static pressure rise coefficient, the static pressure rise coefficient, the freestream efficiency and the row factor for each bladerow are also calculated here. These values are used as inputs when calling the Koch and Smith endwall loss model and values for the endwall loss entropy generation and the endwall boundary layer displacement thickness are supplied when calling the rotor and stator sub-codes. When using another endwall loss model in the rotor or stator sub-code, the entropy generation value from the Koch and Smith model is not used, but the boundary layer displacement thickness parameter is still used for calculating the endwall blockage. Section C.4.2 shows the formatted equations for a stage. In this case, the total-to-total adiabatic efficiency is a function of the sum of the entropy increases and the sum of the stagnation enthalpy increases of the rotor and the stator.

5.4.3 Rotor and Stator sub-sections

The Rotor and Stator sub-sections contain equations for calculating the required rotor and stator variables respectively. Equation sets that are applicable to both the rotor and stator, contained in different sub-sections, are called when needed. These include the equations for minimum loss incidence, deviation, stalling static pressure rise coefficient, operating range, a test to determine whether the cascade is stalled, and the different losses. In the case of the losses, there can be switch between the different models simply by calling the appropriate sub-section and commenting the other calling arguments or assignments in the code.

The author found it very difficult to give the code a sequential structure for increased readability, due to the implicit nature of the code and the fact that several sub-sections are called. Some effort has been made. However, it must again be emphasized that the equations are not solved sequentially in the sub-sections and that the equation order or form has no real importance in EES and solves as long as the number of equations and variables are equal. Section C.4.3 shows the equations and variables used in the Rotor sub-section and Section C.4.4 for the stator. Extensive commentary has been included and a detailed discussion is therefore not given here. The following points should however be noted.

The fluid property calculations were done using built-in EES functions that return the required value with static pressure and temperature given as arguments. C_p and C_v were assumed constant throughout the bladerows, but different values for ρ, μ and a was calculated at the inlet and outlet of each bladerow.

The *ABF* is calculated in a sub-section as a function of the annulus boundary layer displacement thickness parameter, which is calculated by the Koch and Smith endwall loss model in the stage code, and the inlet *ABF* passed from a previous stage or supplied by the user.

For the profile loss calculations, blade blockage has to be taken into account. This was done using a blade blockage factor (*BBF*). The *BBF* increases the outlet freestream velocity, used in the profile loss calculations, due to a reduction in effective area in the blade passages caused by the presence of blade boundary layers. The *BBF* is calculated as a function of the blade boundary layer displacement thickness, given in the code as *block* and calculated by the Koch and Smith profile loss model. When using another loss model, this parameter is returned with a value of zero. At off-minimum loss conditions, the value of this parameter is necessarily assumed to be the same as at minimum loss conditions, because it is only calculated for the minimum profile loss.

The windage loss model can be called if applicable. In this model, the windage loss also leads to a pressure loss and reduces the efficiency through an increase in entropy. It is only applied to the rotor disk.

In order to facilitate the interchanging of the various loss models, a method was devised where the applicable loss model sub-code could return either a pressure loss coefficient or an entropy increase value. The returned value was then also converted into the other parameter, resulting in quantities of pressure loss coefficient and entropy increase for each loss used in the calculation. This was done using a relation derived in Appendix C.6 for the rotor:

$$\Delta s = -R \ln \left(\frac{P_{T_1} - \left(\frac{\varpi q_1 P_{T1}}{P_{01r}} \right)}{P_{T1}} \right) \tag{5.3}$$

A similar relation is used in the stator calculations, but the thermodynamics of the stator applies. The outlet conditions of the rotor are taken to be the inlet conditions of the stator and the required variables are passed accordingly.

5.4.4 Annulus blockage (*ABF*)

It is calculated from an annulus boundary layer parameter returned from the Koch and Smith endwall loss model, the average blade height and the inlet *ABF* value. Section C.4.5 shows this sub-section and includes the limit set by Koch and Smith of $1 \leq ABF \leq 0.83$.

5.4.5 Minimum-loss incidence (Min_{inc})

Section C.4.6 shows the formatted equations for the prediction of the minimum loss incidence. The lines for the different solidities in Figure B.1.2 are distributed evenly enough so that curve fits were only performed for a σ of 0.4 and 2 and linear interpolation was performed for values inbetween. The same applied to the estimation of the slope factor and a single polynomial fit could be found for the deviation in maximum thickness correction factor.

5.4.6 Deviation (*Deviation*)

Section C.4.7 shows the sub-section containing the equations for predicting the deviation at minimum loss and off-minimum loss conditions. Figure B.2.3 was implemented by obtaining polynomial curve fits for the lines σ = 0.4, 1.2 and 2 and performing linear interpolation for the values inbetween. Curve fits were also obtained for Figures B.2.1, B.2.2 and B.2.4 and implemented for finding these values. In Figure B.2.5, the graph is evenly distributed for the lines β_1 = 0, 30, 40 and 50. Polynomial curve fits were obtained for β_1 = 0, 50, 60 and 70 and linear interpolation was used to find the values inbetween.

5.4.7 Stall and choke

A prediction of the operating range, thus the range of inlet flow angle for stable operation, was implemented in a sub-section called Opp_{Range}. Section C.4.8.1 shows the formatted equations for this sub-section. Casey assumes that stall and choke will occur in terms of incidence at the root mean square radius when:

$$\left|i - i_{\min}\right| = 0.8\left(\frac{\delta\beta}{2}\right) \tag{5.4}$$

This criterion, based on the operating range calculated in the sub-section Opp_{Range}, is used as one of the measures to ensure that the rotor or stator is not operating in the stalled range. A sub-section was generated, testing if the cascade is operating in these limits and if not, returns a warning message to the user. This sub-section is shown in Section C.4.8.2. When the endwall loss model by Koch and Smith is used, a further test is conducted and a warning is given when

the static pressure rise increases beyond the predicted stalling static pressure rise coefficient as seen in Section 5.4.3.

The prediction of the maximum static pressure rise coefficient, thus the value at stall according to Koch and modified by Casey were implemented in the sub-section called $Stall_{PRC}$. Curve fits were again performed on the correlation figures as given in Appendix B.3 for implementation purposes. The curve fit for the Reynolds number correction factor was facilitated with the aid of three straight lines as can be seen from the formatted equations for this sub-section given in Section C.4.8.3.

As stated in Chapter 4, this study makes the same assumption as Casey for choking and this is assumed to happen when the stage produces no pressure rise. No additional correlations were therefore implemented for predicting choke.

5.5 Summary and Conclusions

This chapter presented the methodology and generation of a performance prediction code, with general applicability to subsonic multi-stage compressors with different geometries and working fluids, which allows the interchanging of loss models. A software package called EES was used for implementation. A modular approach was followed and different sub-sections were used to structure the code, implement logical operations in EES and limit programming time by calling common sub-sections from the relative and absolute frame respectively.

The correlations were mainly given in the literature in a graphical format and were implemented by obtaining curve fits containing the specific variables. The loss models were implemented as given in the literature, with the exception of the Koch and Smith endwall loss model that was transformed from a stage based approach to a component-based model. The performance prediction was implemented using a separate EES program for each stage that calls sub-sections for the rotor and stator, which in turns uses the loss models from the respective frame. The stage programs are run sequentially from the first stage to the last through exporting outputs from each stage to an ASCII file so that the following stage can import applicable input variables from the previous stage. An EES program was then generated that utilizes the output ASCII files to calculate the multi-stage compressor performance variables. A method was devised where loss models could return either an entropy increase value or a pressure loss coefficient.

Blockage was implemented with the aid of blockage factors. An annulus blockage factor (ABF) is used to reduce the geometrical annulus area to an effective annulus area due to the presence of

an endwall boundary layer. This factor is a function of the endwall boundary displacement thickness calculated by the endwall loss model of Koch and Smith and an inlet annulus boundary layer parameter which can be supplied by the user or obtained from the output blockage value of the previous stage. For the blade blockage due to the blade boundary layers, a blade boundary layer factor (BBF) is used that increases the velocity used for the profile loss models. This factor is a function of the blade boundary layer displacement thickness, which value is zero for the Lieblein profile loss model and calculated by the Koch and Smith profile loss model.

For the prediction of stall, this code uses the endwall loss model from Koch and Smith to test if the static pressure rise is larger than the stalling static pressure rise coefficient as predicted by Koch. Another test, that was implemented, is the correlation and stall criterion given by Casey. Choke was assumed to occur when the stage has no pressure rise.

The generated code must be verified and the methodology validated before it can be used for obtaining interesting conclusions. Chapter 6 verifies the code against a commercial software package called NREC and evaluates the different loss models according to their simplicity and accuracy.

Chapter 6

VERIFICATION AND EVALUATION

Chapter 6 verifies the code, developed in Chapter 5, against a commercial software package called NREC and evaluates the different loss models according to their simplicity and accuracy. A loss model combination is chosen according to the results and the performance prediction from this code is then compared to predictions from NREC. This is first done for a stage and then for a multi-stage compressor.

6.1 Introduction

Chapter 5 presented the reader with the methodology to generate an axial compressor performance prediction code from Chapters 3 and 4, which presented the available literature regarding the loss models and the basic theory for performance prediction respectively. This code aims at having general applicability to subsonic multi-stage compressors with different geometries and working fluids which allows the interchanging of different loss models. It is also envisioned that the code will have the capability to be used for parametric studies, reflecting the influence of input variable changes on particularly the loss magnitudes and this relation to compressor performance.

In this chapter, the accuracy and validity of the code will be verified against a commercial performance prediction package called NREC (Concepts NREC ETI Inc, 2003). The version used in this study is Version 7.5.3 and the module is called Axial. The loss models will be interchanged and evaluated according to their deviation from the norm set by NREC and conclusions are made about the sensitivity of compressor performance prediction to certain aspects of modelling and the different loss models.

6.2 Methodology

A four stage compressor test case was implemented in NREC and EES. It uses helium as working fluid and employs the NACA-65 blade profile for all the blades. Appendix D.1 gives the values of the parameters needed for implementation in EES. Detail verification will be done for a single stage and, because of the time incurred for solving multi-stage compressor cases and the stability problems posed by EES when such a large amount of variables are calculated, a four stage compressor will be used for verification of multi-stage prediction.

It would, of course, be ideal to test a much broader spectrum of cases, with experimental data, especially when evaluating the applicability of the different loss models. It is advised that this be done in further work when more compressor design specifications are available and a more stable solver has been employed. It is, however, thought to be adequate, for the purpose of this study, to verify the methodology used and gain confidence in the code to perform parametrical studies of the loss parameter changes on performance and especially the loss magnitudes.

NREC offers three basic model selection options for fans, compressors and pumps. For each of these basic options, the user can choose to stick to standard models which NREC recommends for this basic choice or different models can be selected according to the user's preference. For this study, the Koch and Smith basic option was selected.

Figure 6.1 illustrates how user inputs can be done in NREC and specifically shows the model selection used for each blade row, in this case the first stage rotor, used for the verification. A description of the standard model used in each case is also included.

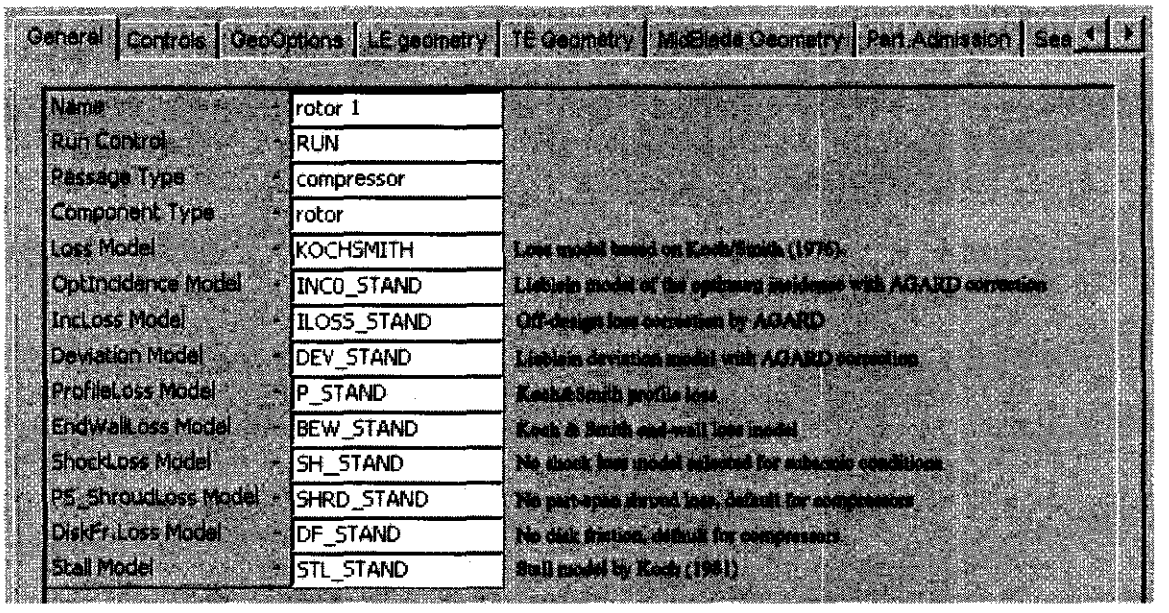

Fig. 6.1 Illustrates inputs and model selection for a bladerow in NREC

It can be seen from Figure 6.1 that models for part span shroud loss and windage loss (Disk friction loss) are by default not included in the NREC simulation for compressors. However, even when specifically selecting models for these values, NREC seems to ignore them and the values are always given as zero. This might be an error in NREC and accordingly, no results were available to verify these models included in EES. It will thus not be verified in this study and assumed that the EES models are correct, until further work can verify these models. This assumption can be supported by the fact that these loss models are usually excluded from compressor performance prediction due to their small values. A constant profile from hub to tip was initially used for the blades in NREC which only requires input values for the RMS location.

In some cases, variables have to be supplied that are not needed for the EES model. In these cases, values representing standard design practices were used according to the assumptions made while constructing the EES model. A forced variable blade profile (twisted blades) was then used to construct a variable blade profile test compressor in NREC, representing a more realistic compressor. NREC uses fixed design rules to obtain reasonable values at the hub and tip for each blade. Figure 6.2 shows the variable blade compressor as represented by NREC.

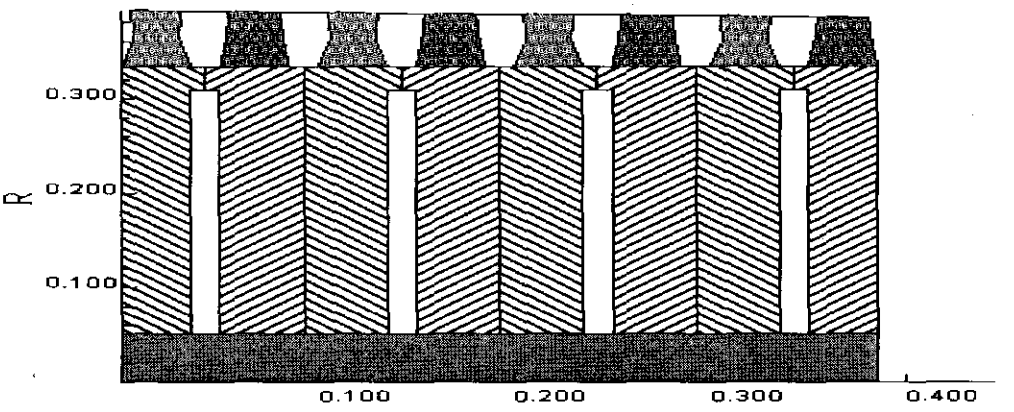

Fig 6.2 Graphical representation of test compressor as given by NREC

The constant profile blade compressor and the variable profile blade compressor were compared against each other, using the same performance and loss models to illustrate the validity of performing an analysis and parameter study at the RMS location as done in this study. The results for the total-to-total adiabatic efficiency at minimum and off-minimum loss cases in the stable operating range are shown in Figure 6.3 for a rotational speed of 9000 rpm.

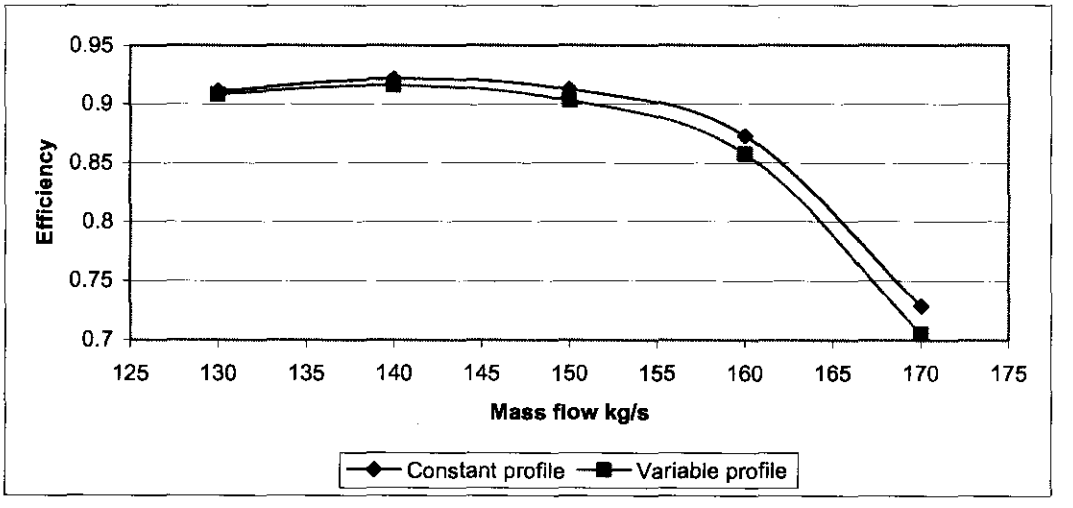

Fig 6.3 Comparison between constant blade profile and variable blade profile efficiency prediction

It can be seen that the comparison is satisfactory, with the variable profile case giving slightly lower efficiency values. The variable blade profile compressor will be used further in this chapter for verification purposes with EES. This is done to emphasize the ability of the EES model to predict multi-stage compressor performance of realistic compressor designs and that realistic trends will be obtained when doing the loss model parametrical study.

The next section presents a detailed verification of the first stage of the compressor as presented above. This verification will display the EES model's ability to predict the performance of a stage, without the influence of inlet blockage, which will be observed at other stages in a multi-stage compressor. A section showing the comparison of the multi-stage compressor data between the two codes then follows.

6.3 Single stage verification and loss model evaluation

The first stage of the test compressor was used for this purpose. The NREC model and EES code was adapted to calculate only the first stage parameters.

6.3.1 Verification of non-loss theory and correlations

In verifying the velocity triangles and non-loss (ideal stage) parameters, the losses and deviation were initially excluded from the simulations. Great discrepancies were observed when comparing the predictions of the fluid properties from NREC and EES. It was found that the values of the fluid properties, for example, specific heat capacity and density are especially critical in the performance prediction, but that EES calculates different values than the NREC code.

After inspection of the method in which NREC and EES calculates the fluid properties, it was found that NREC uses input files from which constants and coefficients for the equation of state are read. The NREC default file gave helium's specific heat capacity at constant pressure, C_p, a constant value of 7899.2 J/kg-K, while EES gives a value of 5190 J/kg-K at the pressure and temperature concerned. After careful consideration, it was decided to adapt the NREC input file to the values, ranges and reference quantities used by EES for successful comparison between the two packages.

EES uses the fundamental equation of state given by Rainer Tiller-Roth in Fundamental Equations of State published in 1998 and ancillary equations are provided by R.D. McCarty and V.D. Arp in "A New Wide Range Equation of State for Helium" published in 1990.

The range of applicability of the thermodynamic properties is from the triple point temperature 2.1768 K to 1500 K at pressures up to 100 MPa. It was further found that the density predicted by EES and NREC still differ by a constant value of 0.18 kg/m^3 at all the evaluation points through the stage and over the entire mass flow range considered. The percentage difference over the entire range, calculated by Equation 6.1, is less than 3%. There are numerous reasons why this might be, but it was deemed to be outside the scope of this study to continue the investigation

and it will be assigned for further work. Consequently, the calculation of density in EES was adapted by simply adding 0.18 kg/m^3 to the result.

Table 6.1 shows the comparison between the major non-loss parameters as well as the percentage error between the two models at the compressor design point. The term 'design point' is used, because this point is not precisely the minimum loss point for the stage as defined in this study and small off-minimum loss values will be present at this point. The values were rounded to the second decimal. Comparisons of these parameters at other mass flows are given in Appendix D.2.

It can be seen that the non-loss parameters compare very well at all the mass flows considered. It can thus be concluded that the non-loss theory and methodology used in the EES code are correctly applied and implemented. In the following paragraphs, the correlations for predicting minimum-loss incidence and deviation are included in the simulations and compared for verification purposes.

The percentage difference was calculated by

$$\%\ Difference = \left| \frac{(x)_{EES} - (x)_{NREC}}{(x)_{EES}} \right| \times 100 \tag{6.1}$$

where x is the value of the parameter being compared from EES and NREC respectively.

Table 6.1: Ideal stage parameter verification at the design point

Variable	NREC	EES	Difference %
C_1	157.95	157.99	0.03
W_1	346.50	346.50	0.00
β_1	-63.52	-63.51	0.02
U_1	342.99	342.99	0.00
C_2	213.06	212.87	0.09
W_2	245.96	247.79	0.73
α_2	44.45	43.96	1.11
β_2	-51.80	-51.80	0.00
U_2	342.49	342.49	0.00

Variable	NREC	EES	Difference %
C_3	166.02	168.33	1.37
W_3	166.02	168.33	1.37
α_3	23.00	23.00	0.00
β_3	23.00	23.00	0.00
P_{03}	4792.34	4788.58	0.08
T_{03}	306.98	306.88	0.03

Figure 6.4 and Figure 6.5 show the prediction of the minimum-loss incidence angle and deviation angle over a range of mass flows for the rotor and stator respectively and how it compares to the values predicted by the NREC model. The verifications are done for a range of mass flows at 9000 rpm. It must be emphasized that, due to the fact that the predictions for the minimum loss incidence, deviation and the losses are based on correlations, this study can merely provide a comparison between the models used in EES and NREC. However, it is not possible to conclude which models are in fact more correct because of the lack of experimental data. NREC will therefore be used as the benchmark, but future work should definitely compare the concluded model with experimental data.

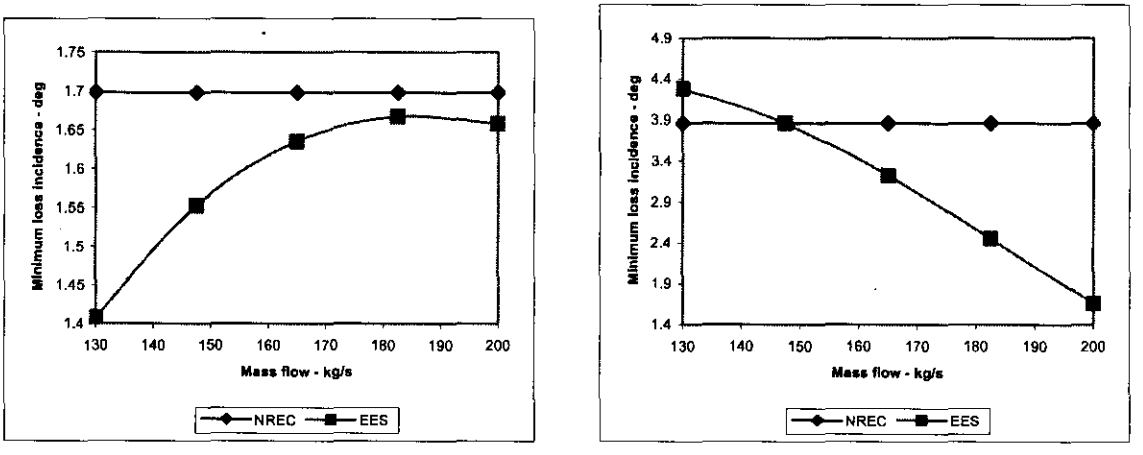

Fig 6.4 Minimum loss incidence angle at design and off-design conditions according to NREC and EES for (a) rotor and (b) stator

NREC assumes the minimum loss incidence angle to be a constant value for both the rotor and the stator at all mass flows. The EES code calculates these values and every effort were made to ensure the correctness of the correlations employed. It can be seen that the difference for the

rotor is relatively small, but that it is quite large for the stator predictions amounting to more than two degrees at the highest mass flow. NREC employs the Lieblein model, but with corrections for 3-D effects for the standard option in this case. However, no change occurs in the prediction when selecting the Lieblein model without the 3-D corrections. At the design point (148 kg/s) for the stator the values compare well, but this is not the case for the rotor. It is suggested that these correlations are revisited in future studies and verified against experimental data and that studies are performed on exactly the sensitivity of compressor performance prediction to the minimum loss incidence.

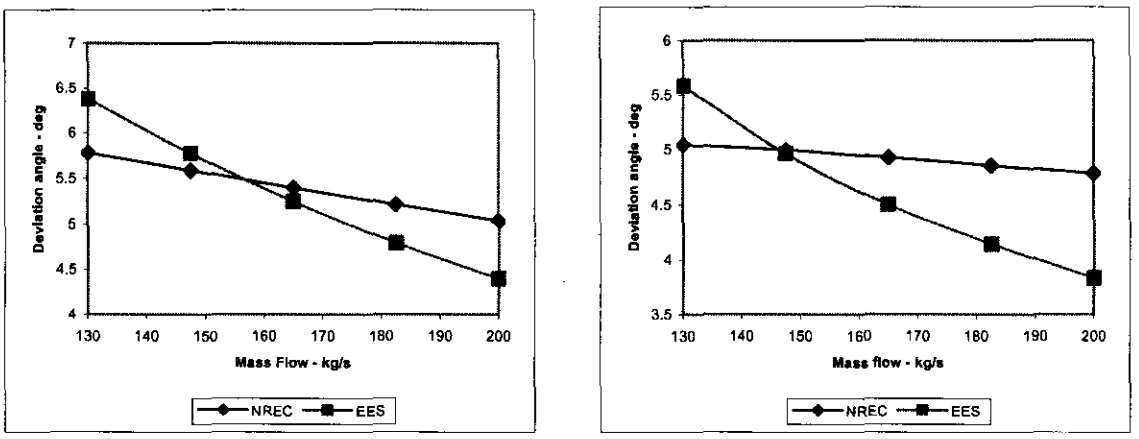

(a) (b)

Fig 6.5 Deviation angle at design and off-design conditions according to NREC and EES for (a) rotor and (b) stator

The predictions for the deviation compare fairly well, with the largest difference of just less than one degree noticeable at the stator for the higher mass flows. NREC and EES follows the same trend, however, the EES model has larger gradients. NREC uses the Lieblein model as employed in the EES code, but apply corrections for 3-D effects. Unfortunately, there is no way of selecting a model without the corrections and it must be assumed that the difference between the NREC and EES predictions can be ascribed to them. It was further noted that, when using only the minimum deviation values, the comparison is better, but no proof could be found that NREC excludes the off-design deviation correction. The values compare well at the design point for both the rotor and the stator. It is, however, again suggested that these correlations are revisited in future work and verified against experimental data and that the EES model be updated with the 3-D corrections.

6.3.2 Verification and evaluation of the loss models

Different combinations of the loss models were used by interchanging the models in the EES code and comparing the results to the NREC model. For easier comparison with NREC, the pressure loss coefficient was used in all the cases and not the entropy increase values as supported by this study.

A potential error was identified in NREC for assigning the profile loss model. According to NREC (see Section 6.2), the default profile loss model for the Koch and Smith basic option is the profile loss model from Koch and Smith. In other words, when choosing the 'standard' model, NREC is supposed to use the profile loss model from Koch and Smith. However, when selecting the 'standard' option for the profile loss calculation, NREC uses a model from Wright and Miller. It was then decided to specifically select the Koch and Smith model in NREC for the profile losses, but after a tedious process it was discovered that this option uses the model from Casey. Furthermore, when selecting the provided user file for the Koch and Smith profile loss, the results are unrealistically high and out of range. It was consequently decided to use the model of Casey in the verification by selecting the Koch and Smith model in the NREC software.

It was necessary to set the deviation and minimum loss incidence to constant values in the NREC and EES models in order to perform an accurate comparison of the loss predictions. This was done because of the differences noted in the prediction of these values between the two models.

For verifying and evaluating the profile loss models, all other losses were excluded and Figure 6.6 and Figure 6.7 were generated for the rotor and stator respectively. When evaluating the stator, the profile loss magnitudes from NREC were inputted in EES for the rotor in order to avoid the repetitive difference resulting from the difference in the rotor comparison. The figures show the prediction of the profile pressure loss coefficient according to the different models and variations thereof according to a variation in mass flow for a constant rotational speed of 9000 rpm.

The models used are the NREC Casey (by selecting Koch and Smith) profile loss model, the EES code with the Koch and Smith profile loss model selected, the EES code with the Lieblein profile loss model selected and the Lieblein profile loss model with the simplified equation for calculating the pressure loss coefficient by assuming the blade boundary layer to be unity. The Lieblein model in EES uses the correlations as provided by Casey and for successful verification should compare almost exactly with the NREC predictions.

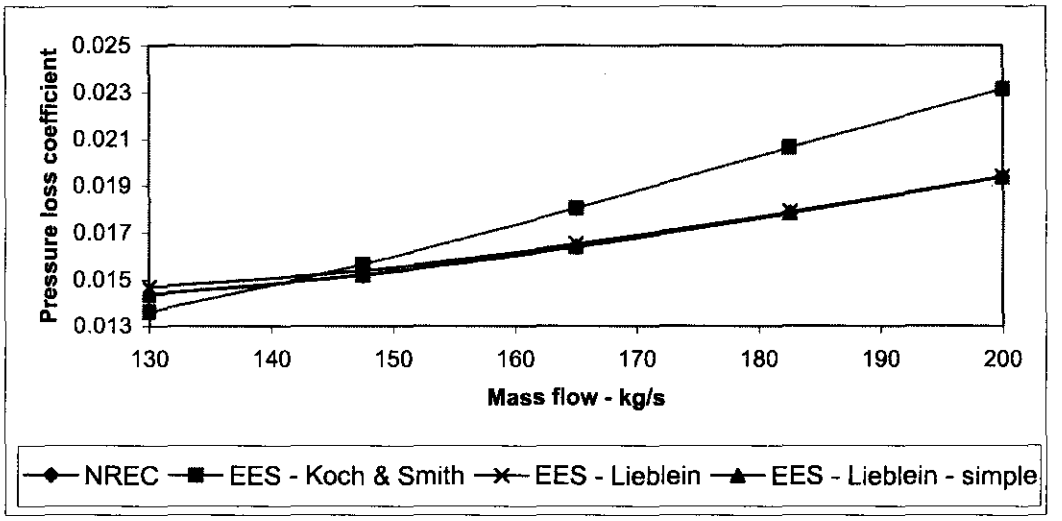

Fig. 6.6 Comparison of profile loss predictions from the various models used in this study for the rotor

From Figure 6.6 it can be seen that the simple Lieblein model in EES, with the simple pressure loss coefficient equation used, compares exactly with the predictions from NREC, with the two lines on top of each other. The reason for this is because NREC uses precisely the same correlations, provided by Casey (1987:275), as this EES model when selecting the Koch and Smith option as mentioned previously. When the form factor is included as a constant value of 1.08 in the pressure loss coefficient equation, the predictions at the lower mass flows are slightly higher, but is expected to have an almost negligible effect on the efficiency predictions.

It can furthermore be seen that the EES Koch and Smith model has a steeper slope than the predictions using the Lieblein model with the Casey correlations. Possible reasons for this could be the fact that the Lieblein model was derived from linear two dimensional cascades and no three-dimensional or compressibility effects are included in the model. The higher loss predictions at the higher mass flows are further also attributed to more parameters taken into account in the Koch and Smith model, like the blade roughness etc.

It is the author's opinion that the Koch and Smith model be used when detail design is required and that the Lieblein simple model be used for predicting the profile losses when quick preliminary values are needed. Unfortunately, it is only possible to validate the Lieblein model employed in EES due to the exact comparison with NREC using the same model. It is, however, seen that the Koch and Smith model is in the correct range and shows the same trend and it is concluded that this model was correctly implemented.

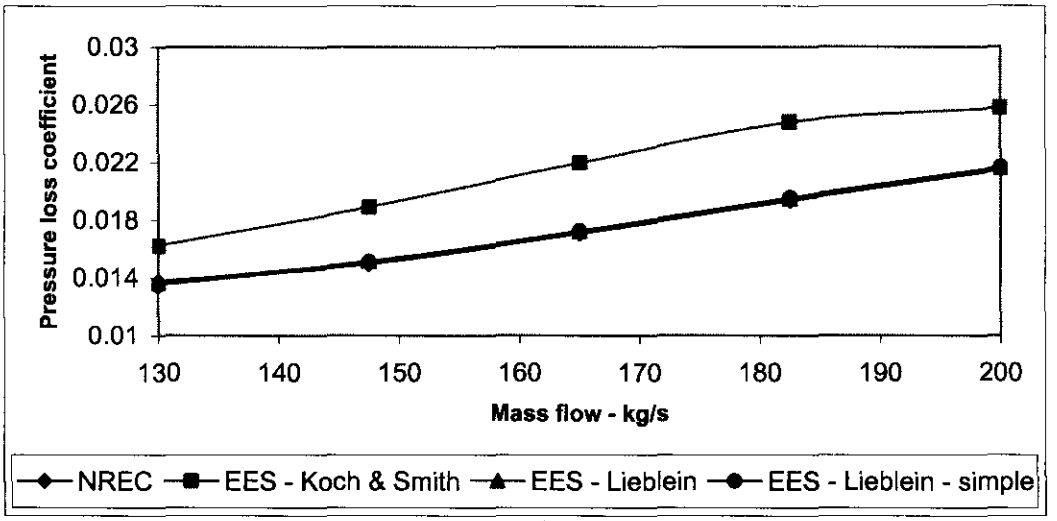

Fig. 6.7 Comparison of profile loss predictions from the various models used in this study for the stator

It can be seen from Figure 6.7 that the trend for the stator is similar to that predicted for the rotor in Figure 6.6 and that the Koch and Smith model in the EES code gives higher values than those predicted by NREC. This might again be attributable to the reasons given in the discussion for the rotor. The predictions from the Lieblein model and the Lieblein model using the simple equation for calculating the pressure loss coefficient gives, as for the rotor almost exactly the same results as NREC with the lines lying almost on top of each other.

The off-minimum loss or incidence loss values are verified and evaluated next. In order to obtain the best possible means of comparing the predictions from NREC and EES, values for the profile loss, obtained from NREC, at the different mass flow increments were inputted into the EES code using the Casey off-minimum loss model. When evaluating the stator, the incidence loss magnitudes from NREC were inputted in EES for the rotor in order to avoid the repetitive difference resulting from the difference in the rotor comparison. For comparing the incidence loss predictions from the Lieblein model, the Lieblein minimum loss profile loss were calculated and subtracted from the total profile loss prediction. This is necessary, because the Lieblein off-minimum loss model gives total values for the profile loss, including the incidence loss component. Figure 6.8 shows the comparison of the incidence loss pressure loss coefficient for the rotor from the two EES models with NREC.

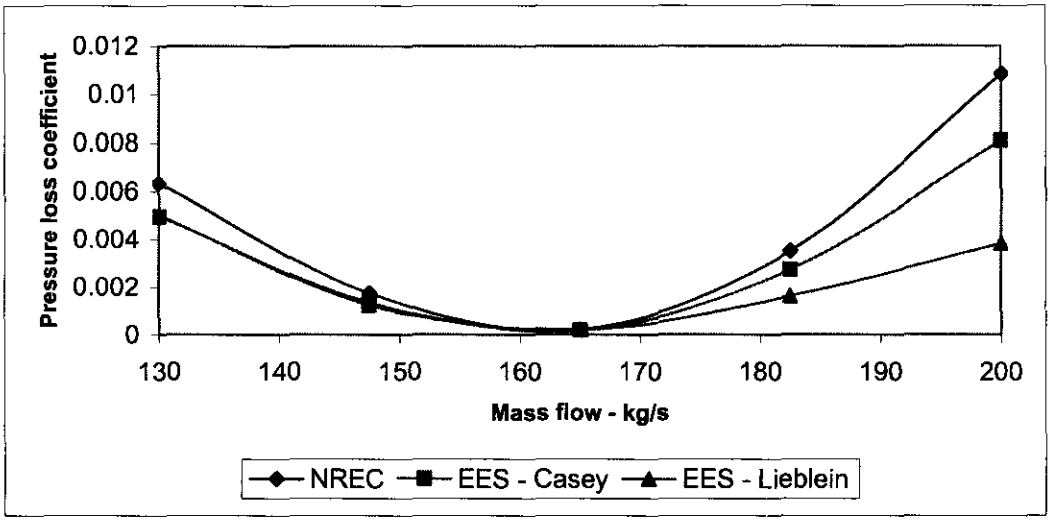

Fig. 6.8 Comparison of incidence loss predictions from the various models for the rotor

Good agreement exists between the NREC model and the Casey and Lieblein models used in the EES code in the region of the minimum loss point. However, a reasonable difference is noticeable at points far removed.

The Lieblein model predicts a more 'open' parabola than both the other models tested, especially for higher mass flows. The comparison between the Lieblein model and Casey model is good at negative incidence only. Reasons for this difference can be attributed to the two-dimensionality and incompressible nature of the cascades used for generating the correlation as well as the high degrees of laminar flow that existed on the cascades. The model uses the pressure loss coefficient equation that includes the boundary layer form factor parameter. It was found that using the simple equation leads to even lower values for the negative incidence region.

It is suggested that this model could be considered for calculations in the region of the minimum-loss point during the preliminary design phase due to its simplicity and the fact that it calculates the total profile loss at minimum and slight off-minimum loss conditions relatively accurately. The Casey model must be used where more accuracy at the off-minimum loss conditions are desired. It is advised that further study be performed, or that verification with experimental data be performed, before making any conclusions about which model (NREC or EES-Casey) is the best to use for this specific test case. Figure 6.9 shows the comparison for the stator.

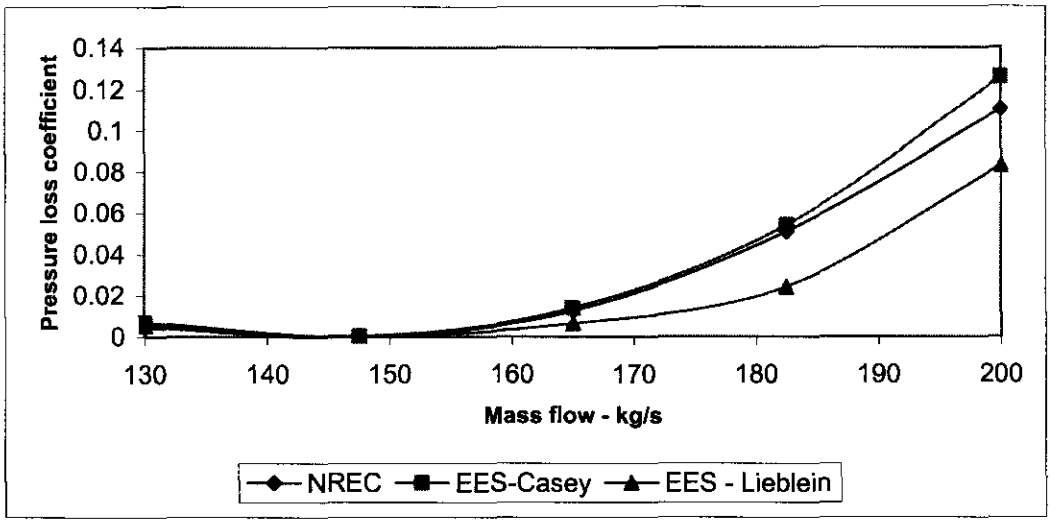

Fig. 6.9 Comparison of off-minimum loss predictions from the various models for the stator

The comparison for the stator leads to the same discussion as for the rotor. The Casey model again shows a good qualitative comparison with the NREC model, with the Lieblein model predicting lower magnitudes for the incidence loss across the range of positive incidence.

The endwall loss models were tediously verified and evaluated by inputting the profile and incidence loss magnitudes predicted by NREC into EES and comparing the endwall loss predictions to those from the NREC model. When evaluating the stator, the endwall loss magnitudes from NREC were also inputted in EES for the rotor in order to avoid the repetitive difference resulting from the difference in the rotor comparison. When other models than the Koch and Smith endwall loss model is used, the value calculated for the Koch and Smith model will be assigned for the endwall boundary layer displacement thickness parameter needed by the EES code to obtain magnitudes for the ABF.

It was seen in Chapter 3 that the endwall loss is the most difficult loss component to understand and predict and virtually all prediction methods rely on very little underlying physics. It was furthermore stated that the correlations come mostly from experimental data from cascades, which is not representative of real compressor bladerows, and that they should be used with great caution. The reader should keep these comments in mind when evaluating the next section. Figure 6.10 shows the comparison of the different endwall loss models used in EES with the NREC prediction for the rotor.

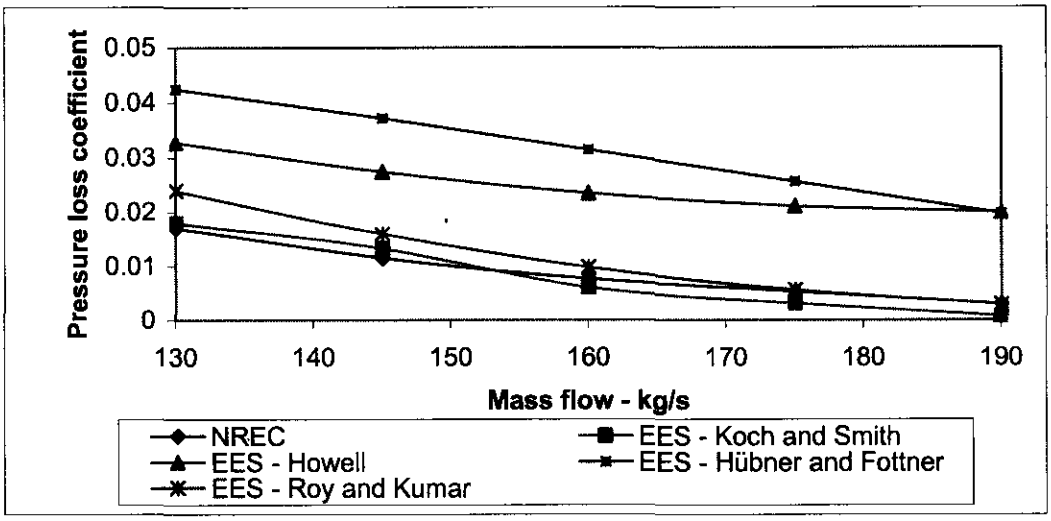

Fig. 6.10 Comparison of the endwall loss predictions from the various models for the rotor

Large variations can be seen in the predictions of the magnitudes of the endwall loss from the various models for the rotor. It can be seen that all the models display the same trend, i.e. a decrease in endwall loss, but their magnitudes differ tremendously. This is an expected result as stated in the aforementioned discussion on the heavy reliance of the correlations on empiricism. The Koch and Smith model compares well to the NREC model, which also uses Koch and Smith, and gives confidence to the methodology employed in this study for applying the stage based correlations to single bladerows. Reasons for the slight difference might be different curve fittings obtained for the correlation figures given in the literature and different methodologies used for applying the model to single bladerows. The Roy and Kumar model also compares reasonable to Koch and Smith, with higher values in the lower mass flow range. These higher values could be the result of the separate prediction of an endwall loss and tip clearance loss magnitudes used in the Roy and Kumar model.

The Howell and "Hübner and Fottner" models both predict much higher values for the endwall loss. In both instances, the correlations were generated from data obtained from linear cascades. Hübner and Fottner used a highly loaded cascade and it was already mentioned that cascade data is not representative of real compressors. The deviation in the predictions from Howell is somewhat understandable due to the extreme simplicity of the model, and the fact that tip clearance is not even taken into account. It can be concluded that the Hübner and Fottner and Howell models are not recommended for endwall loss prediction in detail studies, but that conservative and representative trends can be obtained from these simple models for preliminary design purposes. Figure 6.11 shows the comparison of the different endwall loss models used in EES with the NREC prediction for the stator.

evaluated and conclusions about the loss models were made according to their comparison with each other and NREC.

In this section, the complete stage performance prediction capability of the EES code is verified and evaluated against the NREC model. The loss models will be interchanged in order to investigate the sensitivity of compressor stage efficiency prediction to the prediction of the loss magnitudes. Figures are then generated showing efficiency and pressure ratio against mass flow for constant speed lines for the stage in the stable operating range using the optimum complete EES model and compared to NREC.

The predictions of the stall and choke mass flow for each speed line was done with the NREC software and these boundaries were used to ensure that the simulations were in the stable operating range according to NREC. In Chapter 5, however, methods for predicting stall and choke were discussed and implemented in the EES code, but it is accepted that verification and improvement of these methods will be left for further study due to it falling outside the scope of the current focus. The error functions halting the calculations in such cases were consequently converted to warning functions, warning the user that a bladerow in the stage is outside the operating range according to the EES model, without stopping the simulation.

In a real compressor stage, all the variables and correlations are dependent on each other and different combinations of loss models lead to different performance prediction. The combinations that were chosen for this study are given in Table 6.2 and were chosen in an effort to lead to sensible conclusions about the sensitivity of performance prediction to using different models and with the individual loss comparisons and resulting conclusions in mind. The comparison was done for the constant speed line of 9000 rpm and the predictions for the minimum incidence and deviation angles were unrestrained.

Table 6.2: Loss model combinations used for stage performance prediction

No.	Profile loss	Off-minimum loss	Endwall loss
1	Lieblein	Casey	Koch and Smith
2	Koch and Smith	Casey	Koch and Smith
3	Koch and smith	Casey	Howell
4	Lieblein		Koch and Smith
5	Lieblein		Howell

Figure 6.12 shows the comparison of the models using the loss combinations as given in Table 6.2 with the NREC model for predicting the total-to-total adiabatic efficiency of the stage. The numbers used in the legend corresponds to the numbers in the table.

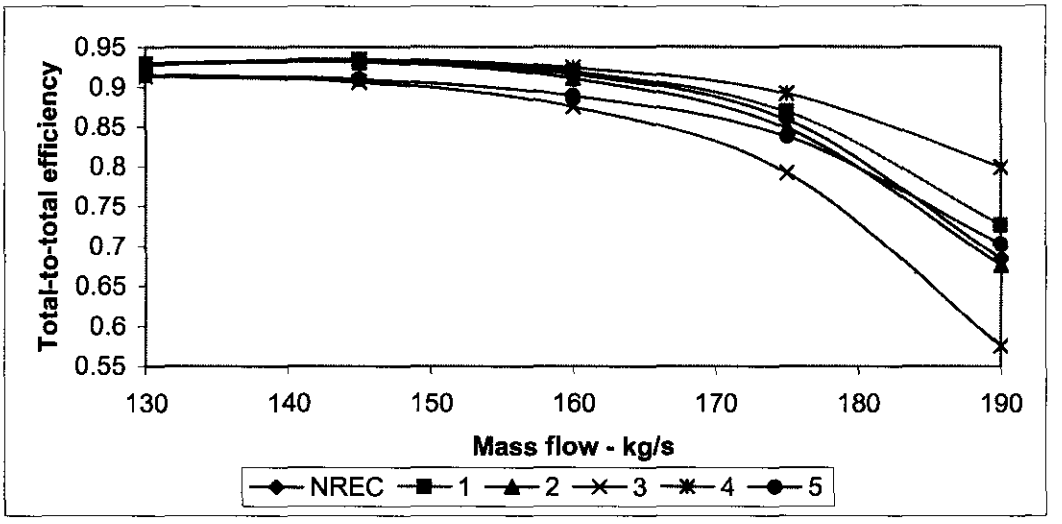

Fig. 6.12 Comparison of total-to-total adiabatic efficiency predictions for a stage using different loss models

From Figure 6.12 it can be seen that the choice of loss models has a noticeable effect on efficiency prediction, especially when nearing choking conditions. It can, however, be concluded that for preliminary design point estimates, it is acceptable to use the simpler loss models. This conclusion is further supported by the results obtained when using Combination 5 and it can be seen that in this instance, the comparison at off-design conditions is also relatively good with the largest deviation from NREC equal to less than 3%. In this study, Combination 2 compares the best with the NREC model and the higher profile loss values is neutralized by the lower incidence loss values from the Casey model at off-design conditions.

From Combinations 1 and 2 it can be concluded that either Lieblein or Koch and Smith can be used for predicting the profile loss at the design point, but a noticeable difference can be seen at the higher mass flows. As mentioned earlier, Koch and Smith is a more comprehensive model and should therefore be used if possible. The same holds for the incidence loss prediction and can be seen from the comparison between Combinations 2 and 4. From the comparison it can be seen that the endwall loss model plays an important role in obtaining accurate results at the design point and it can be recommended that Koch and Smith again be used wherever possible due to its comprehensiveness and the fact that both combinations using the Howell model gives lower design point values.

Combination 2 was used and figures were generated showing efficiency and pressure ratio against mass flow for constant speed lines for the stage in the stable operating range and compared to NREC. This comparison for total-to-total adiabatic efficiency and total-to-total pressure ratio of the stage can be seen in Figure 6.13 and Figure 6.14 respectively.

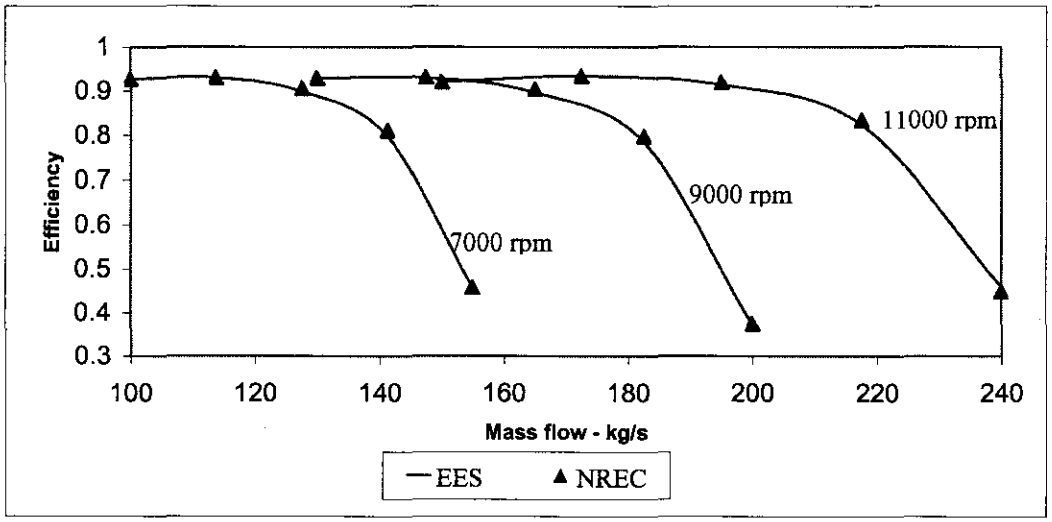

Fig. 6.13 Comparison of stage efficiency prediction between NREC and EES for constant speed lines

It can be seen that the comparison between EES and NREC is excellent for all mass flows and rotational speeds considered. This verifies that the implementation and usage of the EES model is done correctly according to the commercial software package NREC.

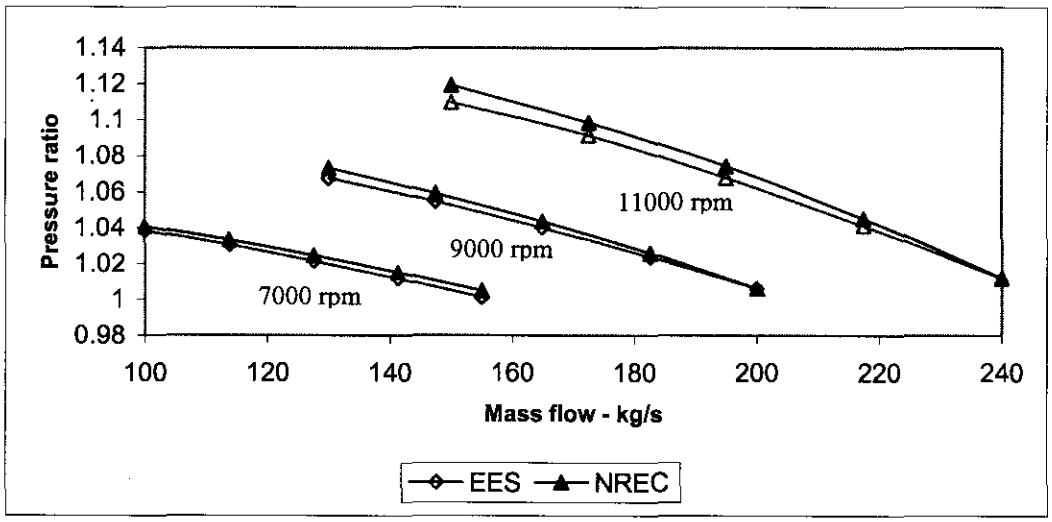

Fig. 6.14 Comparison of stage pressure ratio prediction between NREC and EES for constant speed lines

Figure 6.14 shows that there is a good comparison between the EES code and NREC for the total-to-total stage pressure ratio predictions. However, EES predicts slightly lower values than NREC and this becomes more evident in the higher speed lines. Possible reasons for this deviation in the predictions can be the fact that NREC uses variable blade profiles (twisted blades) for their prediction and differences in the definition of blockage between the two codes.

The EES code was successfully validated in this section for performance prediction of real stage performance. Valuable conclusions were also made regarding the loss models and their influence on performance prediction as well as the penalties induced for using the simple preliminary models. The next chapter uses the validated EES code to perform parametrical studies of the influence of varying the parameters, contained in the models used, on performance prediction. In the next section, however, the EES code's ability to predict multi-stage performance is investigated and again verified against NREC.

6.4 Multi-stage compressor performance prediction

The previous section evaluated the influence of using different loss models on the performance prediction and verified the EES code for stage performance prediction with NREC. This section deals with using the EES code for multi-stage axial compressor performance prediction through comparing its results with that given by NREC. The four stage compressor described in Section 6.2 is used here and was implemented in EES and NREC.

When using the outlet ABF value from the one stage as input ABF to the following stage, the EES model predicted much lower efficiency values than NREC, especially at the higher mass flows. It is possible that the methodology is incorrect and it was decided to simulate the growth of the endwall boundary layer through the compressor by reducing the inlet ABF by one percentage for each stage starting at stage two. Further work needs to be done specifically on multi-stage compressor blockage and how it is increasing throughout the compressor due to it falling outside the scope of this study.

The results of the comparison between NREC and EES for the performance prediction of the four stage compressor are shown in Figure 6.15 and Figure 6.16. Figure 6.15 shows the comparison for the compressor total-to-total adiabatic efficiency and Figure 6.16 shows the comparison for the total-to-total compressor pressure ratio.

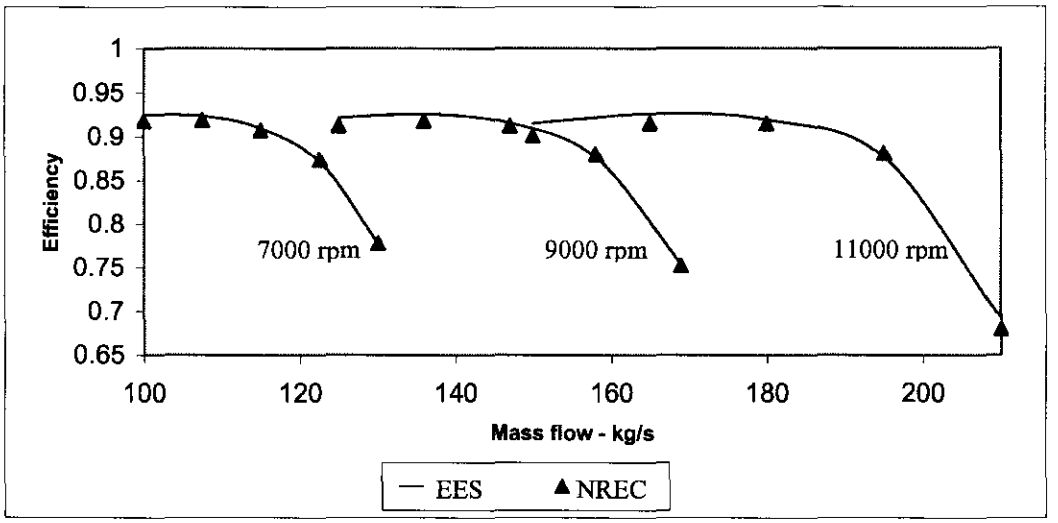

Fig. 6.15 Comparison of compressor total-to-total adiabatic efficiency prediction between NREC and EES for constant speed lines

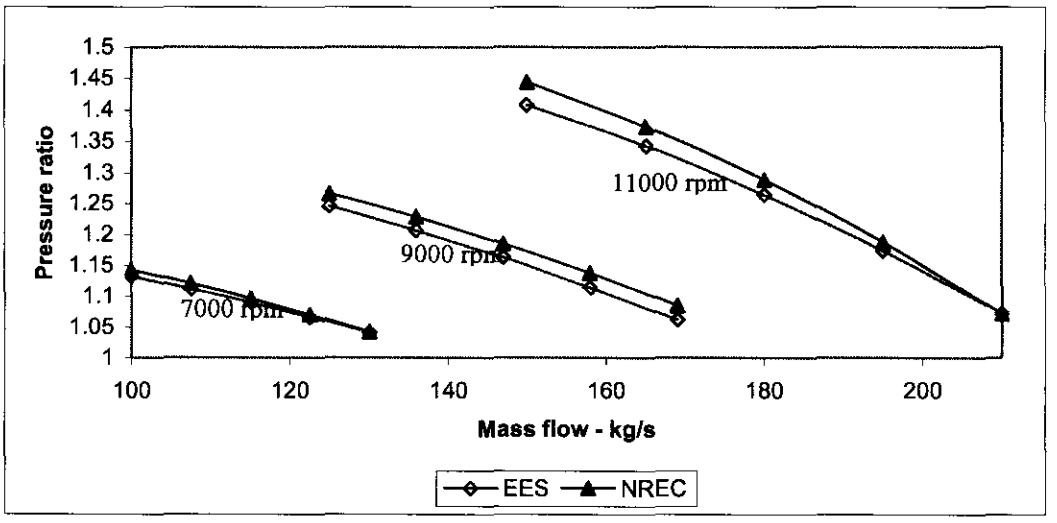

Fig. 6.16 Comparison of compressor pressure ratio prediction between NREC and EES for constant speed lines

It can be seen that the comparison is good and it can be concluded that the EES code is capable of doing successful and accurate performance prediction for multi-stage axial compressors. The slight differences can be ascribed to the same reasons as given in Section 6.4 for the differences in the single stage comparison. It can further be concluded that the loss models and the methodology employed in this study for implementing them in a multi-stage axial compressor performance prediction code are correct and well founded.

6.5 Summary and conclusions

In this chapter, the accuracy and validity of the engineering code generated for axial compressor performance prediction was verified against a commercial performance prediction package called NREC. The loss models were interchanged and evaluated according to their deviation from the norm set by NREC and conclusions were made about the sensitivity of compressor performance prediction to certain aspects of modelling and the different loss models. Furthermore, the ability of the EES code to predict stage and multi-stage compressor performance was verified.

It was seen that the non-loss parameters compare very well at different mass flows and it was thus concluded that the non-loss theory and methodology used in the EES code were correctly applied and implemented. NREC assumes the minimum loss incidence angle to be a constant value for both the rotor and the stator at all mass flows. The EES code calculates these values and it was seen that differences in the stator predictions amounts to more than two degrees at the highest mass flow. The predictions for the deviation compare fairly well, with the largest difference of just less than one degree noticeable at the stator for the higher mass flows. It was accepted that the difference between the NREC and EES predictions can be ascribed to the changes made by NREC to the model for incorporating 3-D effects. It was further noted that, when using only the minimum deviation values, the comparison is better, but no proof could be found that NREC excludes the off-design deviation correction. It was, however, suggested that the minimum loss incidence and deviation correlations should be revisited in future work and verified against experimental data.

For the profile losses, it was suggested that the Koch and Smith model be used when detail design is required and that the Lieblein simple model be used when quick preliminary values are needed. Good qualitative comparison was obtained between the NREC model and the Casey and Lieblein models for the incidence loss predictions in the region of the minimum loss point, although a reasonable difference was noticeable at points far removed. It was suggested that the Lieblein model could be considered for calculations in the region of the minimum-loss point during the preliminary design phase due to its simplicity and the fact that it calculates the total profile loss at minimum and slight off-minimum loss conditions relatively accurately. The Casey model must be used where more accuracy at the off-minimum loss conditions are desired. It was advised that further study should be performed, or that verification with experimental data be performed, before making any conclusions about which model (NREC or EES-Casey) is the best to use for this specific test case.

Large variations were seen in the predictions of the magnitudes of the endwall loss from the various models. This is an expected result because of the heavy reliance of the correlations on empiricism. The Koch and Smith model compares well to the NREC model, which also uses Koch and Smith, and gives confidence in the methodology employed in this study for applying the stage based correlations to single bladerows. Conclusions from the endwall loss verification are that the Howell, "Hübner and Fottner" and "Roy and Kumar" models are not recommended for endwall loss prediction, but that conservative and representative trends can be obtained from these simple models for preliminary design purposes. It was furthermore also recommended that Koch and Smith be used wherever possible. The added bonus of using Koch and Smith is the fact that it eliminates the need for additional blockage correlations.

The choice of loss models has a noticeable effect on efficiency prediction, especially when nearing choking conditions. Valuable conclusions were made regarding the loss models and their influence on performance prediction as well as the penalties induced for using the simple preliminary models. It was, however, concluded that for preliminary design point estimates, it is acceptable to use the simpler loss models. In this study, using the Koch and Smith profile loss model, the Casey incidence loss model and the Koch and Smith endwall loss model were identified as the best combination of loss models to use.

It was seen that the single stage and multi-stage performance prediction comparison between EES and NREC is excellent for all mass flows and rotational speeds considered. A good comparison was also obtained between the EES code and NREC for the total-to-total stage pressure ratio predictions. However, EES predicts slightly lower values than NREC and this becomes more evident in the higher speed lines. It was recommended that further studies be performed on the aspects regarding blockage, especially through a multi-stage compressor.

In Chapter 7, the EES-code is used to perform parametric studies on the influence of varying the geometric input parameters on overall stage loss and efficiency prediction. The aim is to form an idea as to which geometrical input parameters are the key players in improving efficiency and which loss parameters are crucial to accurate predictions.

Chapter 7

PARAMETRIC STUDIES

In this chapter the EES-code is used to perform parametric studies on the influence of varying the geometric input parameters on overall stage loss and efficiency prediction. The aim is to form an idea as to which geometrical input parameters are the key players in improving efficiency and which loss parameters are crucial to accurate predictions.

7.1 Introduction

Chapter 3 presented the reader with the models obtained from the open literature for predicting the losses through an axial compressor. It was, however, found that it would be advantageous to include the models in a performance prediction code, because of their extreme dependence on each other and some of the other variables included in performance prediction and due to the implicit nature of the calculations. Chapter 4 then presented the concepts and theory needed for generating a basic mean line performance prediction code for including the loss models. Chapter 5 discussed the implementation of the models and theory in a software package called EES and in Chapter 6 the accuracy and validity of the generated code was verified against a commercial performance prediction package.

This chapter aims at illustrating the capability of the code, generated in this study, for performing parametric studies. These studies can be used to aid in understanding compressor design and performance or for basic optimization problems. This is done, staying with the focus of this study, by showing the results from several parametric studies where some of the loss parameters were varied in the EES code and also by presenting an illustrative parametric study for optimizing the rotor inlet blade angle.

7.2 Methodology

It was seen in Chapter 5 that the performance prediction for a multi-stage compressor comprised of sequentially obtaining predictions for the individual stages by using the outlet conditions of the one stage as the inputs for the next. It was also seen that each stage uses the same set of equations for obtaining the predictions. It was, therefore, decided that it would be sufficient for this study to do the parametric studies for a single stage only for illustrating the application of the code for design or optimization purposes. Further study can, of course, use the code more extensively to determine, for instance, the influence of varying some geometric parameter in the third stage rotor to overall compressor performance etc.

The stage used is again the first stage of the four stage compressor used in Chapter 5 with its initial input values given in Appendix D.1. Koch and Smith's profile and endwall loss models and the incidence loss model of Casey was used due to the confidence given to their validity by the comparisons to NREC in Chapter 6 and the fact that this combination includes the most input parameters in the loss models. Furthermore, the part span shroud loss model was included for the rotor and the stator and the windage loss model from Denton for the rotor.

Some of the parameters given in Appendix C.2 for the stage geometrical inputs and used as input values for the loss models are parametrically varied and the influence on efficiency prediction is investigated. This is done by keeping all the input parameters constant with the values given in Appendix D.1, except one parameter which is varied. The first set of parametric studies investigates the influence of the loss parameters on stage total-to-total adiabatic efficiency. These parameters were chosen on the grounds that they are input parameters only to the loss models, or other relevant correlations, and would have no effect on a simulation excluding the losses or deviation.

Next, an illustrative parametric case study is presented which investigates the effect of a major variable change (the rotor inlet blade angle), on the loss magnitudes to illustrate their dependence on the performance prediction variables and each other. The effect of this loss change on stage efficiency and pressure ratio are also shown. The EES code was adapted to include the predictions for stall and choke as discussed in Chapter 4 and Chapter 5 and aided in determining the range for the parametric studies. Further restrictions for the range between which the variables are varied are obtained from the correlation figure boundaries. The following sections presents the results as obtained from the parametric studies with the EES code.

7.3 The influence of some loss parameters on stage efficiency

7.3.1 The effect of axial spacing on stage efficiency

The axial spacing between the blade rows were varied between 0.1 and 20 mm. The effect of this parameter is included in the stage performance prediction through the correction factor implemented in the Koch stalling static pressure rise coefficient model and the Koch and Smith endwall loss model. These correction figures are shown in Figure B.3.4 and Figure A.4.2 respectively. Figure 7.1 shows how this influenced the stage efficiency for this compressor stage.

From Figure 7.1 it can be seen that the efficiency decreases with an increase in axial spacing between the bladerows. The slope also decreases with an increase in axial spacing, showing that its effect is most dramatic in the range close to zero spacing.

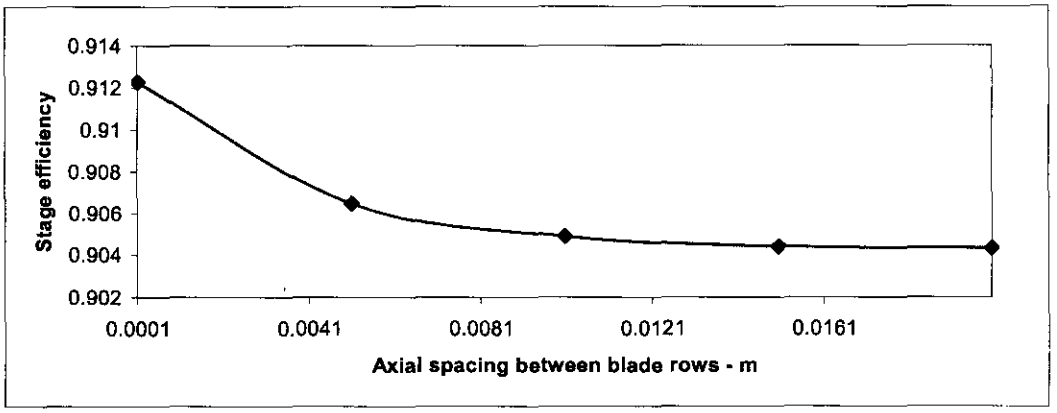

Fig. 7.1 Effect of varying axial spacing between bladerows on stage total-to-total adiabatic efficiency

It can be concluded that the axial spacing between the bladerows has a definite influence with a stage efficiency variation of 0.8 % for the range considered and that closer blades means higher efficiency. It must, however, be remembered that the models used for predicting profile loss and deviation does not take this parameter into account and the influence of extremely close bladerows are therefore unknown on these predictions. Furthermore, this parameter is usually limited mechanically due to the fixing methods and associated stresses due to wake passing excitation.

7.3.2 The effect of tip clearance on stage efficiency

The tip clearance values for the rotor and stator were varied in this investigation to see the influence of tip clearance on the efficiency of an axial compressor stage. The effect of tip clearance is included in the performance prediction in a correction applied to the Koch stalling static pressure rise coefficient model as well as being one of the correlating parameters in the Koch and Smith endwall loss model as seen in Figures B.3.3 and A.4.1 respectively. Both bladerow's tip clearances were varied simultaneously between 0.01 and 2 mm and the effect of this on the stage efficiency is shown in Figure 7.2. Varying the tip clearance for only the rotor and keeping the value for the stator constant and vice versa, showed a similar trend and it is not reproduced here.

It can be seen that the stage efficiency decreased almost linearly when increasing the tip clearance for the range considered. The efficiency decrease is rather large, almost 4%, and it can therefore be concluded that tip clearance plays a major role, as expected, in compressor efficiency. According to Cumpsty (1989:344), however, the endwall loss model from Koch and Smith is the most reliable model available, but it cannot be valid for stages with small or vanishing tip clearance. Flow visualizations have indicated that there exists a definite optimum tip clearance

for bladerows, as opposed to zero clearance, which counteracts detrimental secondary flows, which in turn causes separation in the endwall region. Cumpsty (1989:344) further states that "Although the clearance flow seems to be beneficial when very small, typically not more than 1% of chord, at larger clearances the loss and the inception of stall appears to be dominated by the clearance flow behavior." It can therefore be suggested, according to the aforementioned, that a good preliminary estimate for tip clearance could be about 0.5 % of chord.

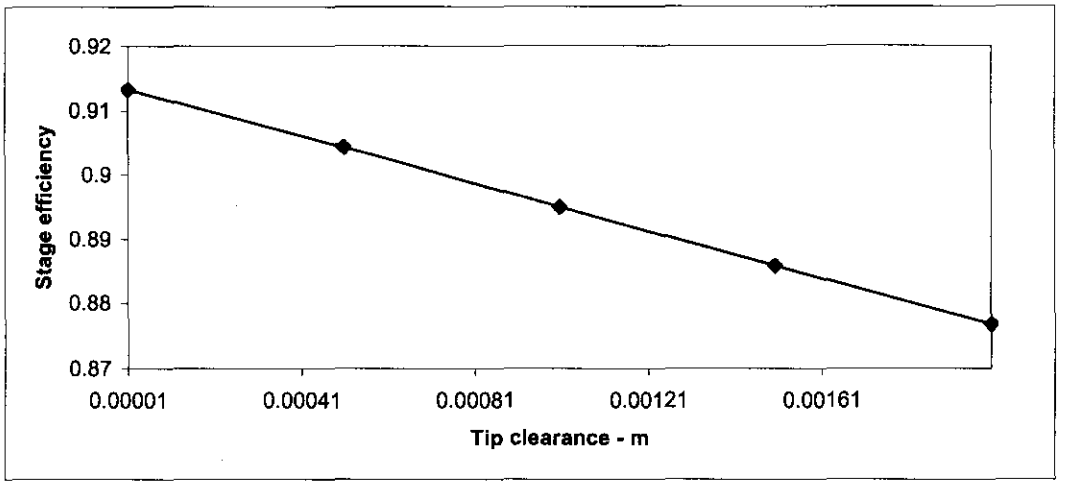

Fig. 7.2 Effect of varying tip clearance of bladerows on stage total-to-total adiabatic efficiency

7.3.3 The effect of maximum blade thickness on stage efficiency

The maximum blade thickness is input parameters to the correlations for the Koch and Smith profile loss model as well as the correlations for the deviation and minimum loss incidence angle predictions. As for the tip clearance study, the thicknesses of the rotor and stator blades were increased simultaneously and the effect on the stage efficiency was investigated. The values were varied between approximately 3% and 11% thickness to chord ratio, which is between 1 and 4 mm for the test stage blades. The effect on stage efficiency is shown in Figure 7.3.

Figure 7.3 shows that the slope of the graph increases with an increase in maximum blade thickness. For this test case it can also be seen that no real efficiency decrease is suffered up to a blade thickness of about 5% thickness to chord ratio. Furthermore it was stated in Chapter 3 that the loss from different profile sections is very nearly the same at subsonic Mach numbers. Cumpsty (1989:141) gives evidence that the result might be correct by stating that, nowadays, most applications would call for much thinner blades, typically around 5% for subsonic inlet flow conditions. According to these results, it can therefore be concluded that the blade thickness should be kept as thin as possible, taking into account manufacturing restraints and strength

considerations. For the test compressor, the efficiency can be increased by 0.5% by using blades with half the maximum thickness it currently uses for the rotor and the stator.

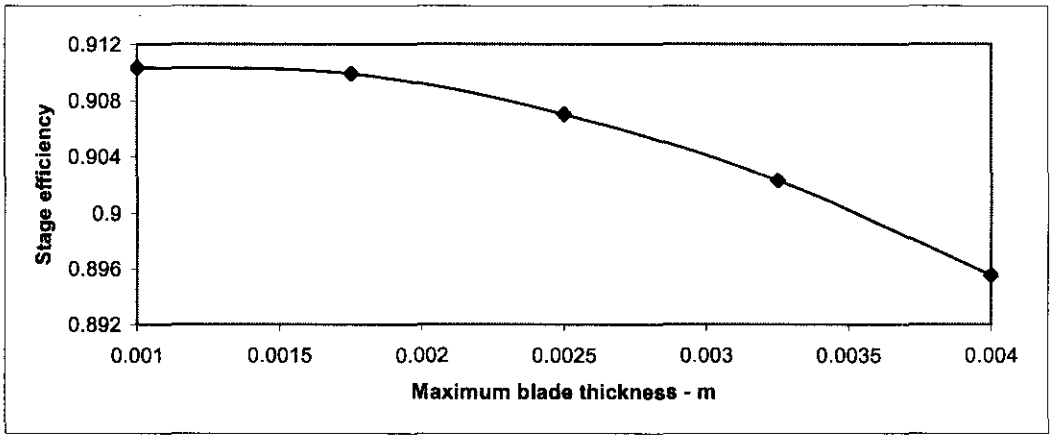

Fig. 7.3 Effect of varying maximum blade thickness on stage total-to-total adiabatic efficiency

7.3.4 The effect of blade chord on stage efficiency

The blade chord parameter is used directly and/or indirectly in all the loss models and performance correlations in the EES code and the performance prediction is very much dependant on this parameter. The blade chord parameter for the rotor was varied between 25 and 50 mm, while the chord value for the stator was kept constant at the given value of 35.6 mm. The same was done for the stator while keeping the rotor chord value constant. Finally, the rotor and stator chord parameters were varied simultaneously between the specified values. The effect of these variations on stage efficiency is shown in Figure 7.4.

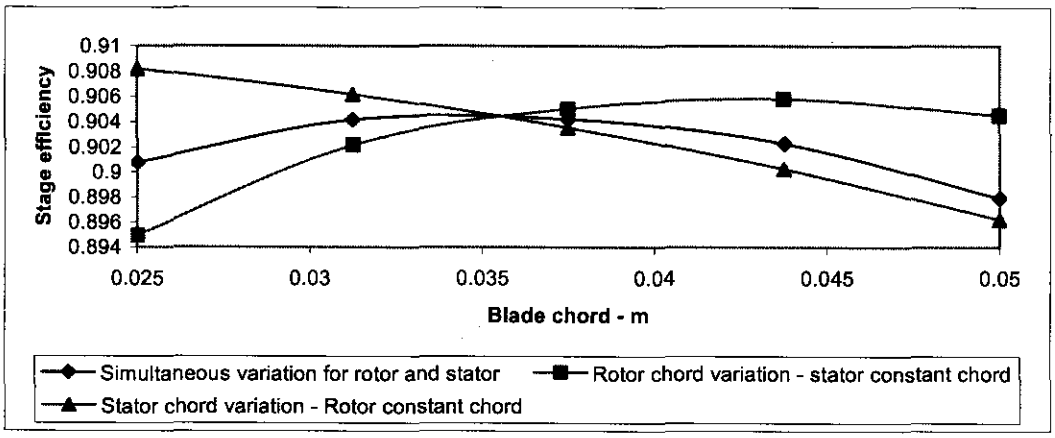

Fig. 7.4 Effect of varying blade chord on stage total-to-total adiabatic efficiency

Figure 7.4 suggests that there is an optimum blade chord length for both the rotor and the stator for the test stage considered. This can be deduced from the fact that, when keeping the stator chord length constant, the stage efficiency reaches a maximum for this test case with the rotor chord length equal to about 44 mm. It can also be deduced that, when keeping the rotor chord constant, the stage efficiency would reach a maximum when the stator chord length is equal to some value smaller than 25 mm. From the graph showing the simultaneous variation of the chord lengths for both the rotor and stator, it can be seen that the maximum stage efficiency according to the EES code would be at the current value of about 35 mm. The difference in stage efficiency was about 1% for the range of chord lengths considered and it can be concluded that there exists an optimum chord length for maximum stage efficiency for each blade row. However, for a preliminary design estimate, chord lengths for the rotor and stator can be taken as equal or according to manufacturing constraints due to the small influence on stage efficiency.

7.3.5 The effect of blade pitch on stage efficiency

The blade pitch parameter for the rotor was varied between 17 and 35 mm, while the pitch value for the stator was kept constant at the given value of 19 mm. The same was done for the stator while keeping the rotor pitch value constant at 19 mm. Also, the rotor and stator pitch parameters were varied simultaneously between the specified values. The effect of these variations on stage total-to-total adiabatic efficiency is shown in Figure 7.5.

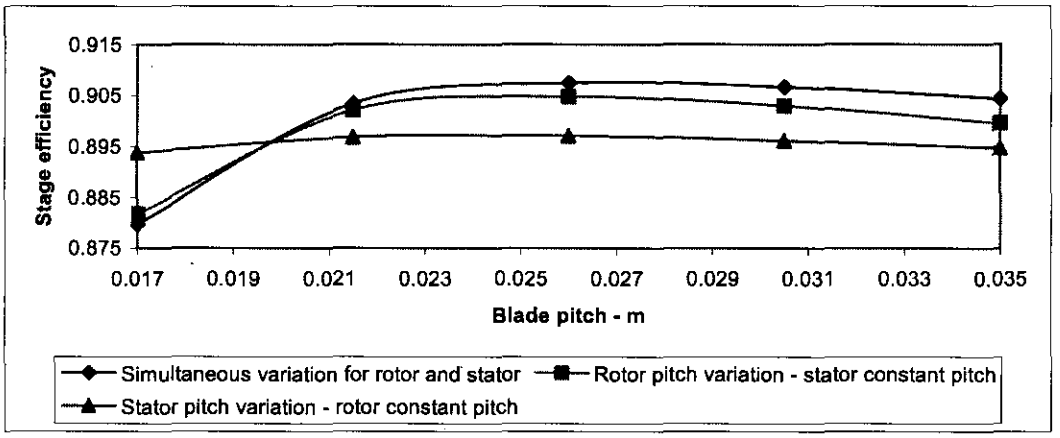

Fig. 7.5 Effect of varying blade pitch on stage total-to-total adiabatic efficiency

It can be seen that, for this specific stage, the influence of varying the stator pitch has a small effect on the stage efficiency and it seems as if the pitch of the rotor has the most influence on the stage efficiency. As with the blade chord, there seems to be an optimum pitch value for the rotor and the stator to obtain maximum stage efficiency with the other parameters constant.

For this study, it can be seen that the maximum efficiency will be achieved with the pitch value for the rotor and stator set to about 27.5 mm. For this test stage, the stage efficiency increases by 0.3% when increasing the pith of the stator from 19 mm to 27.5 mm.

7.3.6 The effect of blade surface roughness on stage efficiency

In this section the effect of using rough blades opposed to blades that with a smooth surface finish is investigated by inspecting the effect that this has on the stage efficiency. The range of the investigation falls outside the criteria for hydraulically smooth blades, which is corrected only for Reynolds number in the Koch and Smith profile loss model. The parameter that is varied is the centerline average of the roughness particles, k_{CLA}, and is defined as the arithmetical average deviation expressed in microns measured normal to the centreline. The parameter is varied between 0.2 and 2 microns for the rotor and stator simultaneously and the effect of this on the stage efficiency can be seen in Figure 7.6.

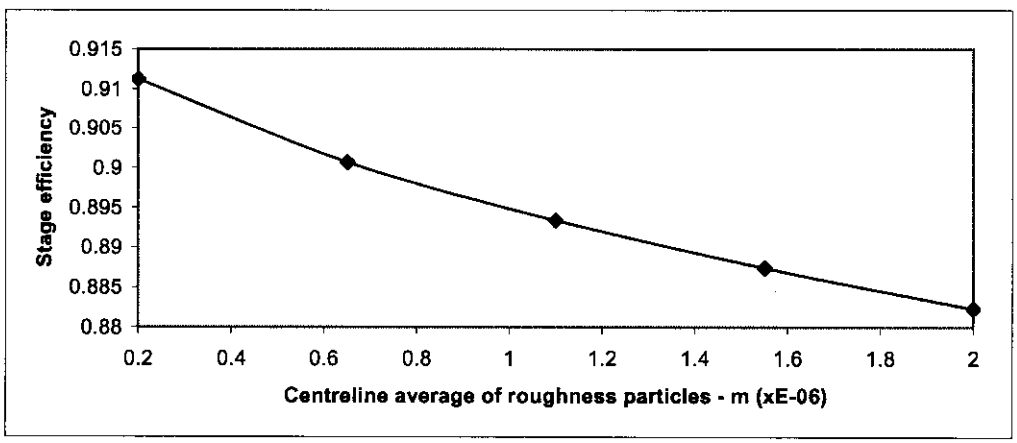

Fig. 7.6 Effect of varying blade surface roughness on stage total-to-total adiabatic efficiency

The effect of increasing the surface finish of the blades is quite dramatic and it can be seen that the stage total-to-total adiabatic efficiency is decreased by almost 3%. Even a small improvement in the surface finish seems to have a relatively significant influence on the stage efficiency and, in practical terms, it can be deduced that fouling during operation must be minimized due to the large effect on efficiency. The test compressor's efficiency can be increased by 0.7% by improving the centreline average particle roughness of the rotor and stator surface finish from 0.5 microns to 0.2 microns. The parametric study can, of course, also be done for only one blade row at a time as well to investigate the effect when the rotor are smooth and the stator are not etc. Also, it would be interesting to perform a study on the cost implication of improving blade roughness compared to the gain in stage efficiency. This will, however, be left for further work.

7.3.7 The effect of the part span shrouds on stage efficiency

There are three parameters which need to be supplied for including the model for the part span shroud loss in the performance prediction code. These are the shroud radius, shroud maximum thickness and the shroud chord. For this investigation, a shroud will be included only for the rotor and the effect on the stage total-to-total adiabatic efficiency will be investigated when varying the respective shroud parameters. Figure 7.7 shows the influence on the stage efficiency for a shroud at a radius of 0.36 m, a thickness of 2 mm and varying shroud chord values between 5 and 20 mm. Figure 7.8 and Figure 7.9 shows the influence on the stage efficiency when varying the rotor shroud thickness and radius respectively while keeping the other parameters constant at their given values. The thickness was varied between 0.5 and 3 mm and the radius was varied between 0.3 and 0.4 m.

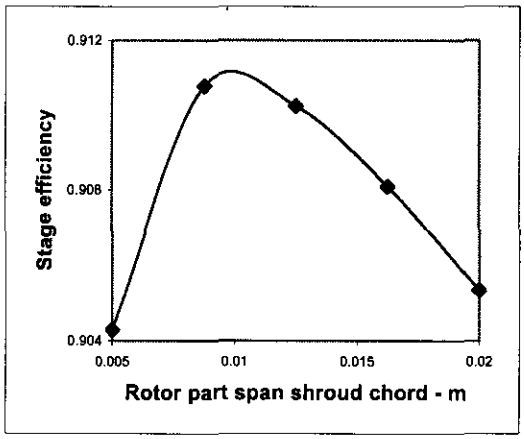

Fig 7.7 Effect of varying rotor part span shroud chord on stage total-to-total adiabatic efficiency

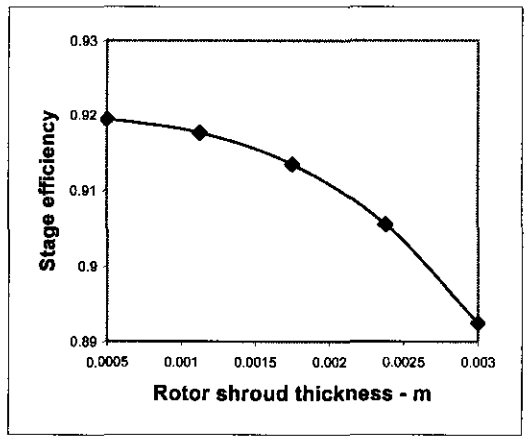

Fig 7.8 Effect of varying rotor part span shroud thickness on stage total-to-total adiabatic efficiency

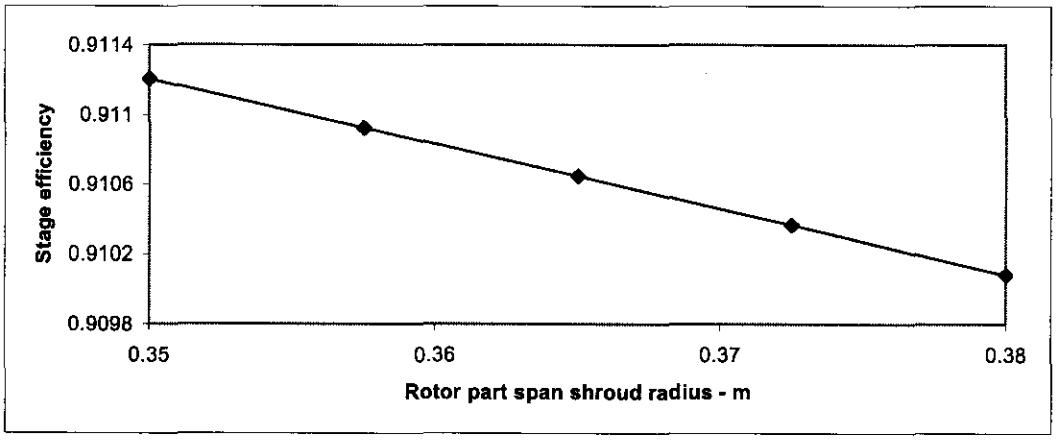

Fig 7.9 Effect of varying rotor part span shroud radius on stage total-to-total adiabatic efficiency

Figure 7.7 shows that there is an optimum chord value for the part span shroud, with the other parameters at their constant values, resulting in maximum stage efficiency. Furthermore, it can be seen from Figure 7.8 that the efficiency decreases with an increasing slope with an increase in shroud thickness, leading to the conclusion that the shroud should be kept as thin as possible. Also, from Figure 7.9, it is seen that when the part span shroud is moved from the hub towards the tip, the efficiency decreases by a small percentage, however, it is uncertain if this correlation takes the boundary layers and the interaction that would occur with them into account. Consequently, it is advised that this correlation should only be used when the part span shroud is placed well away from the endwalls until further study has confirmed the results. This parametric study can similarly be performed for the stator in order to access the influence of a part span shroud and its parameter magnitudes on the stage efficiency. The next section investigates the effect of major variable changes like, for instance, the blade angles on the loss magnitudes to illustrate their dependence on the performance prediction variables and each other. The effect of this loss change on stage efficiency and pressure ratio will also be shown.

7.4 Illustrative parametric case study

A case study is presented in this section for illustrating the capability of the EES code to perform such studies and to try and show the dependence of the loss models on the performance variables and each other. The effect of changing the rotor blade inlet angle on the different loss components, total loss, stage efficiency and pressure ratio will be investigated in an effort to obtain an optimum rotor blade inlet angle value for maximum stage efficiency. The rotor inlet blade angle was varied and the effect on the entropy change values for the different loss components for the rotor and the total entropy change through the rotor was investigated. The effect for the different loss components are shown in Figure 7.10.

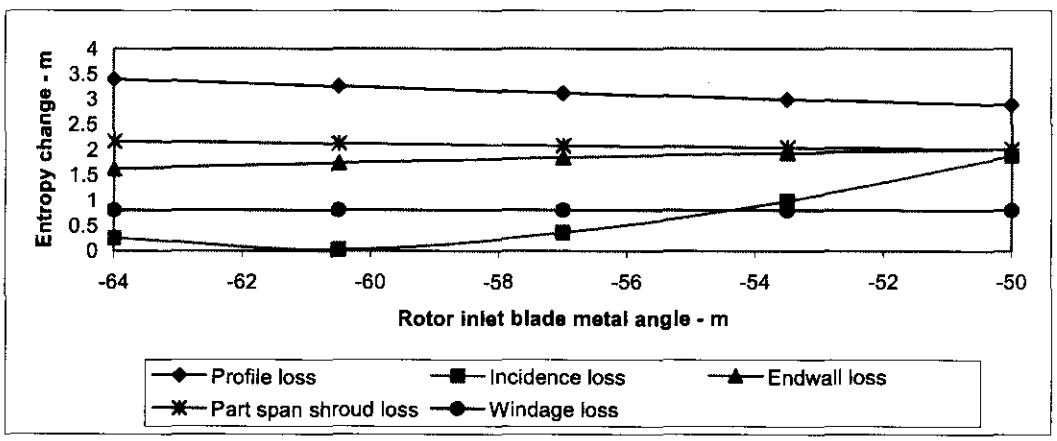

Fig. 7.10 The effect of varying the rotor inlet blade angle on the magnitudes of the loss components

From Figure 7.10 it can be seen that varying the rotor inlet blade angle from -50 to -64 degrees has an influence on all the loss components included in the performance prediction model for the rotor. The profile loss shows a decrease with a blade inlet angle increase. Furthermore, it can be seen that the endwall loss and part span loss values also show a decrease with an increase in inlet rotor blade angle, while there seems to be an optimum inlet blade angle for the smallest incidence loss. This is understandable, because the incidence angle is a function of the inlet blade angle. The windage loss shows a small decrease for the increase in the inlet blade angle values. For this specific compressor stage it was found that excluding the windage loss from the performance prediction caused an increase in stage efficiency of approximately 0.65 % and it can therefore be concluded that the contribution from this loss is somewhat significant. Reasons contributing to large windage loss values are disks that are not smooth or, as in this case, short blades with low flow and loading coefficients, as stated in Chapter 3.

The effect of all the losses are combined by adding their entropy changes and the resulting total entropy change through the rotor, with the specified variation in inlet blade angle, is shown in Figure 7.11. The effect on the total stage entropy change can be seen in Figure 7.12.

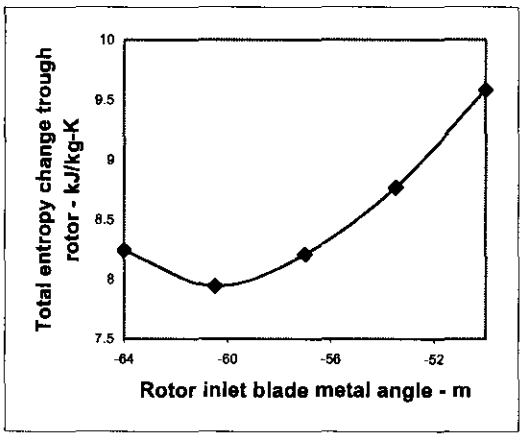

Fig 7.11 Effect of varying rotor inlet blade angle on total entropy change through the rotor

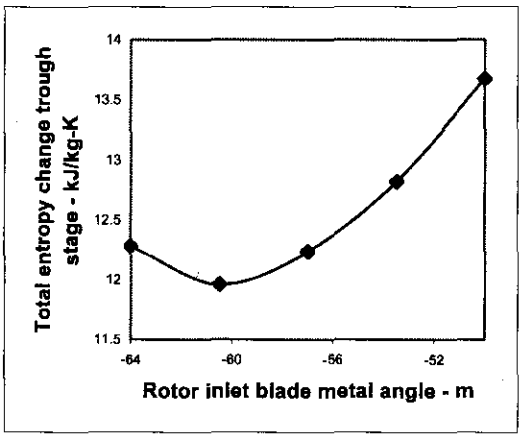

Fig 7.12 Effect of varying rotor inlet blade angle on stage total entropy change

Figure 7.11 and Figure 7.12 shows that there was little change in the total entropy change through the stator because of the variation in the rotor inlet blade angle. This can be deduced from the similar form of the two graphs. To investigate the relationship that this variation on stage entropy change has on the stage efficiency and pressure ratio, Figure 7.13 and Figure 7.14 were generated.

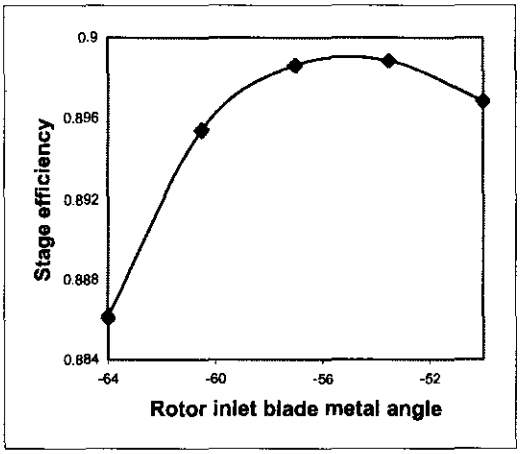

Fig 7.13 Effect of varying rotor inlet blade angle on stage total-to-total adiabatic efficiency

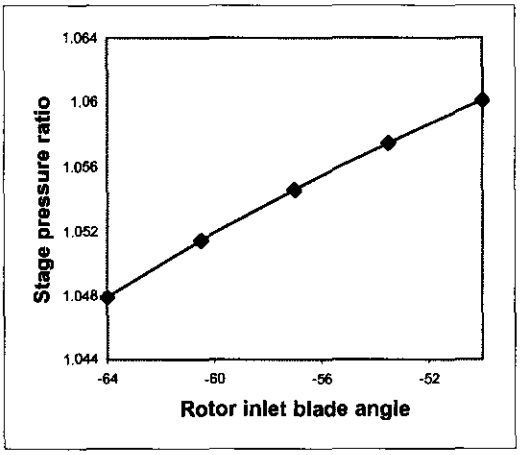

Fig 7.14 Effect of varying rotor inlet blade angle on stage total-to-total pressure ratio

It can be seen that, according to this investigation, there exists a different optimum angle for the rotor inlet blade angle for maximum stage efficiency or minimum entropy generation, i.e. loss. However, the larger the rotor inlet blade angle, the higher the pressure ratio for this case study. From the figures it can be seen that, for maximum stage efficiency, the rotor inlet blade angle must be changed from the current -59.5° to a value of approximately -55°. Although small, this change will increase the stage efficiency by about 0.3% and the pressure ratio by about 0.004.

7.5 Summary and conclusions

Chapter 7 aimed at presenting the reader with an illustration of the capabilities of the performance prediction code that was generated from this study. Furthermore, the influence of varying some of the loss parameters on stage efficiency was investigated in the hope that some conclusions can be made about their relative importance to accurate loss and stage efficiency prediction. In an attempt to illustrate the applicability of the code as an optimization or educational tool, a parametric case study was presented that investigated the influence of varying the rotor blade inlet angle on several performance variables.

It was found, from the parametric study of the influence of the axial spacing between the bladerows on stage efficiency, that closer bladerows leads to lower losses and higher stage efficiency. It was also seen that the effect becomes less important the further the blades are moved apart. However, it must be remembered that the models for deviation and profile loss do not take this parameter into account and further study on this result is advised. For a tip clearance increase, a large efficiency decrease was observed and it can therefore be concluded that tip clearance plays a major role, as expected, in the accurate prediction of efficiency. According to

Cumpsty (1989:344), however, the endwall loss model from Koch and Smith cannot be valid for stages with small or vanishing tip clearance and he further states that "Although the clearance flow seems to be beneficial when very small, typically not more than 1% of chord, at larger clearances the loss and the inception of stall appears to be dominated by the clearance flow behaviour." From the blade thickness investigation, it was concluded that the blade thickness should be kept as thin as possible, taking into account manufacturing restraints and strength considerations. It was also seen that 5% thickness to chord ratio is a good preliminary thickness estimate for modern subsonic compressor blades. Furthermore, it was found that there exists optimum chord and pitch values for the rotor and stator to obtain maximum stage efficiency, but the pitch of the rotor has the most influence. The effect of blade surface roughness also seems to be quite dramatic, and it was found that in this case, even a small improvement in the blade surface finish could improve the stage efficiency noticeably.

For the parametric studies concerning the part span shrouds, it was found that, as for the compressor blades, there exists an optimum shroud chord for maximum efficiency. It was also seen that the shroud should be as thin as possible and rather positioned closer to the hub than the tip.

An illustrative parametric case study was also presented. For this case study, it was investigated which value of the rotor inlet blade angle would give the highest stage efficiency with all the other parameters constant. It was found that there existed an optimum value for this parameter and the capability of using the code for basic optimization purposes was therefore successfully demonstrated.

The following chapter gives a brief summary and a condensed conclusion of the study on the modelling of losses in multi-stage axial compressors with subsonic conditions. It also gives recommendations for further research based on the knowledge gained as to the shortcomings of this study.

Chapter 8

CONCLUSION

Chapter 8 concludes this study by giving a short summary of the preceding chapters, conclusions that can be made from the results obtained and recommendations for future research.

8.1 Summary

In Chapter 1, the background leading to the study as well as a short overview of the main concepts contained in the study was given. Further aspects that received attention were the primary restrictions, the expected contributions and outline of the study. Chapter 2 described the mechanisms mainly responsible for the losses and gave more detail about the mechanisms that are commonly used in loss modelling.

Chapter 3 presented the reader with a comprehensive, but summarized literature survey regarding loss prediction methods for subsonic axial compressors. It was found that the loss mechanisms are interactive and complex by nature and methods of predicting them rely greatly on empirical correlations. Also, the open literature is rather diffused and the main groupings used in this chapter were: Blade profile losses, endwall losses including literature on tip leakage and secondary losses, part span shroud losses, other losses, losses due to high subsonic mach numbers and off-minimum losses.

Chapter 4 attempted to provide the reader with a framework into which the loss models can be integrated through presenting the theory required for a meanline compressor analysis. This chapter included discussions on methods of predicting minimum loss incidence, deviation, stall and choke as well as methods of estimating blade and annulus blockage. Chapter 5 presented the methodology employed for the generation of a performance prediction code, with general applicability to subsonic multi-stage compressors with different geometries and working fluids, which allows the interchanging of loss models. This utilized the models described in Chapters 3 and 4.

In Chapter 6 the code, developed in Chapter 5, was verified against a commercial software package called NREC and the different loss models were evaluated according to their simplicity, ease of implementation and accuracy. Finally, in Chapter 7, the validated EES-code was used to perform parametric studies on the influence of varying the geometric input parameters on overall stage loss and efficiency prediction. The aim is to form an idea as to which geometrical input parameters are the key players in improving efficiency and which loss parameters are crucial to accurate predictions. This was done to illustrate the ability of the code for performing such studies to be used as an aid in understanding compressor design and performance and for basic optimization problems.

8.2 Conclusion

In Chapter 1 it was stated that this study aims to contribute by improving subsonic multi-stage axial compressor expertise through investigating, and serving as a reference on, the internal loss mechanisms, the methods of predicting their magnitudes, their implementation and their use. It was further stated that the possibility of developing performance prediction software, with general applicability to subsonic multi-stage compressors with different geometries and working fluids, would be investigated.

The aforementioned were addressed by firstly providing the reader with a description of the loss mechanisms and the most influential of these were described in more detail. The next step was to present a comprehensive literature survey that improves this thesis's value as a reference on the available methods of quantifying the loss mechanisms. It was seen that it would be advantageous not to view the loss models in isolation from the concepts involved in axial compressor performance prediction. Therefore, this study also presents the theory for axial compressor ideal stage analysis as well as methods of predicting the other basic real fluid effects that are necessary for basic performance prediction. A software package called Engineering Equation Solver (EES) was used to implement the performance prediction theory and models. This code has the capability for the considered loss models to be interchanged and evaluated against each other or predictions from other performance prediction software. Verification was done by comparing the results from the EES-code with those of a commercial software package called NREC at different levels of complexity. This verification showed that the methodology used for implementing the loss models was employed correctly and that the basic performance prediction theory was correct. It is recommended that more test cases be considered for complete verification of the correlations and that, if possible, experimental data should also be used. However, this is not considered part of the scope of this study and will be left for future work.

The EES code was subsequently applied and it was found that the models given by Koch and Smith for the minimum profile loss, endwall loss and part span shroud loss (when applicable) with the model by Casey for the incidence loss and Denton's windage loss model was the most comprehensive combination of the loss models considered. For preliminary estimates near the design point, it was seen that the Lieblein model can be used for calculating the total profile loss, i.e. including the incidence loss. Also, any endwall loss models can be used, due to the large amount of uncertainty involved. Unfortunately, when using another endwall model than the one given by Koch and Smith, additional estimates for annulus blockage have to be included. Furthermore, parametric studies were performed to investigate the influence of some of the loss

parameters on stage efficiency and it was also illustrated how the EES-code can be used as an aid in understanding compressor design and performance and for basic optimization problems.

8.3 Recommendations for further research

The secondary outcome of this study resulted in a preliminary meanline performance prediction code. However, the code needs to be verified in more detail and some further research needs to be done before the code can be considered ready to be used with confidence. The following recommendations can be made regarding further work with the idea of improving the preliminary code:

- The EES-code should be reproduced in a lower-level programming language for increased stability and the equation sets for a whole compressor can then be solved simultaneously, rather than one stage at a time. This approach can be very advantageous when including the code in network analysis software.
- Further research should be conducted regarding the prediction of stall and choke and the models should be upgraded to reflect the state of the art for meanline methods.
- Further research should also be conducted on the aspect of annulus blockage and the prediction thereof. Especially, the blockage and how it is passed in simulations from one stage to the next, i.e. how it "grows" through the compressor, should be investigated and correctly implemented.
- A much broader spectrum of test cases, preferably experimental data, should be used for verification of the correlations used in the code as to derive correlations that would be the most suitable to the most cases and can be accepted as default correlations for all cases.
- More research should be done on methods of predicting the endwall loss due to the large variation seen in this study from the different correlations. Unfortunately, it was noted that great uncertainty surrounds this loss and ways to predict it.
- The code can be improved by including correlations for transonic and supersonic flows.
- It can also be considered to include simulations at other radial stations as the meanline.
- Finally, the conceptualism that internal loss manifests as an entropy increase through the compressor was accepted in this study and it is recommended that future loss modelling be done with this in mind. Denton (1993) did groundbreaking work in this regard and he rightfully suggests that every effort should be focused on understanding exactly how the loss mechanisms work rather than to blindly use the available correlations. It is, therefore, emphasized here that future studies on loss models should try and decrease the dependence on empirical data. The ultimate goal would be to generate models that are totally based on physical laws and are expressed in terms of the entropy increase it generates.

BOTHA, B W, 2002. **Advanced turbomachines.** *School of Mechanical and Materials Engineering. Potchefstroom University for Christian Higher Education,* Course: MEG 841

BROWN, L E, 1972. **Axial flow compressor and turbine loss coefficients: A comparison of several parameters.** *Transactions of the ASME. Journal of Engineering for Power,* 72-GT-18.

CASEY, M V, 1987. **A mean line prediction method for estimating the performance characteristic of an axial compressor stage.** *Turbomachinery – Efficiency prediction and improvement, I. Mech. E.,* Paper C264/87

CETIN, M; ÜCER, A S; HIRSCH, Ch; SEROVY, G K, 1989. **An off-design loss and deviation prediction study for transonic axial compressors.** *Transactions of the ASME. Presented at the Gas Turbine and Aeroengine Congress and Exposition, Toronto.*

COHEN, H; ROGERS, G F C; SARAVANAMUTTOO, H I H, 1996. **Gas turbine theory.** *Pearson Education Limited, Longman Group Limited,* ISBN 0-582-23632-0.

CONCEPTS NREC ETI Inc, 2003. **Concepts NREC - Axial.** Web: http://www.nrec.com. Date of access: September 2003.

CUMPSTY, N A, 1989. **Compressor aerodynamics.** 1st *ed, Longman Scientific & Technical,* ISBN 0-582-01364-X

De RUYCK, J; HIRSCH, C, 1980. **Investigations of an axial compressor end-wall boundary layer prediction method.** *Transactions of the ASME. Journal of Engineering for Power,* 80-GT-53.

DENTON, J D, October 1993. **Loss mechanisms in turbomachines.** *Transactions of the ASME. Journal of Turbomachinery,* 115:621-656

DIXON, S L, 1989. **Fluid mechanics and thermodynamics of turbomachinery.** 4th *ed, Butterworth-Heinemann,* ISBN 0-7506-7059-2

F-CHART SOFTWARE, 2003. **EES - Engineering Equation Solver.** Web: http://www.fchart.com. Date of access: September 2003.

HORLOCK, J H, 2000. **The determination of end-wall blockage in axial compressors: A comparison between various approaches.** *Transactions of the ASME. Journal of Turbomachinery,* 122:218-224

HOWELL, A R, 1945. **Design of axial compressors.** *Proceedings of the Institute if Mechanical Engineers, 153.*

HÜBNER, J; FOTTNER, L, 1996. **Influence of tip clearance, aspect ratio, blade loading, and inlet boundary layer on secondary losses in compressor cascades.** *Transactions of the ASME.* 96-GT-505

JAPIKSE, D; BAINES, N C, 1997. **Introduction to turbomachinery.** *2nd ed, Concepts ETI, Inc. Oxford University Press,* ISBN 0-933283-10-5.

KOCH, C C, October 1981. **Stalling pressure rise capability of axial flow compressor stages.** *Transactions of the ASME. Journal of Engineering for Power,* 103:645-655.

KOCH, C C; SMITH Jr., L H, July 1976. **Loss sources and magnitudes in axial-flow compressors.** *Transactions of the ASME. Journal of Engineering for Power,* 411- 424 p.

KÖNIG, W M; HENNECKE, D K; FOTTNER, L, January 1996. **Improved blade profile loss and deviation angle models for advanced transonic bladings.** *Transactions of the ASME. Journal of Turbomachinery,* 117:81-87 p.

LIEBLEIN, S, September 1959. **Loss and stall analysis of compressor cascades.** *Transactions of the ASME. Journal of Basic Engineering,* 387-400 p.

LIEBLEIN, S, September 1960. **Incidence and deviation angle correlations for compressor cascades.** *Transactions of the ASME. Journal of Basic Engineering,* 575-587 p.

M-TECH INDUSTRIAL (Pty) Ltd., 2003. **Flownex.** Web: http://www.mtechindustrial.com. Date of access: September 2003.

MILLER, D C, 1987. **Off-design prediction of compressor blade losses.** *Turbomachinery – Efficiency prediction and improvement, I. Mech. E.,* Paper C279/87

ROY, B; KUMAR, S, September 1999. **Reduced order loss modelling with tip clearance, aspect ratio and blockage effects for axial flow compressor.** *International Society for Air Breathing Engines and American Institute of Aeronautics & Astronautics.* ISABE 99-7190

SHAMES, I H, 1992. **Mechanics of fluids.** *3rd ed, McGraw Hill, Inc.,* ISBN 0-07-112815-8

SONG, T W; KIM, T S; KIM, J H; RO, S T, 2001. **Performance prediction of axial flow compressors using stage characteristics and simultaneous calculation of interstage parameters.** *Proceedings of the Institution of Mechanical Engineers. Journal of Power and Energy,* 215(A):89-98

STARKE, J, 1980. **The effect of the axial velocity density ratio on the aerodynamic coefficients of compressor cascades.** *Transactions of the ASME. Presented at the Gas Turbine Conference & Products show, New Orleans.*

SWAN, W C, July 1961. **A practical method of predicting transonic compressor performance.** *Transactions of the ASME. Journal of Engineering for Power,* 322-330 p.

WILSON, D G; KORAKIANITIS, T, 1998. **The design of high-efficiency turbomachinery and gas turbines.** *2nd ed, Prentice-Hall, Inc.,* ISBN 0-13-312000-7

Appendix A

ADDITIONAL LOSS MODEL INFORMATION

Appendix A.1

DENTON'S BLADE PROFILE LOSS MODEL

Denton's (1993:633-636) profile loss model for axial compressor blades supports the conceptualism of loss being equivalent to entropy production. Although not used in this study, it is included for the sake of completeness through presenting it in this appendix.

Denton (1993:633-636) estimated the two-dimensional loss coefficient for the blade boundary layers by dividing an expression for the total entropy produced in the boundary layers by the mass flow rate and a reference dynamic head. Thus, for low speed flow, the following expression results

$$\varsigma_s = 2\sum \frac{C_s}{p\cos\beta_1}\int_0^1 C_d\left(\frac{V_{bs}}{W_1}\right)^3 d\left(x/C_s\right) \qquad \text{(A.1.1)}$$

where the summation is for both blade surfaces, C_s is the total length of the blade surface and x is the surface distance. Also, C_d is the dissipation coefficient and resembles a dimensionless entropy production rate in the boundary layer. If the blade surface velocity distribution and the variation of C_d are known, Equation A.1.1 can be used to estimate the loss coefficient. This is, however, rarely the case.

It can be assumed that at the high turbulence levels in turbo machines, the transition from laminar to turbulent boundary layers will be in the Re_θ (Reynolds number based on momentum thickness, $\frac{W\theta}{\nu}$) region of 200 – 500, while the Re_θ at the trailing edge is usually in the range 500 – 2000 with some exceptions. For such conditions, C_d can be assumed constant at 0.002. This is a very crude approximation and, according to Denton, more detailed correlations and estimates for C_d can be found in papers published by Schlichting in 1979 and Truckenbrodt in 1952 for laminar flow. If the inlet and outlet flow angles are specified and a plausible velocity distribution are known or guessed, the pitch to chord ratio can be calculated from the tangential momentum change. An estimate of the loss can then be obtained from Equation A.1.1 while

keeping C_d constant at 0.002. This method produces a value for minimum loss that corresponds to an optimum pith-chord ratio. Varying the velocity distribution until an optimum $\frac{s}{c}$ ratio is found, this minimum loss can be estimated. Denton found that this method underestimates the minimum loss value and the prediction for the corresponding optimum ratio is too high. The minimum loss will occur when the boundary layer is on the verge of separation and this method seems not to take account of this. For more accurate results the loss should rise rapidly with diffusion factors greater than 0.55. The optimum pitch-chord ratio occurs just above that which gives a diffusion ratio of 0.55. For a complete stage the entropy generation should be considered relative to the stage enthalpy change. An isentropic velocity, W_i, is defined as

$$W_i = \sqrt{\frac{\Delta h_i}{0.5}} \tag{A.1.2}$$

and then the overall specific entropy increase due to the blade surface boundary layers may be estimated from

$$\Delta s \approx \Delta h_i 2 \frac{W_i}{V_x} \sum \frac{C_s}{p} \int_0^1 \frac{C_d}{T} \left(\frac{V_{bs}}{C_i} \right)^3 d\left(x / C_s \right) \tag{A.1.3}$$

where V_{bs} is the blade surface velocity. Denton confirms that a major contribution to the blade profile losses is the mixing loss from the blade boundary layers at the trailing edge. Some empirical results have been obtained and published for a large number of trailing edge shapes, but most of these are for turbines and he suggests an alternative method based on subtracting calculated blade boundary layer loss from measured profile losses. Denton (1993:653) presents a trailing edge loss coefficient as

$$\varsigma = \frac{-C_{pb} t}{\varepsilon} + \frac{2\theta}{\varepsilon} + \left(\frac{\delta + t}{\varepsilon} \right)^2 \tag{A.1.4}$$

where the first term on the right hand side is the loss due to the low base pressure acting on the trailing edge and is obtained from empirical data. The second term is the mixed out loss of the boundary layers on the blade surface just before the trailing edge and the third term arises from the combined blockage of the trailing edge and the boundary layers. Further, in Equation A.1.4, ε is the throat width between the blades.

Appendix A.2

KOCH AND SMITH BLADE PROFILE LOSS CORRELATIONS

The correlation figures for the blade profile loss model for axial compressors from Koch and Smith are presented here. The ratio of trailing edge momentum thickness to chord length, θ_{te}/c, and trailing edge form factor, H_{te} can found from Figure A.2.1 and Figure A.2.2 respectively.

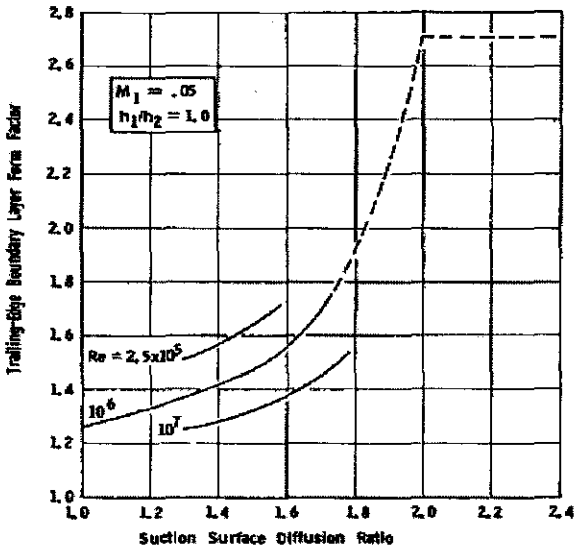

Fig. A.2.1 Koch and Smith correlation for $\frac{\theta_{te}}{c}$

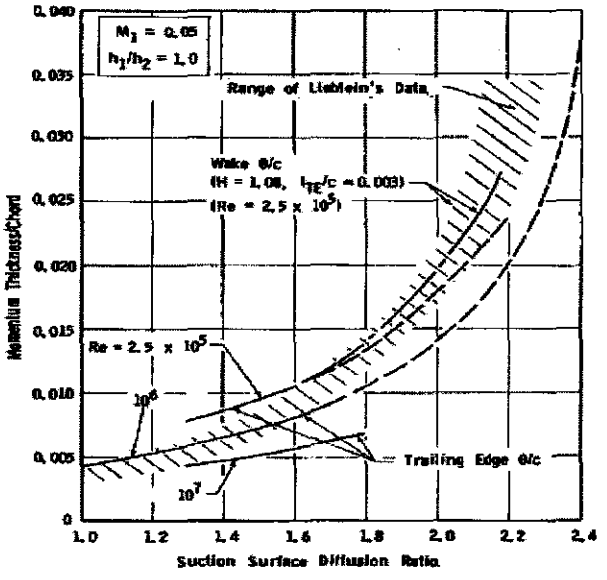

Fig. A.2.2 Koch and Smith correlation for H_{te}

A correction for inlet Mach number other than 0.05 is applied to the momentum thickness and form factor. Multipliers are given in Figure A.2.3.

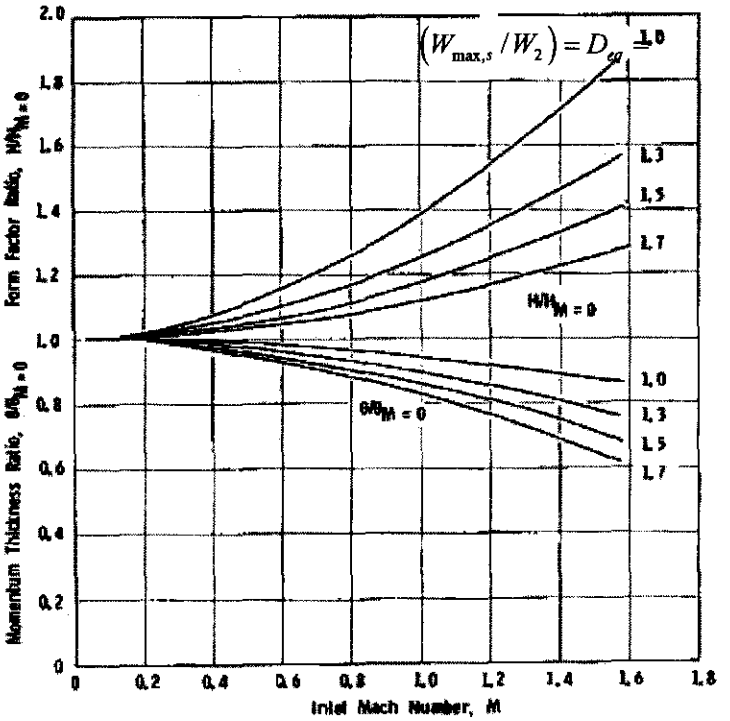

Fig. A.2.3 Effect of inlet Mach number on nominal trailing edge momentum thickness and form factor

Momentum thickness and form factor are corrected to streamtube convergence other than unity from the curves given in Figures A.2.4 and A.2.5.

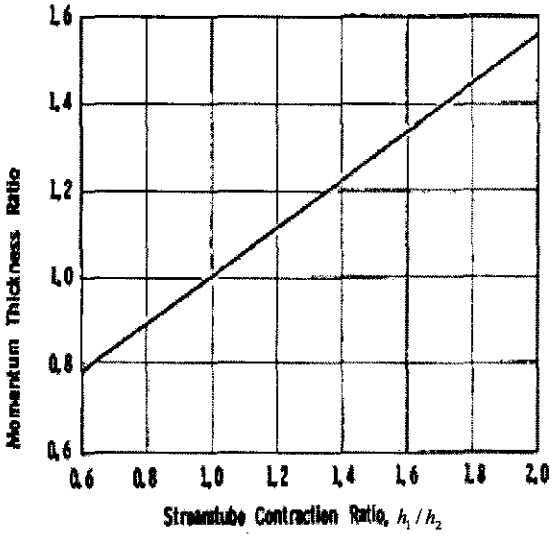

Fig. A.2.4 Effect of streamtube height variation on calculated trailing edge momentum thickness.

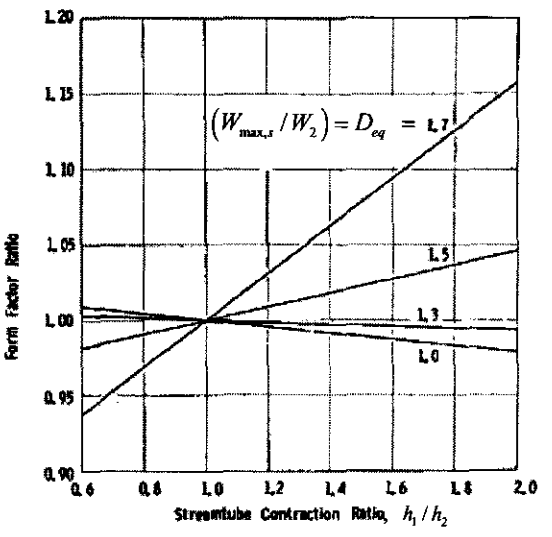

Fig. A.2.5 Effect of streamtube height variation on calculated trailing-edge form factor

A correction for Reynolds numbers other than 1×10^6 and blade surface roughness are then made according to Figure A.2.6 for momentum thickness.

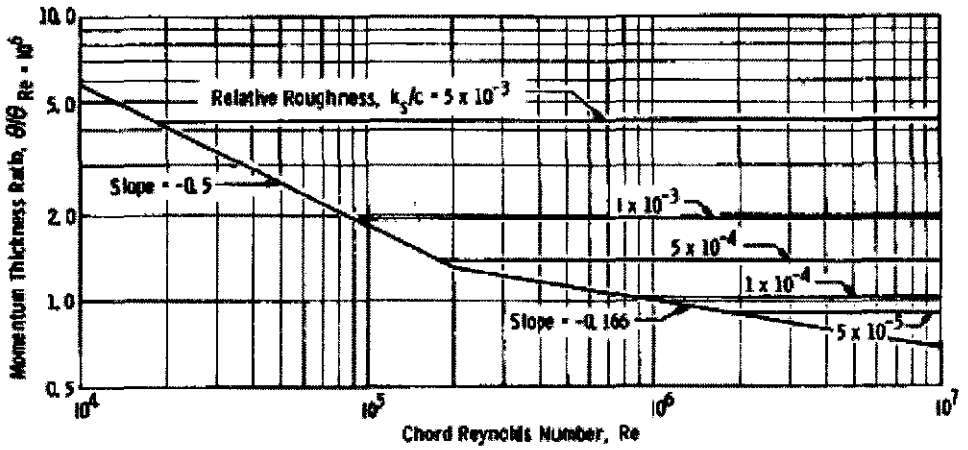

Fig. A.2.6 Effect of Reynolds number and surface finish on calculated trailing edge momentum thickness.

Reynolds number effects are only included for roughness Reynolds number below or equal to 90. Above this value the boundary layer characteristics do not change with Reynolds number and depend only on the ratio of blade surface roughness to chord. A similar correction factor is also applied to the form factor, but a –0.06 power variation is applied for all hydraulically smooth blades over the whole range of Reynolds numbers. In other words no transition effects are assumed for the form factor.

Appendix A.3

DENTON'S ENDWALL LOSS MODEL

Denton (1993:640) presents loss models for the tip clearance losses and endwall losses separately and defines them in terms of entropy generation. His models were included in this section due to his effort to find models that are based less on empirical results and calculate the loss as an entropy increase. The simple theory for the tip leakage flow of unshrouded blades was developed for incompressible flow, but can be extended to compressible flow.

Figure A.3.1 shows a graphical representation of tip leakage viewed as jet in a cross flow.

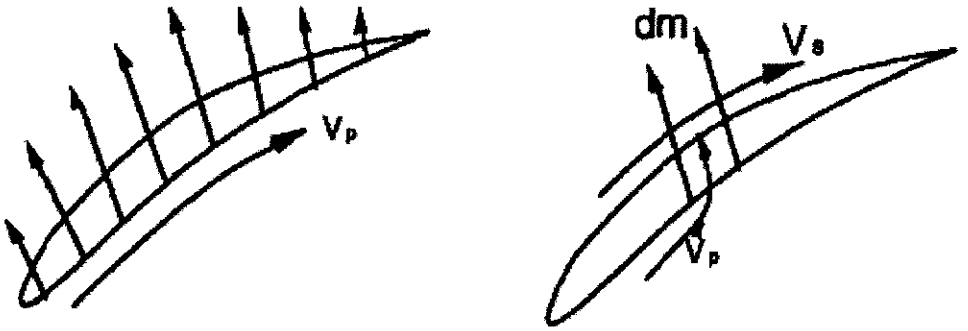

Fig. A.3.1 Tip leakage viewed as a jet in a cross flow

From Figure A.3.1 it can be seen that the leakage flow passes over the blade tip with the same velocity as the surface velocity on the pressure side, V_p, of the blade. The leakage flow rate is determined by a discharge coefficient, C_d, and the static pressure difference between the suction and pressure sides of the blade. The discharge coefficient can be calculated theoretically or determined empirically; Storer finds a typical value to be 0.8. The entropy generation caused by the mixing of the leakage flow, with velocity V_p and the surrounding flow with velocity V_s can be calculated from

$$\Delta s_{total} = \frac{C_d \tau c}{W_1 hp \cos\beta_1} \int_0^1 V_s^2 \left(1 - \frac{V_p}{V_s}\right) \sqrt{\left(V_s^2 - V_p^2\right)} \frac{dz}{c} \Big/_T \qquad \text{(A.3.1)}$$

where the integration is along the cord of the blade for a length dz.

The average values of V_s and V_p can be estimated crudely, if they are not known, by assuming the blade loading uniform along the blade span. From blade circulation

$$V_s - V_p \approx \frac{C_z}{\sigma}(\tan\beta_2 - \tan\beta_1) \tag{A.3.2}$$

and continuity, assuming thin blades,

$$V_s + V_p \approx \frac{2C_z}{\cos\beta} \tag{A.3.3}$$

with C_z the flow velocity in the axial direction. By assuming $\tan\beta$ to vary linearly in the axial direction, $\cos\beta$ may be reasonably estimated. Equation A.3.1 can now be numerically integrated to estimate the leakage loss of a blade.

Denton (1993:640) gives a short overview on the available methods to account for endwall losses, but cannot provide any alternative method to predict these losses and emphasizes the complexity of the flow in the endwall region. He suggests the use of the method proposed by Koch and Smith, but warns that it can only be used reliably with experimental data and on similar compressors.

Appendix A.4

KOCH AND SMITH ENDWALL LOSS CORRELATIONS

This section present the correlations obtained by Koch and Smith for the endwall boundary layer. Figure A.4.1 shows $\frac{2\bar{\delta}}{g}$ plotted against the stage static pressure rise coefficient relative to the maximum static pressure rise coefficient of which the stage is capable. The maximum static pressure rise of which the stage is capable is the static pressure rise coefficient at the stalling point. The different lines are for different stage averaged normalized clearance values, which is the weighted average of the stator and rotor clearances normalized by the staggered spacing at the mean diameter. The weighting function is the inlet dynamic heads of the respective blade rows.

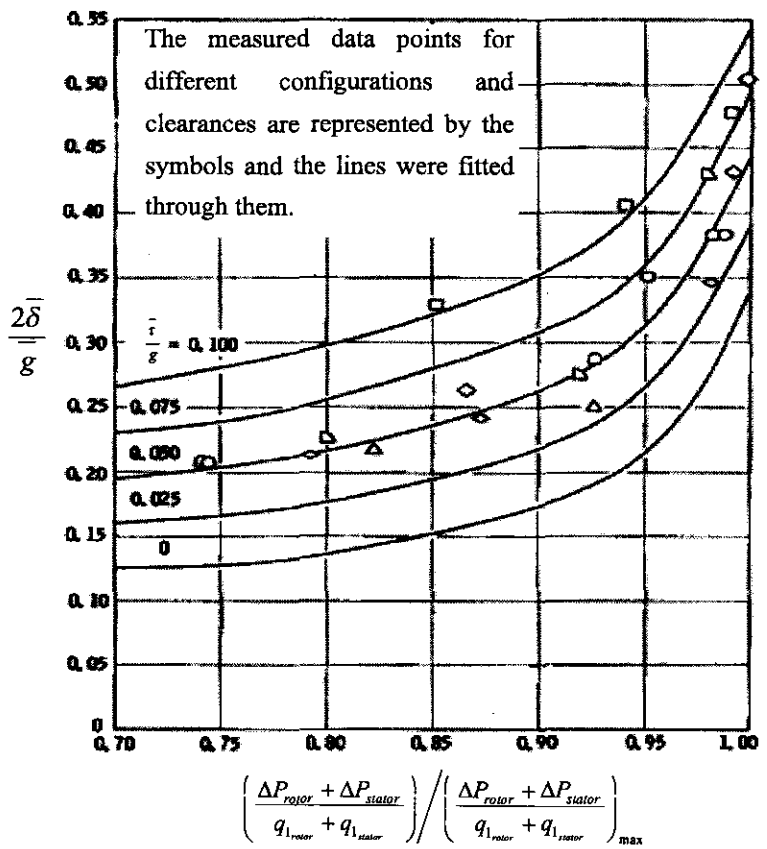

Fig. A.4.1 Sum of the endwall displacement thickness

The lines shown in Figure A.4.1 are related by

$$\frac{2\bar{\delta}}{g} = \left.\frac{2\bar{\delta}}{g}\right|_{\bar{\tau}/g=0} + 2\bar{\tau}/g \left[\left(\frac{\Delta P_{rotor} + \Delta P_{stator}}{q_{1_{rotor}} + q_{1_{stator}}} \right) \Big/ \left(\frac{\Delta P_{rotor} + \Delta P_{stator}}{q_{1_{rotor}} + q_{1_{stator}}} \right)_{\max} \right] \qquad \text{(A.4.1)}$$

Figure A.4.1 was obtained for configurations having axial gap (axial distance between blade rows) / tangential gap (pitch) ratios in the range between 0.3-0.4. For ratios outside this range a correction must be applied to $\bar{\delta}$ according to Figure A.4.2. This applies only to axial gap/pitch ratios of less than 0.7. For ratios larger than 0.7 the effect of the annulus wall skin friction drag should be included.

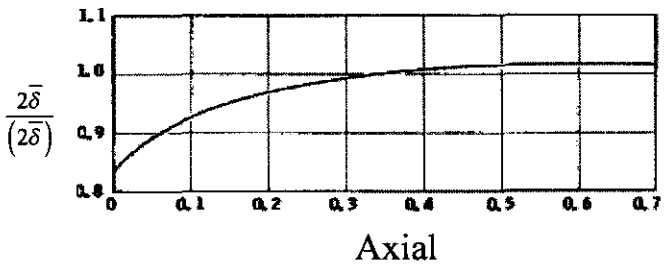

Fig. A.4.2 Effect of axial gap between blade row edges on endwall boundary layer displacement thickness

The tangential force thickness data obtained from the measurements showed no consistent trend in the data and a single line, shown in Figure A.4.3, has been adopted. The data points for the different configurations can also be seen.

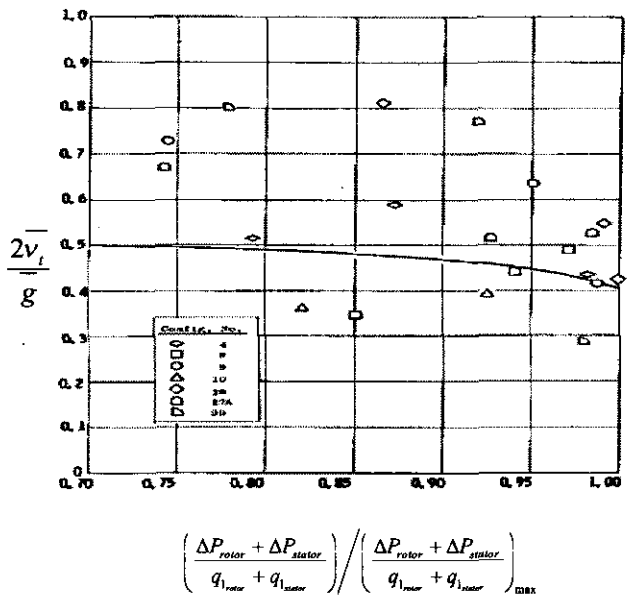

Fig. A.4.3 Sum of hub and tip endwall boundary layer tangential force thicknesses

Appendix B

ADDITIONAL PERFORMANCE PREDICTION INFORMATION

Appendix B.1

MINIMUM LOSS INCIDENCE CORRELATION FIGURES

The minimum loss incidence correlation figures of Lieblein (1960) are presented here. Figure B.1.1 shows the slope of the variation in incidence. Figure B.1.2 presents the minimum loss incidence for a NACA-65 cascade of zero camber and 10 percent thickness to chord ratio and Figure B.1.3 gives the correction factor for different thickness to chord ratios.

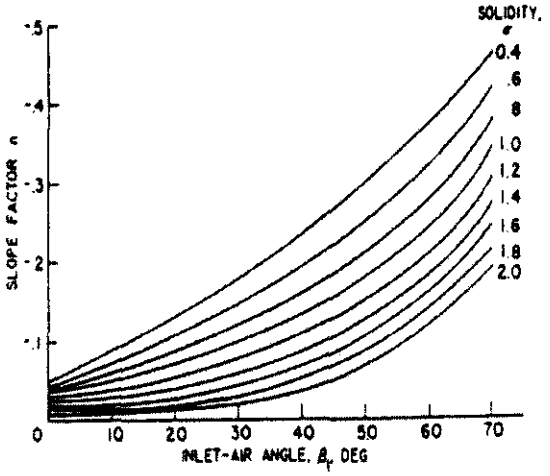

Fig. B.1.1 Minimum loss incidence angle slope factor

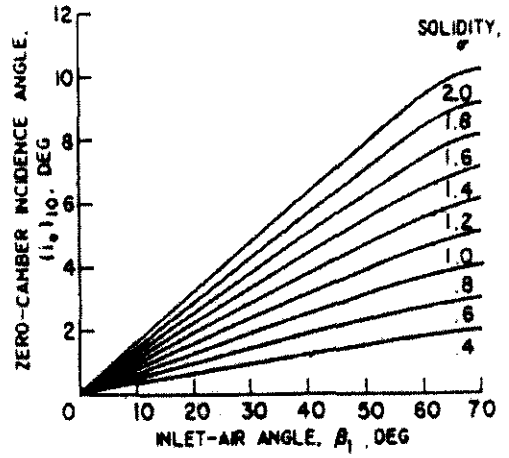

Fig. B.1.2 Minimum loss incidence angle for 10 % *thickness to chord ratio NACA 65 blades*

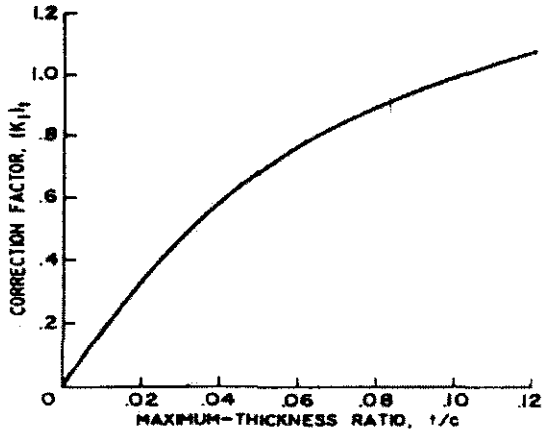

Fig. B.1.3 Correction factor for different thickness to chord ratios

Appendix B.2

DEVIATION CORRELATION FIGURES

In this section the correlation figures for calculating the deviation at minimum loss condition and off-minimum losses are presented as given by Lieblein (1960). Figure B.2.1 gives the slope factor of the deviation angle variation with camber at a solidity of unity. Figure B.2.2 shows the solidity exponent variable with air inlet angle and Figure B.2.3 gives the basic variation for the NACA-65 blade profile with a ten percent thickness distribution. Figure B.2.4 presents the correction necessary for blades with a maximum thickness other than 10 percent. The slope of the deviation angle variation at the minimum-loss incidence angle and can be found from Figure B.2.5.

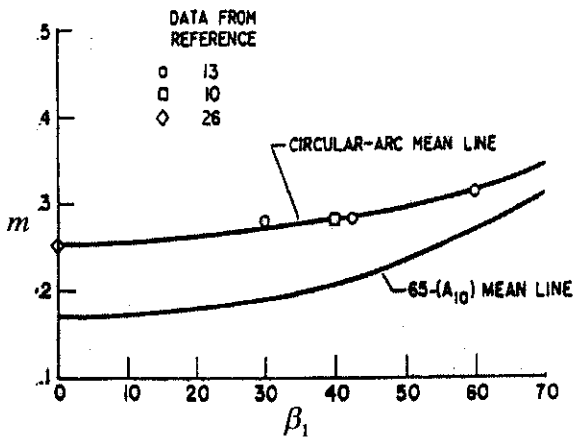

Fig. B.2.1 Slope factor at unity solidity

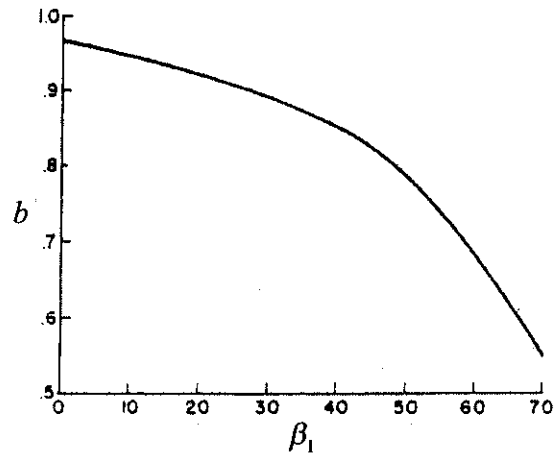

Fig. B.2.2 Solidity exponent in deviation angle rule

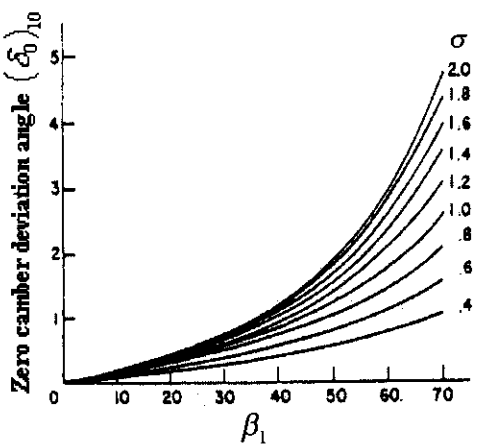

Fig. B.2.3 Basic variation for the NACA-65 blade profile with a ten percent thickness distribution

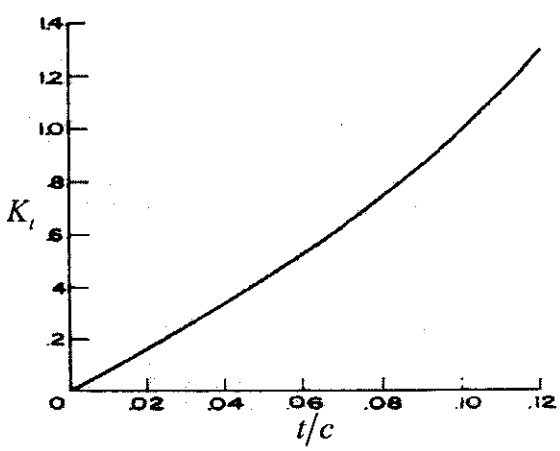

Fig. B.2.4 Correction necessary for blades with a maximum thickness other than 10 percent

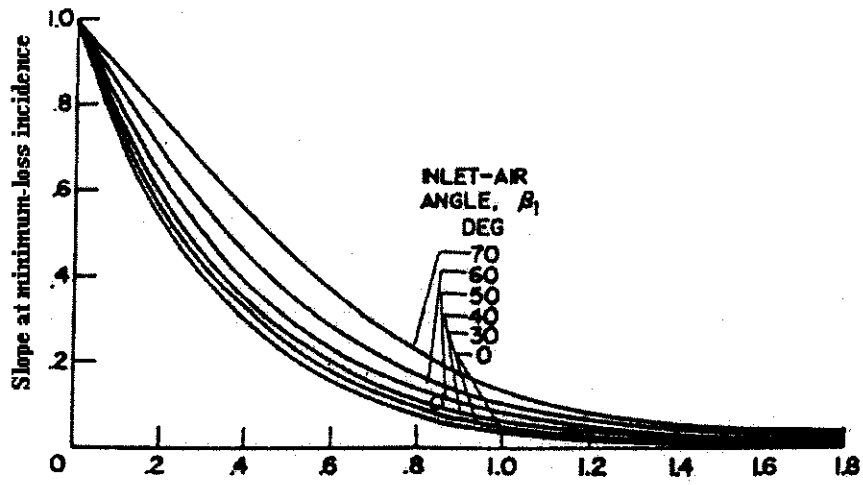

Fig. B.2.5 Slope of the deviation angle variation at the minimum-loss incidence angle

Appendix B.3

KOCH'S STALLING PRESSURE RISE CORRELATION FIGURES

This section gives the correlation figures for predicting the stage stalling static pressure rise coefficient according to Koch (1981) and adjustments made by Casey (1987). Figure B.3.1 gives the modified correlation of Koch according to Casey for the static pressure rise coefficient from the diffuser data to provide even a better fit and also shows the De Haller diffusion limit and the fit used by Koch. Figure B.3.2, B.3.3 and B.3.4 gives the Reynolds number correction factor, a correction for tip clearance effects and the correction for axial spacing between the blade rows respectively.

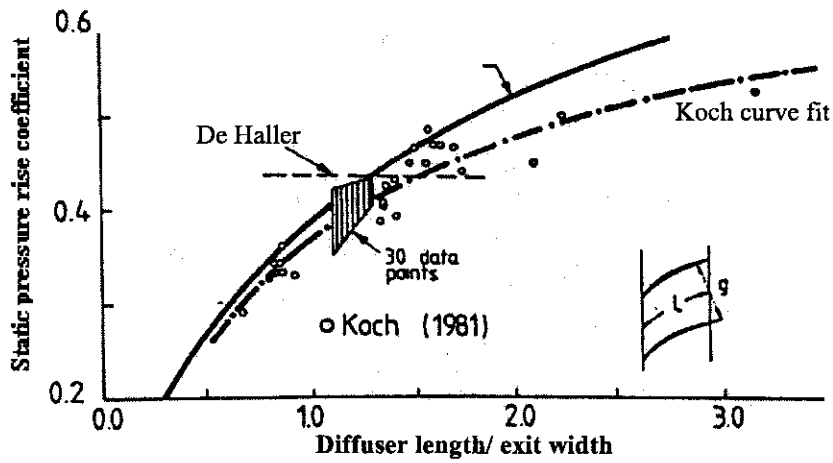

Fig. B.3.1 Modified correlation of Koch according to Casey for diffuser data

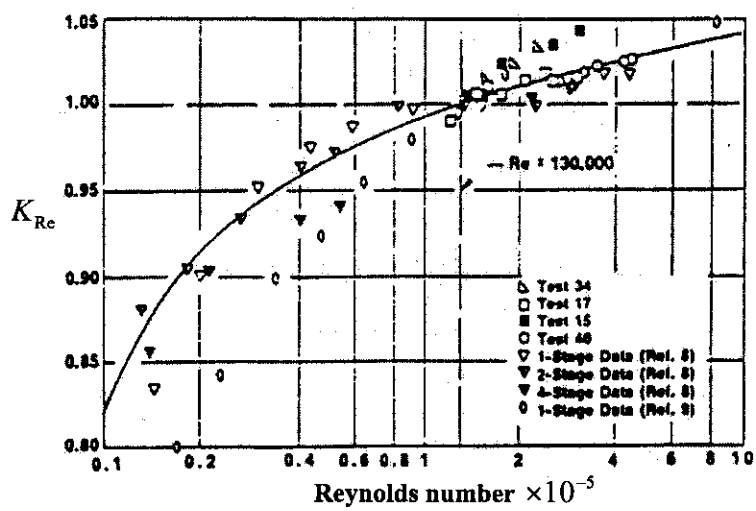

Fig. B.3.2 Reynolds number correction factor

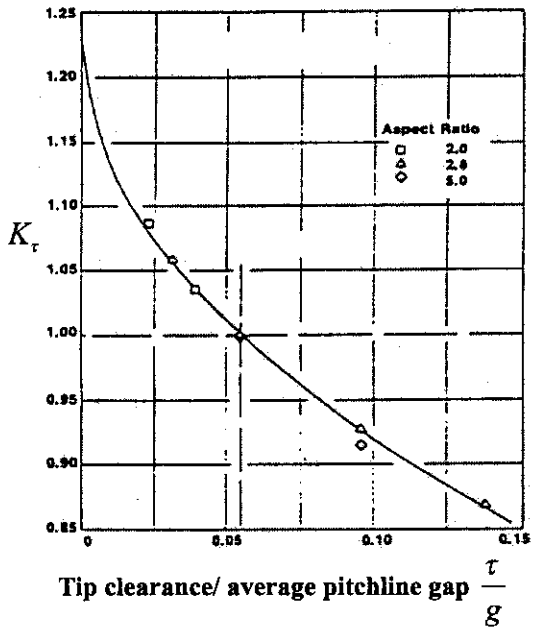

Fig. B.3.3 Correction factor for tip clearance effects

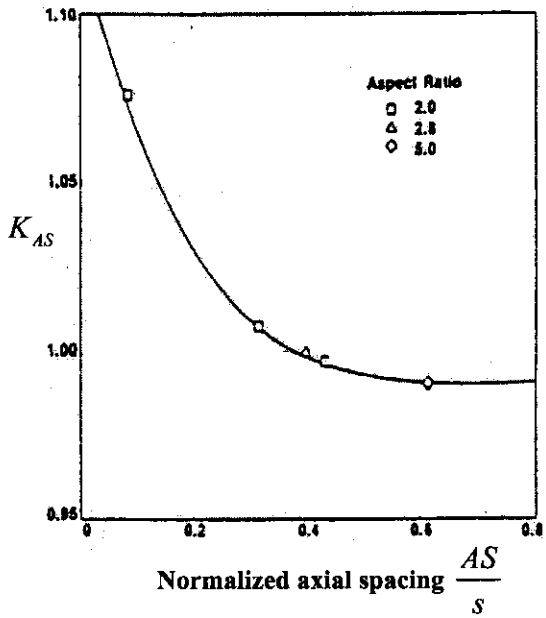

Fig. B.3.4 Correction factor for axial spacing between the blade rows

Appendix C

ADDITIONAL IMPLEMENTATION INFORMATION

Appendix C.1

PROGRAM ALGORITHM

The algorithm given in Figure C.1.1 presents the recommended basic logical structure of the code for axial compressor performance prediction. The arrows point both ways to indicate that inputs are given when called and the necessary outputs are provided to the calling structure. Modules, procedures and functions can be used and updated separate from the code, as long as values for the required input variables are provided. It must be emphasized that the modules are solved implicitly in one equation set with the main program and that the equation order in modules or the calling of program structures are not important. The Koch and Smith endwall loss model is called in the stage module and values for the endwall boundary layer displacement thickness and stage endwall loss are returned with each run to the rotor and stator modules. The endwall boundary layer displacement thickness are used in the annulus blockage factor (*ABF*) calculation and the endwall loss entropy change for the stage are assigned to the respective bladerow by means of a row factor when the Koch and Smith model is used.

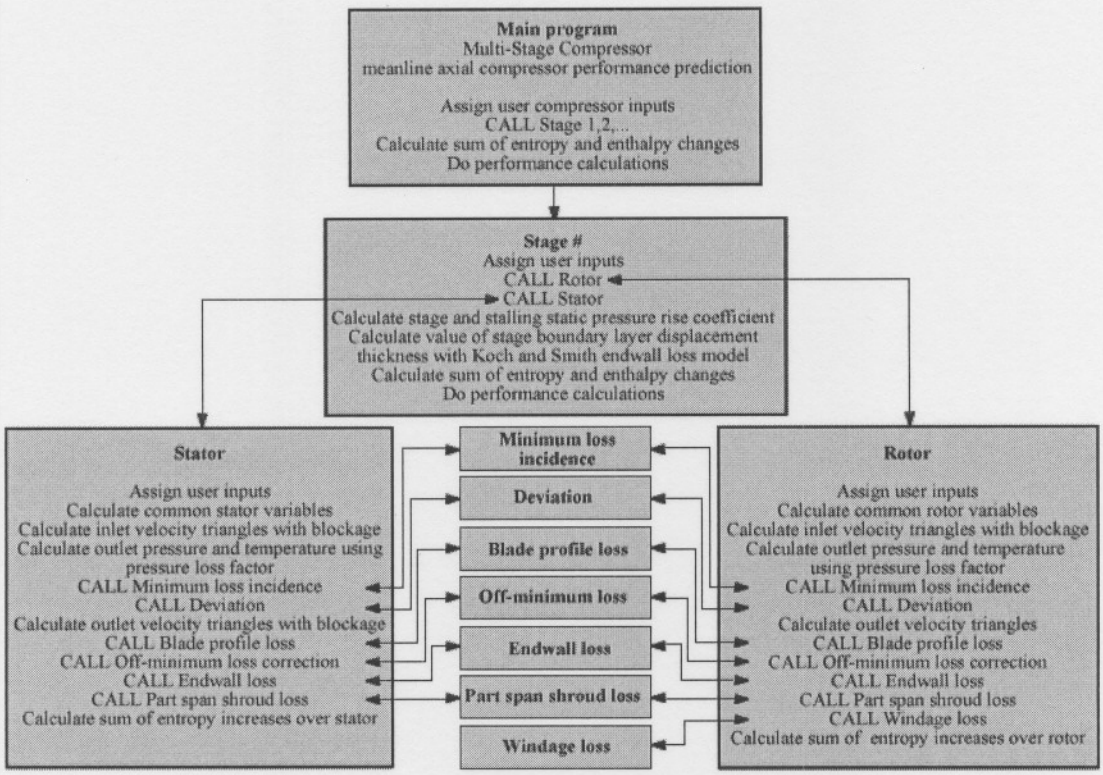

Fig. C.1.1 Basic code algorithm

Appendix C.2

USER VARIABLE INPUTS

The values that need to be supplied by the user for this study are given in Table C.2.1.

Table C.2.1: User supplied variables

General compressor user inputs		
Variable	**Description**	**Units**
N	Compressor rotational speed	rpm
$Fluid$	Defines working fluid – EES variable	-
T_{01}	Compressor inlet stagnation temperature	K
P_{01}	Compressor inlet stagnation pressure	kPa
α_1	Compressor absolute inflow angle – Either from IGV or zero	°
ABF_{in}	Inlet annulus blockage factor	-
$\dot{m}$	Compressor inlet mass flow rate	kg/s
Stage user inputs		
$\dot{m}_{bleed}$	Value to simulate interstage bleed flows and represents the bleed flow rate	kg/s
AS	Axial spacing between blade rows	m
Rotor		
τ_{rtr}	Rotor tip clearance	m
ξ_{rtr}	Rotor stagger angle	°
$\chi_{1_{rtr}}, \chi_{2_{rtr}}$	Rotor blade metal angle at leading and trailing edge	°
r_{t_1}, r_{t_2}	Rotor blade tip radius at leading and trailing edge	m
r_{hb_1}, r_{hb_2}	Rotor blade hub radius at leading and trailing edge	m
$t_{\max_{rtr}}$	Maximum rotor blade thickness	m
c_{rtr}	Rotor blade chord	m
s_{rtr}	Rotor blade pitch	m
$k_{CLA_{rtr}}$	Rotor blade surface roughness	m
r_{sh}, t_{sh}, c_{sh}	Part span shroud radius, thickness and chord	m

Stator		
τ_{str}	Stator tip clearance	m
ξ_{str}	Stator stagger angle	°
$\chi_{2_{str}}, \chi_{3_{str}}$	Stator blade metal angle at leading and trailing edge	°
r_{t_3}	Stator blade tip radius at trailing edge. Leading edge radius assumed equal to rotor trailing edge radius	m
r_{hb_3}	Stator blade hub radius at trailing edge. Leading edge radius assumed equal to rotor trailing edge radius	m
$t_{\max_{str}}$	Maximum stator blade thickness	m
c_{str}	Stator blade chord	m
s_{str}	Stator blade pitch	m
$k_{CLA_{str}}$	Stator blade surface roughness	m
r_{sh}, t_{sh}, c_{sh}	Part span shroud radius, thickness and chord	m

The user inputs are supplied to EES using Lookup tables. The user can change the variables without having to change values in the code. An example of the Lookup tables with representative input values are given in Figure C.2.1 and C.2.2, with each row representing a stage and its position in the compressor in the Stage input table.

Stage inputs | Inlet comp

	1 Fluid [-]	2 N [rpm]	3 T_0 [K]	4 P_0 [kPa]	5 α_1 [degrees]	6 ABF_{in} [-]	7 $\dot{m}$ [kg/s]
Row 1	Helium	9000	299.3	4497	12	1	152

Fig. C.2.1 EES Lookup table for compressor inlet user input

Stage inputs | Inlet comp

	1 $\dot{m}_{bleed}$ [kg/s]	2 AS [m]	3 τ_{rtr} [m]	4 ξ_{rtr} [deg]	5 $\chi_{1,rtr}$ [deg]	6 $\chi_{2,rtr}$ [deg]	7 $r_{t,1}$ [m]	8 $r_{t,2}$ [m]	9 $r_{hb,1}$ [m]	10 $r_{hb,2}$ [m]	11 $t_{max,rtr}$ [m]	12 c_{rtr} [m]
Row 1	0	0.015	0.001	50.9	-59.5	-46	0.392	0.391	0.3335	0.3335	0.002955	0.0356
Row 2	0	0.015	0.001	50.9	-59.5	-46	0.39	0.389	0.3335	0.3335	0.002955	0.0356
Row 3	0	0.015	0.001	50.9	-59.5	-46	0.388	0.387	0.3335	0.3335	0.002955	0.0356
Row 4	0	0.015	0.001	50.9	-59.5	-46	0.386	0.385	0.3335	0.3335	0.002955	0.0356

Fig. C.2.2 Part of EES Lookup table for stage user input, each row represents a stage

Appendix C.3

LOSS MODEL FORMATTED EQUATION SETS

Chapter 5 presents the discussion on the implementation of the loss models into EES for generating the performance prediction code for axial compressors with subsonic conditions. This appendix gives the formatted equations for each loss model and shows how they are implemented in EES using modules, procedures and functions. In the calling arguments for modules and procedures, the variables to the right of the semicolon are returned to the calling program structure.

C.3.1 Profile loss – Lieblein

MODULE $\mathbf{Profile_{Loss,Lieblein}}(\beta_1, \beta_2, \sigma, c : \bar{\omega}_{min}, block)$

$H_{ex} = 1.08$

$$D_{eq} = \frac{\cos(\beta_2)}{\cos(\beta_1)} \cdot \left[1.12 + 0.61 \cdot \frac{\cos^2(\beta_1)}{\sigma} \cdot (\tan(\beta_2) - \tan(\beta_1))\right]$$ Equation 3.3

$$\frac{\theta_{ex}}{c} = \frac{0.0045}{1 - 0.95 \cdot \ln(D_{eq})}$$ Equation 3.2

Profile loss calculation

$$\bar{\omega}_{min} = 2 \cdot \frac{\theta_{ex}}{c} \cdot \frac{\sigma}{\cos(\beta_2)} \cdot \left[\frac{\cos(\beta_1)}{\cos(\beta_2)}\right]^2$$ Equation 3.4

$block = 0$ Module needs to return blockage value

END $\mathbf{Profile_{Loss,Lieblein}}$

C.3.2 Profile loss – Koch and Smith

The implementation of the Koch and Smith profile loss correction factors are done through including them in functions which return their values to the Koch and Smith profile loss module. The correction factor functions are given here below the module, but in EES they need to be above the calling program structure.

MODULE $\mathbf{Profile_{Loss,Koch,Smith}}(r_{rms,1}, r_{rms,2}, C_{theta,1}, C_{theta,2}, Re_o, \mu, c, k_{CLA}, h_{ratio}, A_1, A_2, \sigma, t_{max}, \beta_1, \beta_2, W_1, W_2, M_1, M_{z,1}, \rho_1 : \bar{\omega}_{min}, block)$

$$\Gamma = \frac{r_{rms,1} \cdot C_{\theta,1} - r_{rms,2} \cdot C_{\theta,2}}{\left[\frac{r_{rms,1} + r_{rms,2}}{2}\right] \cdot \sigma \cdot W_1}$$ Equation 3.13

$$A_p = \left[1 - 0.4458 \cdot \sigma \cdot \frac{\frac{t_{max}}{c}}{\cos\left(\frac{\beta_1 + \beta_2}{2}\right)}\right] \cdot \left[1 - \left(\frac{A_1 - A_2}{3 \cdot A_1}\right)\right]$$ Equation 3.11

$$\frac{\rho_p}{\rho_1} = 1 - \left[\left(\frac{M_{z,1}^2}{1 - M_{z,1}^2}\right) \cdot \left(1 - A_p - 0.2445 \cdot \frac{\tan(\beta_1)}{\cos(\beta_1)} \cdot \sigma \cdot \Gamma\right)\right]$$ Equation 3.12

$$\frac{\rho_p}{\rho_1} = 1 - \left[\left(\frac{M_{z,1}^2}{1 - M_{z,1}^2}\right) \cdot \left(1 - A_p - 0.2445 \cdot \frac{\tan(\beta_1)}{\cos(\beta_1)} \cdot \sigma \cdot \Gamma\right)\right]$$ Equation 3.12

$$\frac{V_p}{W_1} = \left[(\sin(\beta_1) - 0.2445 \cdot \sigma \cdot \Gamma)^2 + \left(\frac{\cos(\beta_1)}{A_p \cdot \frac{\rho_p}{\rho_1}}\right)^2\right]^{(1/2)}$$ Equation 3.9

$$\frac{V_{max}}{V_p} = 1 + 0.7688 \cdot \frac{t_{max}}{c} + 0.6024 \cdot \Gamma$$ Equation 3.10

$$D_{eq} = \frac{W_1}{W_2} \cdot \frac{V_{max}}{V_p} \cdot \frac{V_p}{W_1}$$ Equation 3.8

Apply corrections for conditions other than nominal

$K_{e,1} = \mathbf{KMM}(M_1, D_{eq})$ Correction factor for inlet Mach number effect

$K_{e,2} = \mathbf{KSTM}(h_{ratio})$ Correction factor for stream tube contraction effects

$K_{e,3} = \mathbf{KRSM}(Re_c, k_{CLA}, c, W_1, \rho_1, \mu)$ Correction factor for Reynolds numer and surface finish effects

$K_{total,e} = K_{e,1} \cdot K_{e,2} \cdot K_{e,3}$ Calculation of total correction factor for Momentum thickness

$K_{H,1} = \mathbf{KMH}(M_1, D_{eq})$ Correction factor for Mach number effects

$K_{H,2} = \mathbf{KSTH}(h_{ratio}, D_{eq})$ Correction factor for stream tube contraction effects

$K_{H,3} = \mathbf{KRSH}(Re_c, k_{CLA}, c, W_1, \rho_1, \mu)$ Correction factor for Reynolds numer and surface finish effects

$K_{total,H} = K_{H,1} \cdot K_{H,2} \cdot K_{H,3}$ Calculation of total correction factor for From factor

$$\frac{\theta_{te}}{c} = (0.0025 - 0.352407 + 1.23 \cdot D_{eq} - 1.678 \cdot D_{eq}^2 + 1.131 \cdot D_{eq}^3 - 0.3755 \cdot D_{eq}^4 + 0.04933 \cdot D_{eq}^5) \cdot K_{total,e}$$

Figure A.2.1 - 0.0025 adder included

$$H_{te} = (0.5413 - 0.72941463 \cdot D_{eq} + 4.206 \cdot D_{eq}^2 - 3.8628472 \cdot D_{eq}^3 + 1.107 \cdot D_{eq}^4) \cdot K_{total,H}$$ Figure A.2.2

Profile loss calculation

$$\bar{\omega}_{min} = 2 \cdot \frac{\theta_{te}}{c} \cdot \frac{\sigma}{\cos(\beta_2)} \cdot \left[\frac{\cos(\beta_1)}{\cos(\beta_2)}\right]^2 \cdot \left[\frac{2}{3 - \frac{1}{H_{te}}}\right] \cdot \left[1 - \frac{\theta_{te}}{c} \cdot \frac{\sigma \cdot H_{te}}{\cos(\beta_2)}\right]^{-3}$$ Equation 3.1

$block = \theta_{te} \cdot H_{te}$ Calculation of boundary layer displacement thickness - blade blockage

END $\mathbf{Profile}_{Loss,Koch,Smith}$

Koch and Smith profile loss correction factors ==========

Function KMM (M, D_{eq})

Function for calculating correction factors for mach number effects on momentum thickness - Figure A.2.3

If ((1 <= D_{eq}) and (D_{eq} < 1.3)) Then

Y1 := 1 - 0.00151 · M - 0.05544 · M^2 Correction factor equation for D_{eq} = 1

Y2 := 1 - 0.00205 · M - 0.10085 · M^2 Correction factor equation for D_{eq} = 1.3

KMM := Interpol (1, 1.3, Y1, Y2, D_{eq})

Else

If ((1.3 <= D_{eq}) and (D_{eq} < 1.5)) Then

Y1 := 1 - 0.00205 · M - 0.10085 · M^2 Correction factor equation for D_{eq} = 1.3

Y2 := 1 - 0.02936 · M - 0.11103 · M^2 Correction factor equation for D_{eq} = 1.5

KMM := Interpol (1.3, 1.5, Y1, Y2, D_{eq})

Else

If ((1.5 <= D_{eq}) and (D_{eq} <= 1.7)) Then

Y1 := 1 - 0.02936 · M - 0.11103 · M^2 Correction factor equation for D_{eq} = 1.5

Y2 := 1 - 0.02627 · M - 0.151 · M^2 Correction factor equation for D_{eq} = 1.7

KMM := Interpol (1.5, 1.7, Y1, Y2, D_{eq})

```
    Else
      If ((1.3 <= Deq) and (Deq < 1.5)) Then
        Y1 := 1 - 0.00205 · M - 0.10085 · M^2          Correction factor equation for Deq = 1.3
        Y2 := 1 - 0.02936 · M - 0.11103 · M^2          Correction factor equation for Deq = 1.5
        KMM := Interpol (1.3, 1.5, Y1, Y2, Deq)
      Else
        If ((1.5 <= Deq) and (Deq <= 1.7)) Then
          Y1 := 1 - 0.02936 · M - 0.11103 · M^2        Correction factor equation for Deq = 1.5
          Y2 := 1 - 0.02627 · M - 0.151 · M^2          Correction factor equation for Deq = 1.7
          KMM := Interpol (1.5, 1.7, Y1, Y2, Deq)
        Else
          Call WARNING ('Eq Diffusion ratio > 1.7 u..')   Display warning if Deq is out of range
          KMM := 1 - 0.02627 · M - 0.151 · M^2         Use value of Deq = 1.7 for higher values of Deq
        EndIf
      EndIf
    EndIf
End KMM


Function KMH (M, Deq)
Function for calculating correctional multipliers for mach number effects on form factor - Figure A.2.3
  If ((1 <= Deq) and (Deq <= 1.3)) Then
    Y1 := 1 + 0.08796 · M + 0.27474 · M^2              Correction factor equation for Deq = 1
    Y2 := 1 + 0.04192 · M + 0.1995 · M^2               Correction factor equation for Deq = 1.3
    KMH := Interpol (1, 1.3, Y1, Y2, Deq)
  Else
    If ((1.3 <= Deq) and (Deq < 1.5)) Then
      Y1 := 1 + 0.04192 · M + 0.1995 · M^2             Correction factor equation for Deq = 1.3
      Y2 := 1 + 0.01736 · M + 0.14414 · M^2            Correction factor equation for Deq = 1.5
      KMH := Interpol (1.3, 1.5, Y1, Y2, Deq)
    Else
      If ((1.5 <= Deq) and (Deq <= 1.7)) Then
        Y1 := 1 + 0.01736 · M + 0.14414 · M^2          Correction factor equation for Deq = 1.5
        Y2 := 1 + 0.02241 · M + 0.09155 · M^2          Correction factor equation for Deq = 1.7
        KMH := Interpol (1.5, 1.7, Y1, Y2, Deq)
      Else
        KMH := 1 + 0.02241 · M + 0.09155 · M^2         Correction factor equation for Deq = 1.7
      EndIf
    EndIf
  EndIf
End KMH
```

Function **KSTM** (h_{ratio})

Function for calculating correction factor for stream tube contraction ratio effects on momentum thickness - Figure A.2.4

KSTM := 0.45 + 0.55 · h_{ratio}

End **KSTM**

Function **KSTH** (h_{ratio}, D_{eq})

Function for calculating correction factor for stream tube contraction ratio effects on form factor - Figure A.2.5

If ((1 <= D_{eq}) and (D_{eq} < 1.3)) Then

Y1 := 1.02114 − 0.02057 · h_{ratio}

Y2 := 1.00829 − 0.00714 · h_{ratio} Correction factor equation for D_{eq} = 1

KSTH := **Interpol** (1 , 1.3 , Y1 , Y2 , D_{eq})

Else

If ((1.3 <= D_{eq}) and (D_{eq} < 1.5)) Then

Y1 := 1.00829 − 0.00714 · h_{ratio} Correction factor equation for D_{eq} = 1.3

Y2 := 0.95457 + 0.04571 · h_{ratio} Correction factor equation for D_{eq} = 1.5

KSTH := **Interpol** (1.3 , 1.5 , Y1 , Y2 , D_{eq})

Else

If ((1.5 <= D_{eq}) and (D_{eq} <= 1.7)) Then

Y1 := 0.95457 + 0.04571 · h_{ratio} Correction factor equation for D_{eq} = 1.5

Y2 := 0.84457 + 0.15571 · h_{ratio} Correction factor equation for D_{eq} = 1.7

KSTH := **Interpol** (1.5 , 1.7 , Y1 , Y2 , D_{eq})

Else

KSTH := 0.84457 + 0.15571 · h_{ratio} Correction factor equation for D_{eq} = 1.7

EndIf

EndIf

EndIf

End **KSTH**

Function **KRSM** (Re_c, k_{CLA}, c, W_1, ρ, μ)

Function for calculating correction factor for Reynolds number and surface finish effects on Momentum thickness ratio - Figure A.2.6

$k_s := 6.2 \cdot k_{CLA}$ Equation 3.7

$RR := \frac{k_s}{c}$ Relative roughness

$RRe := \frac{k_s \cdot W_1 \cdot \rho}{\mu}$ Roughness Reynolds number

If (RRe <= 90) Then Equation 3.6

If (Re_c < 200000) Then

KRSM := 600.178 · $Re_c^{-0.5}$ Momentum thickness vary as the -0.5 power of chord Reynolds number

Else

KRSM := 10.224 · $Re_c^{-0.166}$ Momentum thickness vary as the -0.166 power of chord Reynolds number

EndIf

Else

KRSM := 23.398 · $RR^{0.347}$ Power fit of relation of Relative roughness to correction

EndIf

End **KRSM**

Function **KRSH** (Re_c, k_{CLA}, c, W_1, ρ, μ)

Function for calculating correction factor for Reynolds number and surface finish effects on Form factor - Figure A.2.6

$k_s := 6.2 \cdot k_{CLA}$ Equation 3.7

$RR := \frac{k_s}{c}$ Relative roughness

$RRe := \frac{k_s \cdot W_1 \cdot \rho}{\mu}$ Roughness Reynolds number

If (RRe <= 90) Then Equation 3.6

KRSH := $2.291 \cdot Re_c^{-0.06}$ Form factor vary as the -0.06 power of chord Reynolds number

Else

KRSH := $23.398 \cdot RR^{0.347}$ Power fit of relation of Relative roughness to correction

EndIf

End **KRSH**

The function below does linear interpolation and are also called from some other sub-programs.

Function to linearly interpolate between two points

Function **Interpol** (A, B, Y1, Y2, X)

If (Y1 >= Y2) Then

$$Interpol := \frac{\left[A - \left(X + 1.0 \times 10^{-15}\right)\right] \cdot \left[\left|Y1 - Y2\right|\right]}{\left|A - B\right|} + Y1$$

Else

$$Interpol := -\left[\frac{\left(A - \left[X + 1.0 \times 10^{-15}\right]\right) \cdot \left(\left|Y1 - Y2\right|\right)}{\left|A - B\right|} - Y1\right]$$

EndIf

End **Interpol**

C.3.3 Off-minimum loss – Casey

MODULE $\mathbf{Off}_{Loss,Casey}$ ($\bar{\omega}_{min}$, i, i_{min}, δ_{beta} : $\bar{\omega}$)

$$\chi = \frac{\left|i - i_{min}\right|}{\frac{\delta_p}{2}}$$ Equation 3.47

$$\frac{\bar{\omega}}{\bar{\omega}_{min}} = 1 + 0.1667 \cdot \chi + 0.8333 \cdot \chi^2$$ Equation 3.46

END $\mathbf{Off}_{Loss,Casey}$

C.3.4 Off-minimum loss – Lieblein

MODULE $\mathbf{Off}_{Loss,Lieblein}$ (β_1, β_2, σ, c, i, i_{min} : $\bar{\omega}$)

k = 0.0117

$$D_{eq,off} = \frac{\cos(\beta_2)}{\cos(\beta_1)} \cdot \left[1.12 + k \cdot \left(\left|i - i_{min}\right|\right)^{1.43} + 0.61 \cdot \frac{\cos^2(\beta_1)}{\sigma} \cdot (\tan(\beta_2) - \tan(\beta_1))\right]$$ Equation 3.48

$H_{ex} = 1.08$

$$\frac{\theta_{ex}}{c} = \frac{0.0045}{1 - 0.95 \cdot \ln(D_{eq,off})}$$ Equation 3.2

$$\bar{\omega} = 2 \cdot \frac{\theta_{ex}}{c} \cdot \frac{\sigma}{\cos(\beta_2)} \cdot \left[\frac{\cos(\beta_1)}{\cos(\beta_2)}\right]^2 \cdot \left[\frac{2}{3 - \frac{1}{H_{ex}}}\right] \cdot \left[1 - \frac{\theta_{ex}}{c} \cdot \frac{\sigma \cdot H_{ex}}{\cos(\beta_2)}\right]^{-3}$$ Equation 3.1

END $\mathbf{Off}_{Loss,Lieblein}$

C.3.5 Endwall loss – Howell

MODULE $\mathbf{Endwall}_{loss,Howell}(\beta_1, \beta_2, s, h, \sigma : \bar{\omega})$

$$\tan(\beta_m) = 0.5 \cdot (\tan(\beta_1) + \tan(\beta_2))$$ Equation 3.17

$$C_{D,A} = 0.02 \cdot \frac{s}{h}$$ Equation 3.14

$$C_L = \frac{2}{\sigma} \cdot (\tan(\beta_1) - \tan(\beta_2)) \cdot \cos(\beta_m)$$ Equation 3.16

$$C_{D,S} = 0.018 \cdot C_L^2$$ Equation 3.15

$$\bar{\omega} = \frac{(C_{D,A} + C_{D,S}) \cdot \sigma \cdot \cos^2(\beta_1)}{\cos^3(\beta_m)}$$ Equation 3.18

END $\mathbf{Endwall}_{loss,Howell}$

C.3.6 Endwall loss - Hübner and Fottner

MODULE $\mathbf{Endwall}_{loss,Hub,Fott}(h, c, \beta_1, \beta_2, \tau : \bar{\omega})$

$$\bar{\omega}_t = \left[\frac{0.165}{\frac{h}{c}} \cdot (\tan^{-2}(\beta_1 - 90) - \tan^{-2}(\beta_2 - 90)) \cdot \sin^2(\beta_1 - 90)\right] \cdot \tanh\left[35 \cdot \frac{\tau}{c}\right] + 0.0288$$ Equation 3.22

$$\bar{\omega}_{hb} = 2 \cdot \frac{c}{h} \cdot (0.0505 \cdot (\tan^{-2}(\beta_1 - 90) - \tan^{-2}(\beta_2 - 90)) - 0.01313) \cdot \sin^2(\beta_1 - 90)$$ Equation 3.23

$$\bar{\omega} = \frac{\bar{\omega}_t + \bar{\omega}_{hb}}{2}$$ Equation 3.21

END $\mathbf{Endwall}_{loss,Hub,Fott}$

C.3.7 Endwall loss – Roy and Kumar

MODULE $\mathbf{Endwall}_{loss,Roy,Kumar}(\beta_1, \beta_2, \sigma, h, c, \rho_1, \tau, C_P, W_1, \bar{U}, q_1, \theta_{camber} : \bar{\omega})$

$A = 1$ Assume uniform tip gap - from Table 3.1

$B = -0.24$

$C_d = 0.84$

$\tan(\beta_m) = 0.5 \cdot (\tan(\beta_1) + \tan(\beta_2))$

$$C_L = \frac{2}{\sigma} \cdot (\tan(\beta_1) - \tan(\beta_2)) \cdot \cos(\beta_m)$$

$$\bar{\omega}_{ew} = 0.04 \cdot C_L^2 \cdot \frac{\sigma \cdot c \cdot \cos^2(\beta_1)}{h \cdot \cos^3(\beta_m)}$$ Equation 3.24

$$\Delta_{P,total} = \Delta_{P,gap} + \Delta_{P,mixing}$$ Equation 3.26

$$\Delta_{P,gap} = 0.5 \cdot c \cdot \rho_1 \cdot \tau \cdot W_1^3 \cdot B \cdot |C_P|^{1.5}$$ Equation 3.27

$$\Delta_{P,mixing} = 0.5 \cdot c \cdot \rho_1 \cdot \tau \cdot V_{jet}^3$$ Equation 3.28

$$\frac{V_{rjet}}{W_1} = C_d \cdot \sqrt{|C_P|}$$ Equation 3.29

$$\frac{V_{njet,max}}{W_1} = A \cdot \sqrt{|C_P|}$$ Equation 3.30

$V_{jet} = V_{jet}(\overline{U}, \theta_{camber}, V_{njet,max}, V_{njet}, \sigma)$ Call function to return V_{jet}

$$\overline{\omega_t} = \frac{\Delta_{P,total}}{q_1 \cdot 1000}$$ Equation 3.25

$$\overline{\omega} = \overline{\omega_{ew}} + \overline{\omega_t}$$ Equation 3.33

END **Endwall**$_{loss,Roy,Kumar}$

Function $V_{jet}(\overline{U}, \theta_{camber}, V_{njet,max}, V_{njet}, \sigma)$

If $(\overline{U} \cdot \cos(\theta_{camber}) > V_{njet,max})$ Then

$V_{jet} := 1.05 \cdot V_{njet} + 0.5 \cdot \sigma \cdot (\overline{U} \cdot \cos(\theta_{camber}) - V_{njet,max})$ Equation 3.35

Else

$V_{jet} := 1.05 \cdot V_{njet}$ Equation 3.36

EndIf

End V_{jet}

C.3.8 Endwall loss – Koch and Smith

Procedure **Endwall**$_{loss,Koch,Smith}$ $(\Delta_{s,fs}, h_{stg}, \Delta_{h,0}, T_{0,3}, \eta_{fs}, K_1, K_2, stg, C_{P,eff}, C_{P,max}, \tau_{wtd}, AS_{wtd}, g_{stg} : \overline{\delta}, \Delta_{s,ks,tr}, \Delta_{s,ks,str})$

$$X := \frac{C_{P,eff}}{C_{P,max}}$$

If $((X > 0.7)$ and $(X <= 1))$ Then

$Y := -74.0578 + 493.6841 \cdot X - 1306.4354 \cdot X^2 + 1719.0773 \cdot X^3 - 1125.3951 \cdot X^4 + 293.4619 \cdot X^5$ Polinomial fit of correlation for tau/g = 0 - Figure A.4.1

Else

If $(X > 1)$ Then

Call WARNING ('Stage XXXA is stalled', stg) Error procedure to halt calculations if $C_P > C_{P,max}$

$Y := 0.126$

Else

$Y := 0.126$ For X <= 0.7

EndIf

EndIf

$$\delta_{initial} := \frac{(Y + 2 \cdot \tau_{wtd} \cdot X) \cdot g_{stg}}{2}$$ Relation for lines with other tau/g values - Equation A.4.1

If $(AS_{wtd} < 0.7)$ Then

$AGP := 0.8301 + 1.50436 \cdot AS_{wtd} - 6.51982 \cdot AS_{wtd}^2 + 16.1595 \cdot AS_{wtd}^3 - 20.05944 \cdot AS_{wtd}^4 + 9.55128 \cdot AS_{wtd}^5$ Only applicable for gap/pitch ratios < 0.7 - Figure A.4.2

Else

$AGP := 1.02$

EndIf

$\overline{\delta} := \delta_{initial} \cdot AGP$ Corrected boundary layer displacement thickness

If $(X > 0.7)$ Then

$\overline{v} := (2.9464 - 9.29627 \cdot X + 11.8667 \cdot X^2 - 5.11111 \cdot X^3) \cdot \overline{\delta}$ Polinomial fit of correlation for tangential force thickness - Figure A.4.3

Else

$\overline{v} := 0.5 \cdot \overline{\delta}$ For X <= 0.7

EndIf

$$\Delta_s := \left[1 - \eta_{ts} \cdot \left(\frac{1 - \frac{2 \cdot \bar{\delta}}{g_{stg}} \cdot \frac{g_{stg}}{h_{stg}}}{1 - \frac{2 \cdot \bar{v}}{2 \cdot \bar{\delta}} \cdot \frac{2 \cdot \bar{\delta}}{g_{stg}} \cdot \frac{g_{stg}}{h_{stg}}}\right)\right] \cdot \frac{\Delta_{h,0}}{T_{0,3}} - \Delta_{s,ts}$$

Rewrite 3.19 to give entropy increase rather than new efficiency

$\Delta_{s,ks,rr} := \Delta_s \cdot K_1$ Assign entropy change for rotor according to row factor

$\Delta_{s,ks,str} := \Delta_s \cdot K_2$ Assign entropy change for stator according to row factor

End **Endwall**$_{loss,Kooh,Smith}$

C.3.9 Part span shroud loss – Koch and Smith

MODULE **Pss**$_{loss}$ ($\beta_1, \beta_2, C_z, a, r_{sh}, N_b, c_{sh}, t_{sh}, \bar{A}, R, \gamma : \Delta_s$)

$$\tan(\beta_m) = \frac{\tan(\beta_1) + \tan(\beta_2)}{2}$$

$$W_m = C_z \cdot \frac{1}{\cos(\beta_m)}$$

$$M_m = \frac{W_m}{a}$$ Equation 3.39

$$P_M = (1 - M_m^2 \cdot \cos^2(\beta_m))^{\left[\frac{-1}{2}\right]}$$ Equation 3.37

$$b = \frac{2 \cdot \pi \cdot r_{sh}}{N_b}$$ Equation 3.38

$$C_{D,sh} = 1.8 \cdot \left[0.012 \cdot \left(\frac{\frac{c_{sh}}{t_{sh}}}{\cos(\beta_m)} + 2 + 60 \cdot P_M^3 \cdot \left[\frac{t_{sh}}{c_{sh}}\right]^2\right) + 3 \cdot P_M^3 \cdot \frac{t_{sh}}{b} \cdot \frac{t_{sh}}{c_{sh}}\right]$$ Equation 3.36

$$A_{sh} = 2 \cdot \pi \cdot r_{sh} \cdot t_{sh}$$ Equation 3.35

$$\Delta_s = C_{D,sh} \cdot \frac{\gamma}{2} \cdot M_m^2 \cdot \frac{A_{sh}}{\bar{A}} \cdot R$$ Equation 3.40

END **Pss**$_{loss}$

C.3.10 Windage loss - Denton

MODULE **Windage**$_{loss}$ ($C_z, U, r_{hb,1}, r_{hb,2}, Re, \Delta_{h,0}, \bar{h}, T_{0,2} : \Delta_s$)

$$\psi = \frac{C_z}{U}$$ Equation 3.46

$$\phi = \frac{\Delta_{h,0}}{U^2}$$ Equation 3.47

$$D_{hb} = r_{hb,1} + r_{hb,2}$$

$$C_m = 0.12654 \cdot Re^{-0.222}$$ Power fit for Reynolds numbers between 10^5 and 10^{11} - Figure 3.4

$$C_f = 0.398 \cdot C_m$$ Equation 3.58

$$\frac{\Delta_{W,windage}}{\Delta_{h,0}} = 0.1 \cdot \frac{C_f}{\phi \cdot \psi} \cdot \frac{D_{hb}}{\bar{h}} \cdot \left[\frac{1}{1 + \frac{4 \cdot \bar{h}}{D_{hb}}}\right]$$ Equation 3.45

$$\Delta_s = \frac{\Delta_{W,windage}}{T_{0,2}}$$ Entropy increase due to windage

END **Windage**$_{loss}$

Appendix C.4

PERFORMANCE PREDICTION FORMATTED EQUATION SETS

Chapter 5 gives the methodology used to generate a performance prediction code from the literature as presented in Chapter 3 and 4. This appendix gives the formatted equations as implemented in EES for the performance prediction code and utilizes the loss models a given in Appendix C.3.

C.4.1 Compressor code

COMPRESSOR PROGRAM

$T_{0,in}$ = **Lookup** ('Inlet comp', 1, 'T_0')	Assign compressor inlet total temperature from lookup table
$T_{0,out}$ = **Lookup** ('STAGE4', run, 'Column1')	Assign compressor outlet total temperature from lookup table
$P_{0,in}$ = **Lookup** ('Inlet comp', 1, 'P_0')	Assign compressor inlet total pressure from lookup table
$P_{0,out}$ = **Lookup** ('STAGE4', run, 'Column2')	Assign compressor outlet total temperature from lookup table
$\Delta_{s,1}$ = **Lookup** ('STAGE1', run, 'Column5')	Assign entropy change of stage 1 from lookup table
$\Delta_{s,2}$ = **Lookup** ('STAGE2', run, 'Column5')	Assign entropy change of stage 2 from lookup table
$\Delta_{s,3}$ = **Lookup** ('STAGE3', run, 'Column5')	Assign entropy change of stage 3 from lookup table
$\Delta_{s,4}$ = **Lookup** ('STAGE4', run, 'Column5')	Assign entropy change of stage 4 from lookup table
$\Delta_{h,0,1}$ = **Lookup** ('STAGE1', run, 'Column4')	Assign enthalpy change of stage 1 from lookup table
$\Delta_{h,0,2}$ = **Lookup** ('STAGE2', run, 'Column4')	Assign enthalpy change of stage 2 from lookup table
$\Delta_{h,0,3}$ = **Lookup** ('STAGE3', run, 'Column4')	Assign enthalpy change of stage 3 from lookup table
$\Delta_{h,0,4}$ = **Lookup** ('STAGE4', run, 'Column4')	Assign enthalpy change of stage 4 from lookup table
$\Delta_s = \Delta_{s,1} + \Delta_{s,2} + \Delta_{s,3} + \Delta_{s,4}$	Calculates sum of entropy changes through all the stages
$\Delta_{h,0} = \Delta_{h,0,1} + \Delta_{h,0,2} + \Delta_{h,0,3} + \Delta_{h,0,4}$	Calculates sum of enthalpy changes through all the stages
$TR_{tt} = \frac{T_{0,out}}{T_{0,in}}$	Total-to-total temperature ratio
$PR_{tt} = \frac{P_{0,out}}{P_{0,in}}$	Total-to-total pressure ratio
$\eta = 1 - \frac{T_{0,out} \cdot \Delta_s}{\Delta_{h,0}}$	Total-to-total adiabatic efficiency
run = 1	Indicates the run in the parametrical table and is varied according to mass flow

C.4.2 Stage code

This section presents the formatted equations for the stage code. The calling arguments to the rotor and stator are too long to be displayed here, but can be seen in the source code in Appendix C.6 if desired.

Assigns user inputs from Lookup table

fluid$ = **Lookup$** ('Inlet comp', 1, 'Fluid') — Defines working fluid for use in fluid property calculations

N = **Lookup** ('Inlet comp', 1, 'N') — Rotational speed

$T_{0,1}$ = **Lookup** ('Inlet comp', 1, 'T_0') — Inlet stagnation temperature

$P_{0,1}$ = **Lookup** ('Inlet comp', 1, 'P_0') — Inlet stagnation pressure

α_1 = **Lookup** ('Inlet comp', 1, '$alpha_1$') — Absolute flow inlet angle measured from axial direction

ABF_{in} = **Lookup** ('Inlet comp', 1, 'ABF_{in}') — Inlet blade blockage factor

$\dot{m}$ = **Lookup** ('Inlet comp', 1, 'm_{dot}') — Flow rate in kg/s

stg = 1

Call rotor and stator sub-codes

Call **Rotor** (δ_{ks}, $\Delta_{s,ks,rtr}$, $\dot{m}$, ABF_{in}, stg, $T_{0,1}$, $P_{0,1}$, α_1, P_1, T_1, $r_{rms,2}$, α_2, M_{2a}, P_2, T_2, $P_{0,2}$, $T_{0,2}$, C_2, A_2, $M_{z,2}$, $C_{e,2}$, $C_{z,2}$, C_1, U_1, U_2, β_1, q_1

Call **Stator** (δ_{ks}, $\Delta_{s,ks,str}$, $\dot{m}$, ABF_{rtr}, α_1, stg, $r_{rms,2}$, α_2, M_{2a}, P_2, T_2, $P_{0,2}$, $T_{0,2}$, C_2, A_2, $M_{z,2}$, $C_{e,2}$, $C_{z,2}$, C_1, U_1, U_2, β_1, P_3, T_3, $T_{0,3}$, $P_{0,3}$, α_2

$$h_{stg} = \frac{\textbf{Lookup}('Stage\ inputs', stg, 'r_{t,1}') - \textbf{Lookup}('Stage\ inputs', stg, 'r_{hb,1}') + \textbf{Lookup}('Stage\ inputs', stg, 'r_{t,3}') - \textbf{Lookup}('Stage\ inputs', stg, 'r_{hb,3}')}{2}$$

Average blade height

$$L_{wtd} = \left[\frac{q_1}{q_1 + q_2}\right] \cdot \frac{L_{rtr}}{g_{rtr}} + \left[\frac{q_2}{q_1 + q_2}\right] \cdot \frac{L_{str}}{g_{str}}$$ — Weighted average for L/g, where L is the diffuser length needed to calculate stallPRC

$$\tau_{wtd} = \left[\frac{q_1}{q_1 + q_2}\right] \cdot \frac{\textbf{Lookup}('Stage\ inputs', stg, 'tau_{rtr}')}{g_{rtr}} + \left[\frac{q_2}{q_1 + q_2}\right] \cdot \frac{\textbf{Lookup}('Stage\ inputs', stg, 'tau_{str}')}{g_{str}}$$ — Weighted average for tau/g

$$g_{stg} = \left[\frac{q_1}{q_1 + q_2}\right] \cdot g_{rtr} + \left[\frac{q_2}{q_1 + q_2}\right] \cdot g_{str}$$ — Weighted average for g

$$AS_{wtd} = \left[\frac{q_1}{q_1 + q_2}\right] \cdot \frac{\textbf{Lookup}('Stage\ inputs', stg, 'AS')}{\textbf{Lookup}('Stage\ inputs', stg, 's_{rtr}')} + \left[\frac{q_2}{q_1 + q_2}\right] \cdot \frac{\textbf{Lookup}('Stage\ inputs', stg, 'AS')}{\textbf{Lookup}('Stage\ inputs', stg, 's_{str}')}$$ — Weighted average for AS/pitch

$$C_{P,max} = \textbf{StallPRC}\left[L_{wtd}, \frac{Re_{rtr} + Re_{str}}{2}, \tau_{wtd}, AS_{wtd}\right]$$ — Stalling static pressure rise coefficient for stage from correlation

$$C_{P,stg} = \frac{P_3 - P_1}{q_1 + q_2}$$ — Static pressure rise coefficient of stage

$$K_1 = \frac{q_{1,eff}}{q_2 + q_1}$$ — Row factor for use with Koch and Smith endwall loss model for rotor

$$K_2 = \frac{q_{2,eff}}{q_2 + q_1}$$ — Row factor for use with Koch and Smith endwall loss model for stator

$$\Delta_{s,fs} = \Delta_{s,fs,rtr} + \Delta_{s,fs,str}$$ — Freestream entropy change through stage

$$\eta_{fs} = 1 - \frac{T_{0,3} \cdot \Delta_{s,fs}}{\Delta_{h,0}}$$ — Stage freestream total-to-total adiabatic efficiency

Call **Endwall**$_{loss,Koch,Smith}$ ($\Delta_{s,fs}$, h_{stg}, $\Delta_{h,0}$, $T_{0,3}$, η_{fs}, K_1, K_2, stg, $C_{P,stg}$, $C_{P,max}$, τ_{wtd}, AS_{wtd}, g_{stg} : δ_{ks}, $\Delta_{s,ks,rtr}$, $\Delta_{s,ks,str}$)

$$\Delta_s = \Delta_{s,rtr} + \Delta_{s,str}$$ — Sum of the total rotor and stator entropy increases

$$TR_{tt} = \frac{T_{0,3}}{T_{0,1}}$$ — Stage total-to-total temperature ratio

$$PR_{tt} = \frac{P_{0,3}}{P_{0,1}}$$ — Stage total-to-total pressure ratio

$$\eta = 1 - \frac{T_{0,3} \cdot \Delta_s}{\Delta_{h,0}}$$ — Stage total-to-total adiabatic efficiency

$T_{0,3}$,$P_{0,3}$,alpha,3,DELTAh,0,DELTAs,TR,tt,PR,tt,eta ---- Export file format

C.4.3 Rotor

MODULE **Rotor** (δ_{ks}, $A_{s,ks,rtr}$, $\dot{m}_o$, ABF_{in}, stg, $T_{0,1}$, $P_{0,1}$, α_1, P_1, T_1, $r_{rms,2}$, α_2, M_{2a}, P_2, T_2, $P_{0,2}$, $T_{0,2}$, C_2, A_2, $M_{z,2}$, $C_{theta,2}$, $C_{z,2}$, C_1, U_1, U_2, β_1, q_1, $q_{1,ef}$

τ_{rtr} = **Lookup** ('Stage inputs', stg , 'tau_{rtr}') Tip clearance

ξ_{rtr} = **Lookup** ('Stage inputs', stg , 'xi_{rtr}') Blade stagger angle

$\chi_{1,rtr}$ = |**Lookup** ('Stage inputs', stg , '$chi_{1,rtr}$') | Blade inlet angle

$\chi_{2,rtr}$ = |**Lookup** ('Stage inputs', stg , '$chi_{2,rtr}$') | Blade outlet angle

$r_{t,1}$ = **Lookup** ('Stage inputs', stg , '$r_{t,1}$') Inputs from lookup table Tip radius at inlet of blade row

$r_{t,2}$ = **Lookup** ('Stage inputs', stg , '$r_{t,2}$') Tip radius at outlet of blade row

$r_{hb,1}$ = **Lookup** ('Stage inputs', stg , '$r_{hb,1}$') Hub radius at inlet of blade row

$r_{hb,2}$ = **Lookup** ('Stage inputs', stg , '$r_{hb,2}$') Hub radius at outlet of blade row

$t_{max,rtr}$ = **Lookup** ('Stage inputs', stg , '$t_{max,rtr}$') Midspan maximum thickness

c_{rtr} = **Lookup** ('Stage inputs', stg , 'c_{rtr}') Blade chord at midspan

s_{rtr} = **Lookup** ('Stage inputs', stg , 's_{rtr}') Blade pitch at mid span

$k_{CLA,rtr}$ = **Lookup** ('Stage inputs', stg , '$k_{CLA,rtr}$') Blade roughness - arithmetical svarage deviation normal to the centre line

$\dot{m}$ = $\dot{m}_c$ − **Lookup** ('Stage inputs', stg , '$m_{dot,bleed}$') Flow rate, compressor inlet flow rate minus bleed flow

r_{sh} = **Lookup** ('Stage inputs', stg , '$r_{sh,rtr}$') Part span shroud radius

t_{sh} = **Lookup** ('Stage inputs', stg , '$t_{sh,rtr}$') Part span shroud thickness

c_{sh} = **Lookup** ('Stage inputs', stg , '$c_{sh,rtr}$') Part span shroud chord

Calculate other geometrical rotor parameters

$$\sigma = \frac{c_{rtr}}{s_{rtr}}$$ Solidity

$$N_b = \mathbf{Round}\left[\frac{2 \cdot \pi \cdot \left(\frac{r_{rms,1} + r_{rms,2}}{2}\right)}{s_{rtr}}\right]$$ Number of blades if trailing edge is assumed infinitly small

$$h_{ratio} = \frac{r_{t,1} - r_{hb,1}}{r_{t,2} - r_{hb,2}}$$ Blade heigth ratio

$$\bar{h} = \frac{r_{t,1} - r_{hb,1} + r_{t,2} - r_{hb,2}}{2}$$ Average blade height

$\theta_{camber} = \chi_{1,rtr} - \chi_{2,rtr}$ Blade camber angle

$g = s_{rtr} \cdot \cos(\xi_{rtr})$ Rotor staggerd spacing

$$L = \frac{c_{rtr} \cdot \pi \cdot \theta_{camber}}{360 \cdot \sin\left[\frac{\theta_{camber}}{2}\right]}$$ Meanline length of circular arc airfoil

Thermodynamic fluid properties assumed constant throughout bladerow

$$C_p = \mathbf{Cp}\left[\text{fluid\$}, T=\frac{T_1 + T_2}{2}, P=\frac{P_1 \bullet P_2}{2}\right]$$ Bladerow specific heat at constant pressure

$$C_v = \mathbf{Cv}\left[\text{fluid\$}, T=\frac{T_1 + T_2}{2}, P=\frac{P_1 + P_2}{2}\right]$$ Bladerow specific heat at constant volume

$R = C_p - C_v$ Gas constant

$$\gamma = \frac{C_p}{C_v}$$ Relation of C_p to C_v

ROTOR INLET CALCULTIONS

Rotor inlet pressure and temperature calculations

$$T_1 = T_{0,1} - \frac{C_1^2}{2 \cdot C_p}$$ Calculation for T - static temperature

$$P_1 = \frac{P_{0,1}}{\left[\frac{T_{0,1}}{T_1}\right]\left[\frac{\gamma}{\gamma - 1}\right]}$$ Calculation for P - static pressure

$$T_{0,1r} = T_{0,1} + \frac{W_1^2 - C_1^2}{2 \cdot C_p}$$ Calculates relative stagnation temperature

$$P_{0,1r} = P_{0,1} \cdot \left[\frac{T_{0,1r}}{T_{0,1}}\right]\left[\frac{\gamma}{\gamma - 1}\right]$$ Calculates relative stagnation pressure

$$h_T = C_p \cdot T_{0,1r} - 0.5 \cdot U_1^2$$ Rothalpy at rotor inlet, equal to rothalpy at rotor outlet

$$P_{T,1} = P_1 \cdot \left[\frac{h_T}{C_p \cdot T_1}\right]\left[\frac{\gamma}{\gamma - 1}\right]$$ Calculates pressure based on rothalpy at rotor inlet

Rotor inlet thermodynamical property calculations from built in EES functions

$\rho_1 = \rho(\text{fluid\$}, T=T_1, P=P_1)$ Density of fluid at bladerow inlet

$a1 = \sqrt{\gamma \cdot R \cdot T_1}$ Velocity of sound, m/s at bladerow inlet

$\mu_1 = \textbf{Visc}(\text{fluid\$}, T=T_1, P=P_1)$ Viscosity of fluid at bladerow inlet

Inlet velocity triangle equations

$A_1 = (\pi \cdot r_{t,1}^2 - \pi \cdot r_{hb,1}^2) \cdot ABF$ Inlet annulus area with ABF taken into account

$$r_{rms,1} = \sqrt{\frac{r_{t,1}^2 + r_{hb,1}^2}{2}}$$ Rms diameter at inlet of blade row

$$U_1 = \frac{2 \cdot \pi \cdot N}{60} \cdot r_{rms,1}$$ Blade pheripheral speed at rms_1

$$U_1 = \frac{2 \cdot \pi \cdot N}{60} \cdot r_{rms,1}$$ Blade pheripheral speed at rms_1

$$C_{z,1} = \frac{\dot{m}}{\rho_1 \cdot A_1}$$ Inlet axial velocity, calculated from the continuity

$$W_1 = \sqrt{(U_1 - C_{\theta,1})^2 + C_{z,1}^2}$$ Inlet relative velocity

$$C_1 = \frac{C_{z,1}}{\cos(\alpha_1)}$$ Inlet Absolute velocity

$C_{\theta,1} = C_{z,1} \cdot \tan(\alpha_1)$ *Tangential component of absolute inlet velocity*

$$\beta_1 = -\arccos\left[\frac{C_{z,1}}{W_1}\right]$$ Calculates angle relative to rotor at inlet

Other required inlet variables

$i = -\chi_{1,rtr} - \beta_1$ Incidence

$$M_{z,1} = \frac{C_{z,1}}{a1}$$ Inlet axial Mach number, based on axial velocity

$$M_1 = \frac{W_1}{a1}$$ Relative inlet Mach number

$q_1 = P_{0,1r} - P_1$ Inlet dynamic head to rotor

$$q_{1,eff} = q_1 \cdot \left[\frac{1 + 2.5 \cdot (C_1 \cdot \sin(\alpha_1 + \beta_1))^2 + 0.5 \cdot U_1^2}{4 \cdot C_1^2}\right]$$ Effective inlet dynamic head for rotor

ROTOR OUTLET CALCULTIONS

Rotor outlet pressure and temperature calculations

$$T_{0,2r} = \frac{h_T + 0.5 \cdot U_2^2}{C_p}$$ Outlet relative temperature, rothalpy at rotor outlet = rothalpy at rotor inlet

$$P_{T,2} = P_{T,1} - \frac{\overline{\omega} \cdot q_1 \cdot P_{T,1}}{P_{0,1r}}$$ Outlet pressure based on rothalpy incorporating presure losses

$$P_{T,2} = P_{T,1} - \frac{\bar{\omega} \cdot q_1 \cdot P_{T,1}}{P_{0,1r}}$$ Outlet pressure based on rothalpy incorporating presure losses

$$P_2 = \frac{P_{T,2}}{\left[\frac{h_T}{C_p \cdot T_2}\right]^{\left[\frac{\gamma}{\gamma - 1}\right]}}$$ Static pressure at outlet

$$T_{0,2} = T_{0,2r} - \left[\frac{W_2^2 - C_2^2}{2 \cdot C_p}\right]$$ Stagnation temperature at outlet

$$P_{0,2} = P_2 \cdot \left[\frac{T_{0,2}}{T_2}\right]^{\left[\frac{\gamma}{\gamma - 1}\right]}$$ Stagnation pressure at outlet

$$P_{0,2r} = P_{0,2} \cdot \left[\frac{T_{0,2r}}{T_{0,2}}\right]^{\left[\frac{\gamma}{\gamma - 1}\right]}$$ Relative outlet stagnation pressure

$$T_2 = T_{0,2} - \frac{C_2^2}{2 \cdot C_p}$$ Calculation for static temperature at outlet

Rotor outlet thermodynamical property calculations from built in *EES* functions

$\rho_2 = \rho(\text{fluid\$}, T=T_2, P=P_2)$ Density of fluid at bladerow outlet

$a2 = \sqrt{\gamma \cdot R \cdot T_2}$ Velocity of sound, *m/s* at bladerow outlet

$\mu_2 = \textbf{Visc}(\text{fluid\$}, T=T_2, P=P_2)$ Viscosity of fluid at bladerow outlet

Outlet velocity triangle equations

$$A_2 = (\pi \cdot r_{t,2}^2 - \pi \cdot r_{hb,2}^2) \cdot ABF$$ Outlet annulus area with ABF taken in account

$$r_{rms,2} = \sqrt{\frac{r_{t,2}^2 + r_{hb,2}^2}{2}}$$ Mean diameter at exit of blade row

$$U_2 = \frac{2 \cdot \pi \cdot N}{60} \cdot r_{rms,2}$$ Blade pheripheral speed at $r_{rms,2}$

$$C_{z,2} = \frac{\dot{m}}{\rho_2 \cdot A_2}$$ Outlet axial velocity - calculated from continuity

$$W_2 = \sqrt{(U_2 - C_{\theta,2})^2 + C_{z,2}^2}$$ Outlet relative velocity

$$C_2 = \frac{C_{z,2}}{\cos(\alpha_2)}$$ Outlet absolute velocity

$$C_{\theta,2} = C_{z,2} \cdot \tan(\alpha_2)$$ Tangential component of absolute outlet velocity

$$\beta_2 = -\arccos\left[\frac{C_{z,2}}{W_2}\right]$$ Calculates angle relative to rotor at outlet

Call **Deviation**$\left[i, i_{min}, |\beta_1|, t_{max,rtr}, c_{rtr}, \theta_{camber}, \sigma : \delta_{min}, \delta\right]$ *Call* sub-section for deviation at min loss and off-min loss

$\beta_2 = -\chi_{2,rtr} - \delta$ Definition of deviation

Other required outlet variables

$$M_{z,2} = \frac{C_{z,2}}{a2}$$ Outlet axial Mach number, based on axial velocity

$$M_2 = \frac{W_2}{a2}$$ Outlet Mach number, based on relative exit velocity

$$M_{2a} = \frac{C_2}{a2}$$ Outlet Mach number, based on absolute exit velocity

$$BBF = 1 - \left[\frac{2 \cdot block}{g + t_{max,rtr}}\right]$$ Blade blackage factor - block is value returned from profile loss module

$$W_{2,fs} = \frac{W_2}{BBF}$$ Freestream outlet velocity due to BBF - blade blockage factor from and to profile loss

$ABF = \textbf{ABF}(ABF_{in}, \bar{\delta}, \bar{\Pi})$ Annulus blockage factor - from Function ABF

Other variables needed for calculations

$\Delta_{h,0} = C_p \cdot (T_{0,2} - T_{0,1})$ Stagnation enthalpy change accross bladerow

$\Delta_h = C_p \cdot (T_2 - T_1)$ Static enthalpy change accross bladerow

$$Re_c = \frac{\left[\left(\frac{\rho_1 + \rho_2}{2}\right) \cdot \left(\frac{W_1 + W_2}{2}\right)\right] \cdot c_{rtr}}{\frac{\mu_1 + \mu_2}{2}}$$ Chord Reynolds number

$$Re = \frac{\left[\left(\frac{\rho_1 + \rho_2}{2}\right) \cdot \left(\frac{C_{z,1} + C_{z,2}}{2}\right)\right] \cdot \sqrt{4 \cdot \frac{\left[\frac{A_1 + A_2}{2}\right]}{\pi}}}{\frac{\mu_1 + \mu_2}{2}}$$ Reynolds number based in equivalent diameter

Call **Blade**$_{Stall}$ (stg , i , i_{min} , δ_β : inop$) Test if blade is in stall and halt calculations with error message

Call **Min**$_{inc}$ [$|\beta_1|$, σ , $t_{max,rtr}$, c_{rtr} , θ_{camber} : i_{min}] Minimum loss or reference incidence from sub-section Min_{inc}

Call **Opp**$_{Range}$ (M_1 , $\chi_{1,rtr}$, σ , θ_{camber} : δ_{beta}) Operating range of cascade from sub-section Opp-Range

$\bar{\delta} = \delta_{ks}$ Sets endwall boundary layer displacement thickness parameter equal to Koch and Smith value calculated in calling module

CALLS TO LOSS MODEL SUB-SECTIONS

Call **Profile**$_{Loss}$, The Koch and Smith or Lieblein profile loss model is called here depending on which one is not commented

Call **Off**$_{Loss}$, The Casey or Lieblein incidence loss model is called here depending on which one is not commented

Call **Pss**$_{loss}$

$\Delta_{s,ew} = \Delta_{s,ks,rtr}$

Call **Windage**$_{loss}$

The Koch and Smith, Hubner and Fottner, Roy and Kumar or Howell endwall loss model is called here. In this case the Koch and Smith model is used because the endwall entropy parameter is set to the value provided from the stage section

Equations nessacary to obtain both pressure loss and entropy increase for losses

$$\Delta_s = C_p \cdot \ln\left[\frac{T_2}{T_1}\right] - R \cdot \ln\left[\frac{P_2}{P_1}\right]$$ Total entropy change through rotor

$\Delta_{s,fs} = \Delta_{s,p} + \Delta_{s,pss}$ Freestream entropy change through rotor

$\Delta_s = \Delta_{s,fs} + \Delta_{s,ew} + \Delta_{s,windage}$ Windage loss only influence efficiency, not pressure loss

$$\Delta_{s,ew} = -R \cdot \ln\left[\frac{P_{T,1} - \frac{\bar{\omega}_{ew} \cdot q_1 \cdot P_{T,1}}{P_{0,1r}}}{P_{T,1}}\right]$$ Calculates pressure loss coefficient from endwall loss

$$\Delta_{s,pss} = -R \cdot \ln\left[\frac{P_{T,1} - \frac{\bar{\omega}_{pss} \cdot q_1 \cdot P_{T,1}}{P_{0,1r}}}{P_{T,1}}\right]$$ Calculates pressure loss coefficient from part span shroud loss

$\bar{\omega} = \bar{\omega}_{ew} + \bar{\omega}_p + \bar{\omega}_{pss} + \bar{\omega}_{windage}$ Sum of pressure loss coefficients for use in pressure loss equations

END **Rotor**

C.4.4 Stator

MODULE **Stator** (δ_{ks}, $\Delta_{s,ks,str}$, $\dot{m}_o$, ABF$_{in}$, α_1, stg, $r_{rms,2}$, α_2, M_{2a}, P_2, T_2, $P_{0,2}$, $T_{0,2}$, C_2, A_2, $M_{z,2}$, $C_{theta,2}$, $C_{z,2}$, C_1, U_1, U_2, β_1, P_3, T_3, $T_{0,3}$, $P_{0,3}$, α_3, ABF

τ_{str} = **Lookup** ('Stage inputs', stg , 'tau_{str}') — Tip clearance

ξ_{str} = **Lookup** ('Stage inputs', stg , 'xi_{str}') — Blade stagger angle

$\chi_{2,str}$ = **Lookup** ('Stage inputs', stg , '$chi_{2,str}$') — Blade inlet angle

$\chi_{3,str}$ = **Lookup** ('Stage inputs', stg , '$chi_{3,str}$') — Blade outlet angle

$r_{t,2}$ = **Lookup** ('Stage inputs', stg , '$r_{t,2}$') — Tip radius at inlet of blade row

$r_{t,3}$ = **Lookup** ('Stage inputs', stg , '$r_{t,3}$') — Tip radius at outlet of blade row

$r_{hb,2}$ = **Lookup** ('Stage inputs', stg , '$r_{hb,2}$') — Hub radius at inlet of blade row

$r_{hb,3}$ = **Lookup** ('Stage inputs', stg , '$r_{hb,3}$') Inputs from lookup table — Hub radius at outlet of blade row

$t_{max,str}$ = **Lookup** ('Stage inputs', stg , '$t_{max,str}$') — Midspan maximum thickness

c_{str} = **Lookup** ('Stage inputs', stg , 'c_{str}') — Blade chord at midspan

s_{str} = **Lookup** ('Stage inputs', stg , 's_{str}') — Blade pitch at mid span

$k_{CLA,str}$ = **Lookup** ('Stage inputs', stg , '$k_{CLA,str}$') — Blade roughness - arithmetical avarage deviation normal to the centre line

$\dot{m}$ = $\dot{m}_o$ − **Lookup** ('Stage inputs', stg , '$m_{dot,bleed}$') — Stage flow rate

r_{sh} = **Lookup** ('Stage inputs', stg , '$r_{sh,str}$') — Part span shroud radius

t_{sh} = **Lookup** ('Stage inputs', stg , '$t_{sh,str}$') — Part span shroud thickness

c_{sh} = **Lookup** ('Stage inputs', stg , '$c_{sh,str}$') — Part span shroud chord

Calculate other geometrical stator parameters

$$\sigma = \frac{c_{str}}{s_{str}}$$ — Solidity

$$N_b = \textbf{Round}\left[\frac{2 \cdot \pi \cdot \left(\frac{r_{rms,2} + r_{rms,3}}{2}\right)}{s_{str}}\right]$$ — Number of blades if trailing edge is assumed infinitly small

$$h_{ratio} = \frac{r_{t,2} - r_{hb,2}}{r_{t,3} - r_{hb,3}}$$ — Blade heigth ratio

$$\overline{h} = \frac{r_{t,2} - r_{hb,2} + r_{t,3} - r_{hb,3}}{2}$$ — Average blade height

$$\theta_{camber} = \chi_{2,str} - \chi_{3,str}$$ — Blade camber angle

$$g = s_{str} \cdot \textbf{cos}\,(\xi_{str})$$ — Stator staggerd spacing

$$L = \frac{c_{str} \cdot \pi \cdot \theta_{camber}}{360 \cdot \textbf{sin}\left[\frac{\theta_{camber}}{2}\right]}$$ — Meanline length of circular arc airfoil

Thermodynamic fluid properties assumed constant throughout bladerow

$$C_p = \textbf{Cp}\left[\text{fluid\$}, T=\frac{T_2 + T_3}{2}, P=\frac{P_2 + P_3}{2}\right]$$ — Bladerow specific heat at constant pressure

$$C_v = \textbf{Cv}\left[\text{fluid\$}, T=\frac{T_2 + T_3}{2}, P=\frac{P_2 + P_3}{2}\right]$$ — Bladerow specific heat at constant volume

$$R = C_p - C_v$$ — Gas constant

$$\gamma = \frac{C_p}{C_v}$$ — Relation of C_p to C_v

STATOR INLET CALCULATIONS

Mostly done in Rotor sub-section

$$q_2 = P_{0,2} - P_2$$ — Inlet dynamic head to stator

$$q_{2,eff} = q_2 \cdot \left[\frac{1 + 2.5 \cdot U_2^2 + 0.5 \cdot U_2^2}{4 \cdot C_2^2}\right]$$ — Effective inlet dynamic head for stator

Stator inlet thermodynamical property calculations from built in EES functions

$\rho_2 = \rho(\text{fluid\$}, T=T_2, P=P_2)$ — Density of fluid at bladerow inlet

$a2 = \sqrt{\gamma \cdot R \cdot T_2}$ — Velocity of sound at bladerow inlet

$\mu_2 = \textbf{Visc}(\text{fluid\$}, T=T_2, P=P_2)$ — Viscosity of fluid at bladerow inlet

$i = \alpha_2 - \chi_{2,str}$ — Incidence

STATOR OUTLET CALCULATIONS

Rotor outlet pressure and temperature calculations

$T_{0,3} = T_{0,2}$ — Constant h_0 over stator

$P_{0,3} = P_{0,2} - \bar{\omega} \cdot q_2$ — Calculation for P_0 at outlet of stator

$$T_3 = T_{0,3} - \frac{C_3^2}{2 \cdot C_p}$$ — Calculation for T - static at outlet

$$P_3 = \frac{P_{0,3}}{\left[\frac{T_{0,3}}{T_3}\right]\left[\frac{\gamma}{\gamma - 1}\right]}$$ — Calculation for P - static at outlet

Stator outlet thermodynamical property calculations from built in EES functions

$\rho_3 = \rho(\text{fluid\$}, T=T_3, P=P_3)$ — Density of fluid at bladerow outlet

$a3 = \sqrt{\gamma \cdot R \cdot T_3}$ — Velocity of sound at bladerow outlet

$\mu_3 = \textbf{Visc}(\text{fluid\$}, T=T_3, P=P_3)$ — Viscosity of fluid at bladerow outlet

Outlet velocity triangle equations

$A_3 = (\pi \cdot r_{t,3}^2 - \pi \cdot r_{hb,3}^2) \cdot ABF$ — Calculates outlet annulus area, ABF_{out} is due to the endwall boundary layer of this stage

$$r_{rms,3} = \sqrt{\frac{r_{t,3}^2 + r_{hb,3}^2}{2}}$$ — Rms diameter at outlet of blade row

$U_3 = 0$ — Blade pheripheral speed at $r_{rms,3}$

$$C_{z,3} = \frac{\dot{m}}{\rho_3 \cdot A_3}$$ — Outlet axial velocity - calculated from continuity

$W_3 = \sqrt{(U_3 - C_{\theta,3})^2 + C_{z,3}^2}$ — Outlet relative velocity

$$C_3 = \frac{C_{z,3}}{\textbf{cos}(\alpha_3)}$$ — Outlet absolute velocity

$C_{\theta,3} = C_3 \cdot \textbf{sin}(\alpha_3)$ — Tangential component of absolute outlet velocity

$$\beta_3 = \textbf{arccos}\left[\frac{C_{z,3}}{W_3}\right]$$ — Calculates angle relative to stator at outlet

Call **Deviation** (i , i_{min} , α_2 , $t_{max,str}$, c_{str} , θ_{camber} , σ : δ_{min} , δ) — Call sub-section for deviation at min loss and off-min loss

$\alpha_3 = \chi_{3,str} + \delta$ — Definition of deviation

Other required outlet variables

$$M_{z,3} = \frac{C_{z,3}}{a3}$$ — Outlet axial Mach number, based on axial velocity

$$M_3 = \frac{C_3}{a3}$$ — Outlet Mach number, based on absolute velocity

$$BBF = 1 - 2 \cdot \left[\frac{block}{g - t_{max,str}}\right]$$ — Blade blockage factor - block is value returned from profile loss boundary layer equations

$$C_{3,fs} = \frac{C_3}{BBF}$$ — Freestream outlet velocity due to BBF - blade blockage factor from and to profile loss

$ABF = \textbf{ABF}(ABF_{in}, \bar{\delta}, \bar{h})$ — Annulus blockage factor, from function ABF

Other variables needed for calculations

$\Delta_h = C_p \cdot (T_3 - T_2)$ — Static enthalpy rise across stator

$$Re_c = \frac{\left[\left(\frac{\rho_2 + \rho_3}{2}\right) \cdot \left(\frac{C_2 + C_3}{2}\right)\right] \cdot c_{str}}{\frac{\mu_2 + \mu_3}{2}}$$ Chord Reynolds number

$$Re = \frac{\left[\left(\frac{\rho_2 + \rho_3}{2}\right) \cdot \left(\frac{C_{z,2} + C_{z,3}}{2}\right)\right] \cdot \sqrt{4 \cdot \frac{\left[\frac{A_2 + A_3}{2}\right]}{\pi}}}{\frac{\mu_2 + \mu_3}{2}}$$ Reynolds number based on equivalent diameter

Call **Blade**$_{Stall}$ (stg , i , i_{min} , δ_ρ : inop$) Test if blade is in stall and halt calculations with error message

Call **Min**$_{inc}$ (α_2 , σ , $t_{max,str}$, c_{str} , θ_{camber} : i_{min}) Minimum loss or reference incidence from sub-section Min_{inc}

Call **Opp**$_{Range}$ (M_{2a} , $\chi_{2,str}$, σ , θ_{camber} : δ_{beta}) Calcualtion of operating range of cascade from sub-section Opp-Range

$\bar{\delta} = \delta_{ks}$ Sets endwall boundary layer displacement thickness parameter equal to Koch and Smith value calculated in calling module

CALLS TO LOSS MODEL SUB-SECTIONS

Call **Profile**$_{Loss}$ Koch and Smith or Lieblein profile loss model is called here depending on which model is not commented

Call **Off**$_{Loss}$ Casey or Lieblein profile loss model is called here depending on which model is not commented

Call **Pss**$_{loss}$ The Koch and Smith, Hubner and Fottner, Roy and Kumar or Howell endwall loss model is called here. In this case the Koch and Smith model is used because the endwall entropy parameter is set to the value provided from

$\Delta_{s,ew} = \Delta_{s,ks,s}$ the stage section

Equations nessacary to obtain both pressure loss and entropy increase for losses

$$\Delta_s = C_p \cdot \ln\left[\frac{T_3}{T_2}\right] - R \cdot \ln\left[\frac{P_3}{P_2}\right]$$ Total entropy change through rotor

$\Delta_{s,fs} = \Delta_{s,p} + \Delta_{s,pss}$ Freestream entropy change through rotor

$\Delta_s = \Delta_{s,fs} + \Delta_{s,ew}$

$\Delta_{s,fs} = \Delta_{s,p} + \Delta_{s,pss}$ Freestream entropy change through rotor

$\Delta_s = \Delta_{s,fs} + \Delta_{s,ew}$

$$\Delta_{s,ew} = -R \cdot \ln\left[\frac{P_{0,2} - \bar{\omega}_{ew} \cdot q_2}{P_{0,2}}\right]$$ Calculates pressure loss coefficient from endwall loss

$$\Delta_{s,pss} = -R \cdot \ln\left[\frac{P_{0,2} - \bar{\omega}_{pss} \cdot q_2}{P_{0,2}}\right]$$ Calculates pressure loss coefficient from part span shroud loss

$\bar{\omega} = \bar{\omega}_{ew} + \bar{\omega}_p + \bar{\omega}_{pss}$ Sum of pressure loss coefficients for use in pressure loss equations

END **Stator**

C.4.5 Annulus blockage

Function **ABF** (ABF_{in}, $\bar{\delta}$, $\bar{h}$)

Function to calculate annulus blockage factor and to limit it accroding to Koch and Smith

If $\left[\frac{2 \cdot \bar{\delta}}{\bar{h}} < 0.17\right]$ Then

$ABF_1 := 1 - 2 \cdot \frac{\bar{\delta}}{\bar{h}}$ Annulus blockage factor with delta calculated in endwall loss module

Else

$ABF_1 := 0.83$ Limiting value for annulus blockage factor

Endif

If ($ABF_1 \cdot ABF_{in} < 0.83$) Then

$ABF := 0.83$ Limiting value for annulus blockage factor

Else

$ABF := ABF_1 \cdot ABF_{in}$ Inlet ABF taken into account

Endif

End **ABF**

C.4.6 Minimum loss incidence

Module to calculate minimum loss (reference) incidence, $i_{0,10}$ and n approximated by interpolating between sigma 0.4 and 2 due to even distribution of solidity lines

MODULE **Min**$_{inc}$ (β_1, σ, t, c, θ_{camber} : i_{min})

$i_{0,10,1} = 0.02857143 \cdot \beta_1$ — Figure B.1.2 for sigma = 0.4

$i_{0,10,2} = -0.01525 + 0.20391 \cdot \beta_1 - 0.00342769 \cdot \beta_1^2 + 0.0000862955 \cdot \beta_1^3 - 7.04167 \times 10^{-7} \cdot \beta_1^4$ — Figure B.1.2 for sigma = 2

$i_{0,10} =$ **Interpol** (0.4 , 2 , $i_{0,10,1}$, $i_{0,10,2}$, σ)

$n_1 = -0.0522 - 0.00302 \cdot \beta_1 - 0.0000393 \cdot \beta_1^2$ — Figure B.1.1 for sigma = 0.4

$n_2 = -0.011821 + 0.00017691 \cdot \beta_1 + 0.00000606 \cdot \beta_1^2 - 6.12 \times 10^{-7} \cdot \beta_1^3$ — Figure B.1.1 for sigma = 2

$n =$ **Interpol** (0.4 , 2 , n_1 , n_2 , σ)

$K_{sh} = 1$ — Shape factor for NACA 65 blades

$K_t = 0.001499 + 18.395 \cdot \frac{t}{c} - 105.283 \cdot \left[\frac{t}{c}\right]^2 + 260.4167 \cdot \left[\frac{t}{c}\right]^3$ — Figure B.1.3

$i_0 = K_{sh} \cdot K_t \cdot i_{0,10}$ — Equation 4.15

$i_{min} = i_0 + n \cdot \theta_{camber} - 1$ — Equation 4.14

END **Min**$_{inc}$

C.4.7 Deviation

Procedure **Deviation** (i, i_{min}, β_1, t, c, θ_{camber}, σ : δ_{min}, δ) Procedure to calculate deviation - according to Lieblein 1960

$K_t := 0.01277 + 6.386 \cdot \frac{t}{c} + 36.074 \cdot \left[\frac{t}{c}\right]^2$ — Figure B.2.4

$K_{sh} := 1$ — Shape factor for NACA 65 blades

If ((σ >= 0.4) and (σ < 1.2)) Then

$\delta_{0,10,1} := 0.0043 + 0.00629 \cdot \beta_1 + 0.0000374 \cdot \beta_1^2 + 0.00000109 \cdot \beta_1^3$ — Figure B.2.3 for sigma = 0.4

$\delta_{0,10,2} := -0.01483 + 0.0176 \cdot \beta_1 - 0.000214 \cdot \beta_1^2 + 0.00000821 \cdot \beta_1^3$ — Figure B.2.3 for sigma = 1.2

$\delta_{0,10} :=$ **Interpol** (0.4 , 1.2 , $\delta_{0,10,1}$ $\delta_{0,10,2}$ σ)

Else

$\delta_{0,10,1} := -0.01483 + 0.0176 \cdot \beta_1 - 0.000214 \cdot \beta_1^2 + 0.00000821 \cdot \beta_1^3$ — Figure B.2.3 for sigma = 1.2

$\delta_{0,10,2} := -0.0016575 + 0.0102 \cdot \beta_1 + 0.000962 \cdot \beta_1^2 - 0.0000255 \cdot \beta_1^3 + 3.26 \times 10^{-7} \cdot \beta_1^4$ — Figure B.2.3 for sigma = 2

$\delta_{0,10} :=$ **Interpol** (1.2 , 2 , $\delta_{0,10,1}$ $\delta_{0,10,2}$ σ)

EndIf

$\delta_0 := K_{sh} \cdot K_t \cdot \delta_{0,10}$ — Equation 4.17

$m := 0.255 + 0.000583 \cdot \beta_1 - 0.00000969 \cdot \beta_1^2 + 2.652 \times 10^{-7} \cdot \beta_1^3$ — Figure B.2.1

$b := 0.964 - 0.00304 \cdot \beta_1 + 0.0000622 \cdot \beta_1^2 - 0.00000147 \cdot \beta_1^3$ — Figure B.2.2

$\delta_{min} := \delta_0 + \frac{m}{\sigma^b} \cdot \theta_{camber}$ — Equation 4.16

Off minimum loss deviation angle

If ((β_1 <= 70) and (β_1 >= 60)) Then

$slope_1 := 1.006 - 1.526 \cdot \sigma + 0.475 \cdot \sigma^2 + 0.276 \cdot \sigma^3 - 0.132 \cdot \sigma^4$ — Figure B.2.5 for beta$_1$ = 60 degrees

```
    slope2 := 1.003 - 0.903 · σ - 0.696 · σ^2 + 1.02 · σ^3 - 0.289 · σ^4        Figure B.2.5 for beta1 = 70 degrees
    slope := interpol ( 60 , 70 , slope1 , slope2 , β1 )
  Else
    If ((β1 <= 60) and (β1 > 50)) Then
      slope1 := 0.978 - 1.955 · σ + 1.49 · σ^2 - 0.475 · σ^3 + 0.046 · σ^4      Figure B.2.5 for beta1 = 50 degrees
      slope2 := 1.006 - 1.528 · σ + 0.475 · σ^2 + 0.276 · σ^3 - 0.132 · σ^4     Figure B.2.5 for beta1 = 60 degrees
      slope := interpol ( 50 , 60 , slope1 , slope2 , β1 )
    Else
      slope1 := 0.972 - 2.563 · σ + 2.685 · σ^2 - 1.288 · σ^3 + 0.234 · σ^4     Figure B.2.5 for beta1 = 0 degrees
      slope2 := 0.978 - 1.955 · σ + 1.49 · σ^2 - 0.475 · σ^3 + 0.046 · σ^4      Figure B.2.5 for beta1 = 50 degrees
      slope := interpol ( 0 , 50 , slope1 , slope2 , β1 )
    EndIf
  EndIf
  δ := δmin + ( i - imin ) · slope                                              Equation 4.18
End Deviation
```

C.4.8 Stall and Choke

The following sections shows the formatted equations for calculating the bladerow operating range according to Casey, a sub-section to determine and warn the user if a bladerow is outside the operating range and the stalling static pressure rise coefficient from Koch.

C.4.8.1 Operating range according to Casey

```
Procedure Opp_Range (M, χ1, σ, θcamber : δbeta)        Procedure to calculate operating range of cascade
  If ( M < 0.2 ) Then
    KM := 1                                                                     Equation 4.21
  Else
    KM := 10^( -2.5 · ( M - 0.2 )^2 )                                           Equation 4.21
  EndIf
  K := 0.001 · ( -40 - 7 · ( χ1 - 45 ) + 0.25 · ( χ1 - 45 )^2 - 0.02 · ( χ1 - 45 )^3 )   Equation 4.20
  δbeta,i := 21 + K · [ (1 + √σ) / (σ · θcamber) ]
  δbeta := δbeta,i · KM                                                         Equation 4.19
End Opp_Range
```

C.4.8.2 Test to determine if bladerow is stalled

```
Procedure Blade_Stall (stg, i, imin, δbeta : inop$)    Procedure to determine if blade is stalled
  If [ | i - imin | > 0.8 · δbeta / 2 ] Then                                    Equation 4.22
    Call WARNING ( 'A bladerow in stage XXXA i..' , stg )
  inop$ := 'In operating range'
End Blade_Stall
```

C.4.8.3 Stalling static pressure rise coefficient

Function **StallPRC** ($L_{div,g}$, $\overline{Re}$, $\tau_{div,g}$, $AS_{div,s}$) Function to calculate stalling, thus maximum pressure rise coefficient - Koch(1981) and Casey(1987)

```
If ((10000 <= Re) and (Re < 20000)) Then                                   Figure B.3.2
   K_Re1 := 0.725 + 0.95 · Re · 10^-5
  Else
   If ((20000 <= Re) and (Re < 40000)) Then
      K_Re1 := 0.87 + 0.225 · Re · 10^-5
     Else
      If ((40000 <= Re) and (Re < 130000)) Then
         K_Re1 := 0.942 + 0.044 · Re · 10^-5
        Else
         K_Re1 := 0.994 + 0.00459 · Re · 10^-5
      EndIf
   EndIf
EndIf
If (K_Re1 < 1.05) Then                                                     Ensuring that maximum value is not more than correlation value
   K_Re := K_Re1                                                           due to assumption of straight lines for high Re values
  Else
   K_Re := 1.05
EndIf
EndIf
K_tau := 1.22436 - 8.18377 · τ_div,g + 112.12121 · τ_div,g^2 - 829.09091 · τ_div,g^3 + 2230 · τ_div,g^4      Figure B.3.3
K_AS := 1.1421 - 0.926 · AS_div,s + 2.333 · AS_div,s^2 - 2.753 · AS_div,s^3 + 1.22 · AS_div,s^4              Figure B.3.4
StallPRC := (0.1636 + 0.2428 · L_div,g - 0.0394 · L_div,g^2) · K_Re · K_tau · K_AS                           Figure B.3.1 and corrections
End StallPRC
```

Appendix C.5

DERIVATION OF PRESSURE LOSS – ENTROPY INCREASE RELATION

For a perfect gas the entropy change can be given by:

$$\Delta s = C_p \ln\left(\frac{T}{T_{ref}}\right) - R\ln\left(\frac{P}{P_{ref}}\right) \tag{C.5.1}$$

From the definition of entropy, Equation H.1 can be written as:

$$\Delta s = C_p \ln\left(\frac{T_{T1}}{T_{T2}}\right) - R\ln\left(\frac{P_{T1}}{P_{T2}}\right) \tag{C.5.2}$$

Using the fact that rothalpy is constant through a rotor and the definition of the pressure loss coefficient for a rotor,

$$\varpi = \frac{P_{T1} - P_{T2}}{P_{01r} - P_1}\frac{P_{01r}}{P_{T1}} \tag{C.5.3}$$

the following relation was obtained:

$$\Delta s = -R\ln\left(\frac{P_{T_1} - \left(\frac{\varpi q_1 P_{T1}}{P_{01r}}\right)}{P_{T1}}\right) \tag{C.5.4}$$

Appendix C.6

EES SOURCE CODE

This appendix presents the source code that was generated and used during this study. Section C.6.1 gives the code for reading the output values from the four stages used for the multi-stage axial compressor performance prediction verification and evaluation, whereas Section C.6.2 gives the code used to obtain these output files for each stage. These codes can easily be combined in a more stable solver than EES to give the performance prediction of a complete multi-stage compressor by simultaneously solving all the stages and their equations and not by using a stage stacking approach.

C.6.1 Compressor code source code

```
"LOSS MODELLING IN MULTI STAGE SUBSONIC AXIAL COMPRESSORS"

T_0_in     =  LOOKUP('Inlet comp',1,3)      "Assign compressor inlet total temperature from lookup table"
T_0_out    =  LOOKUP('STAGE4',run,1)        "Assign compressor outlet total temperature from lookup table"

P_0_in     =  LOOKUP('Inlet comp',1,4)      "Assign compressor inlet total pressure from lookup table"
P_0_out    =  LOOKUP('STAGE4',run,2)        "Assign compressor outlet total temperature from lookup table"

DELTA_s_1  =  LOOKUP('STAGE1',run,5)        "Assign compressor inlet total temperature from lookup table"
DELTA_s_2  =  LOOKUP('STAGE2',run,5)        "Assign compressor inlet total temperature from lookup table"
DELTA_s_3  =  LOOKUP('STAGE3',run,5)        "Assign compressor inlet total temperature from lookup table"
DELTA_s_4  =  LOOKUP('STAGE4',run,5)        "Assign compressor inlet total temperature from lookup table"

DELTA_h_0_1 =  LOOKUP('STAGE1',run,4)       "Assign compressor inlet total temperature from lookup table"
DELTA_h_0_2 =  LOOKUP('STAGE2',run,4)       "Assign compressor inlet total temperature from lookup table"
DELTA_h_0_3 =  LOOKUP('STAGE3',run,4)       "Assign compressor inlet total temperature from lookup table"
DELTA_h_0_4 =  LOOKUP('STAGE4',run,4)       "Assign compressor inlet total temperature from lookup table"

DELTA_s    =  DELTA_s_1+DELTA_s_2+DELTA_s_3+DELTA_s_4          "Calculates sum of entropy
changes through all the stages"
DELTA_h_0  =  DELTA_h_0_1+DELTA_h_0_2+DELTA_h_0_3+DELTA_h_0_4  "Calculates sum of enthalpy
changes through all the stages"

TR_tt      =  T_0_out/T_0_in                "Total-to-total temperature ratio"
PR_tt      =  P_0_out/P_0_in                "Total-to-total pressure ratio"
eta        =  1- ((T_0_out*(DELTA_s))/(DELTA_h_0))     "Total-to-total adiabatic efficiency"

{run =1 }      "Indicates the run according to the parametrical table and is varied according to mass flow"
```

C.6.2 Stage code source code

```
"!Function to linearly interpolate between two points"
FUNCTION Interpol (A,B,Y1,Y2,X)
        IF (Y1>=Y2) THEN
                Interpol  = ((((A-(X+1E-15))*ABS(Y1-Y2))/ABS(A-B))+Y1)
        ELSE
                Interpol  = -((((A-(X+1E-15))*ABS(Y1-Y2))/ABS(A-B))-Y1)
        ENDIF
END
```

```
"Koch and Smith profile loss correction factors ======================="
"!Function for calculating correction factors for mach number effects on momentum thickness - Figure A.2.3 "
FUNCTION KMM (M,D_eq)
        IF (1 <= D_eq) AND (D_eq < 1.3) THEN
                Y1      =       1 - 0.00151*M - 0.05544*M^2         "Correction factor equation for D_eq = 1"
                Y2      =       1 - 0.00205*M - 0.10085*M^2         "Correction factor equation for D_eq = 1.3"
                KMM     =       Interpol(1,1.3,Y1,Y2,D_eq)
        ELSE
                IF (1.3 <= D_eq) AND (D_eq < 1.5) THEN
                        Y1      =       1 - 0.00205*M - 0.10085*M^2"Correction factor equation for D_eq = 1.3"
                        Y2      =       1 - 0.02936*M - 0.11103*M^2"Correction factor equation for D_eq = 1.5"
                        KMM     = Interpol(1.3,1.5,Y1,Y2,D_eq)
                ELSE
                        IF (1.5 <= D_eq) AND (D_eq <=1.7) THEN
                                Y1=1 - 0.02936*M - 0.11103*M^2      "Correction factor equation for D_eq = 1.5"
                                Y2=1 - 0.02627*M - 0.151*M^2        "Correction factor equation for D_eq = 1.7"
                                KMM = Interpol(1.5,1.7,Y1,Y2,D_eq)
                        ELSE
                                CALL WARNING('Eq Diffusion ratio > 1.7 use value of correlation for 1.7') "Display
warning if D_eq is out of range"
                                KMM = 1 - 0.02627*M - 0.151*M^2"Use value of D_eq = 1.7 for higher values of
D_eq"
                        ENDIF
                ENDIF
        ENDIF
END

"!Function for calculating correctional multipliers for mach number effects on form factor - Figure A.2.3"
FUNCTION KMH (M,D_eq)
        IF (1 <= D_eq) AND (D_eq < 1.3) THEN
                Y1=1 + 0.08796*M + 0.27474*M^2                      "Correction factor equation for D_eq = 1"
                Y2=1 + 0.04192*M + 0.1995*M^2                       "Correction factor equation for D_eq = 1.3"
                KMH= Interpol(1,1.3,Y1,Y2,D_eq)
        ELSE
                IF (1.3 <= D_eq) AND (D_eq < 1.5) THEN
                        Y1=1 + 0.04192*M + 0.1995*M^2               "Correction factor equation for D_eq = 1.3"
                        Y2=1 + 0.01736*M + 0.14414*M^2              "Correction factor equation for D_eq = 1.5"
                        KMH= Interpol(1.3,1.5,Y1,Y2,D_eq)
                ELSE
                        IF (1.5 <= D_eq) AND (D_eq <= 1.7) THEN
                                Y1=1 + 0.01736*M + 0.14414*M^2      "Correction factor equation for D_eq = 1.5"
                                Y2=1 + 0.02241*M + 0.09155*M^2      "Correction factor equation for D_eq = 1.7"
                                KMH= Interpol(1.5,1.7,Y1,Y2,D_eq)
                        ELSE
                                KMH = 1 + 0.02241*M + 0.09155*M^2"Correction factor equation for D_eq = 1.7"
                        ENDIF
                ENDIF
        ENDIF
END

"!Function for calculating correction factor for stream tube contraction ratio effects on momentum thickness - Figure
A.2.4"
FUNCTION KSTM (h_ratio)
        KSTM    =0.45 + 0.55*h_ratio
END

"!Function for calculating correction factor for stream tube contraction ratio effects on form factor - Figure A.2.5"
FUNCTION KSTH (h_ratio,D_eq)
        IF (1 <= D_eq) AND (D_eq < 1.3) THEN
                Y1      =       1.02114 - 0.02057*h_ratio
                Y2      =       1.00829 - 0.00714*h_ratio           "Correction factor equation for D_eq = 1"
                KSTH = Interpol(1,1.3,Y1,Y2,D_eq)
        ELSE
                IF (1.3 <= D_eq) AND (D_eq < 1.5) THEN
                        Y1      =       1.00829 - 0.00714*h_ratio   "Correction factor equation for D_eq = 1.3"
                        Y2      =       0.95457 + 0.04571*h_ratio   "Correction factor equation for D_eq = 1.5"
                        KSTH = Interpol(1.3,1.5,Y1,Y2,D_eq)
                ELSE
                        IF (1.5 <= D_eq) AND (D_eq <= 1.7) THEN
                                Y1=0.95457 + 0.04571*h_ratio        "Correction factor equation for D_eq = 1.5"
```

```
                    Y2=0.84457 + 0.15571*h_ratio      "Correction factor equation for D_eq = 1.7"
                    KSTH = Interpol(1.5,1.7,Y1,Y2,D_eq)
                ELSE
                    KSTH = 0.84457 + 0.15571*h_ratio  "Correction factor equation for D_eq = 1.7"
                ENDIF
            ENDIF
        ENDIF
END

"!Function for calculating correction factor for Reynolds number and surface finish effects on Momentum thickness ratio - Figure A.2.6"
FUNCTION KRSM (Re_c,k_CLA,c,W_1,rho,mu)
        k_s = 6.2*k_CLA                                          "Equation 3.7"
        RR = k_s/c                                               "Relative roughness"
        RRe = (k_s*W_1*rho)/mu                                   "Roughness Reynolds number"
        IF (RRe <= 90) THEN                                      "Equation 3.6"
            IF (Re_c < 200000) THEN
                KRSM = 600.178*Re_c^(-0.5)                       "Momentum thickness vary as the -0.5 power of chord Reynolds number"
            ELSE
                KRSM = 10.224*Re_c^(-0.166)                      "Momentum thickness vary as the -0.166 power of chord Reynolds number"
            ENDIF
        ELSE
            KRSM = 23.398*RR^(0.347)                             "Power fit of relation of Relative roughness to correction"
        ENDIF
END

"!Function for calculating correction factor for Reynolds number and surface finish effects on Form factor - Figure A.2.6"
FUNCTION KRSH (Re_c,k_CLA,c,W_1,rho,mu)
        k_s = 6.2*k_CLA                                          "Equation 3.7"
        RR = k_s/c                                               "Relative roughness"
        RRe = (k_s*W_1*rho)/mu                                   "Roughness Reynolds number"
        IF (RRe <= 90) THEN                                      "Equation 3.6"
            KRSH = 2.291*Re_c^(-0.06)        "Form factor vary as the -0.06 power of chord Reynolds number"
        ELSE
            KRSH = 23.398*RR^(0.347)         "Power fit of relation of Relative roughness to correction"
        ENDIF
END
"End of correction factor functions for Koch and Smith profile loss model ================="

"!Function to calculate annulus blockage factor and to limit it according to Koch and Smith"
FUNCTION ABF(ABF_in,delta_bar,h_bar)
        IF (((2*(delta_bar))/h_bar) < 0.17) THEN
            ABF_1=(1 - 2*delta_bar/h_bar)    "Annulus blockage factor with delta_bar calculated in endwall loss module"
        ELSE
            ABF_1=0.83                       "Limiting value for annulus blockage factor"
        ENDIF

        IF (ABF_1*ABF_in < 0.83) THEN
            ABF= 0.83                        "Limiting value for annulus blockage factor"
        ELSE
            ABF=  ABF_1*ABF_in               "Inlet ABF taken into account"
        ENDIF

END

"!Module to calculate minimum loss (reference) incidence, i_0_10 and n approximated by interpolating between sigma 0.4 and 2 due to even distribution of solidity lines"
MODULE Min_inc(beta_1,sigma,t,c,theta_camber:i_min)
        i_0_10_1        =   0.02857143*beta_1                                    "Figure B.1.2 for sigma = 0.4"
        i_0_10_2        =   -0.01525 + 0.20391*beta_1 - 3.42769E-03*beta_1^2 + 8.62955E-05*beta_1^3 - 7.04167E-07*beta_1^4
                                                                                 "Figure B.1.2 for sigma = 2"
        i_0_10          =   Interpol(0.4,2,i_0_10_1,i_0_10_2,sigma)
        n_1             =   -0.0522- 0.00302*beta_1 - 3.93E-05*beta_1^2"Figure B.1.1 for sigma = 0.4"
        n_2             =   -0.011821 + 1.7691E-04*beta_1 + 6.06E-06*beta_1^2 - 6.12E-07*beta_1^3
        "Figure B.1.1 for sigma = 2"
        n               =   Interpol(0.4,2,n_1,n_2,sigma)
        K_sh            =   1                                                    "Shape factor for NACA 65 blades"
```

```
        K_t             =       1.499E-03 + 18.395*(t/c) - 105.283*(t/c)^2 + 260.4167*(t/c)^3   "Figure B.1.3"
        i_0             =       K_sh*K_t*i_0_10                                                 "Equation 4.15"
        i_min           =       i_0 + n*theta_camber - 1                                        "Equation 4.14"
END

"!Procedure to calculate deviation - according to Lieblien 1960"
PROCEDURE Deviation(i,i_min,beta_1,t,c,theta_camber,sigma:delta_min,delta)
        K_t = 0.01277 + 6.386*(t/c) + 36.074*(t/c)^2                                            "Figure B.2.4"
        K_sh = 1                                                                                "Shape factor for NACA 65 blades"
        IF (sigma >= 0.4) AND (sigma < 1.2) THEN
                delta_0_10_1 = 0.0043 + 0.00629*beta_1 + 3.74E-05*beta_1^2 + 1.09E-06*beta_1^3 "Figure B.2.3 for
sigma = 0.4"
                delta_0_10_2 = -0.01483 + 0.0176*beta_1 - 2.14E-04*beta_1^2 + 8.21E-06*beta_1^3 "Figure B.2.3 for
sigma = 1.2"
                delta_0_10 = Interpol(0.4,1.2,delta_0_10_1,delta_0_10_2,sigma)
        ELSE
                delta_0_10_1 = -0.01483 + 0.0176*beta_1 - 2.14E-04*beta_1^2 + 8.21E-06*beta_1^3 "Figure B.2.3 for
sigma = 1.2"
                delta_0_10_2 = -0.0016575 + 0.0102*beta_1 + 9.62E-04*beta_1^2 - 2.55E-05*beta_1^3 + 3.26E-
07*beta_1^4                                                                                     "Figure B.2.3 for sigma = 2"
                delta_0_10 = Interpol(1.2,2,delta_0_10_1,delta_0_10_2,sigma)
        ENDIF
        delta_0 = K_sh*K_t*delta_0_10                                                           "Equation 4.17"
        m = 0.255 + 5.83E-04*beta_1 - 9.69E-06*beta_1^2 + 2.652E-07*beta_1^3"Figure B.2.1"
        b =0.964- 0.00304*beta_1 + 6.22E-05*beta_1^2 - 1.47E-06*beta_1^3    "Figure B.2.2"

        delta_min = delta_0 + (m/sigma^b)*theta_camber                                          "Equation 4.16"

        "Off minimum loss deviation angle"
        IF (beta_1 <= 70) AND (beta_1 > 60) THEN
                slope_1 = 1.006 - 1.526*sigma + 0.475*sigma^2 + 0.276*sigma^3 - 0.132*sigma^4 "Figure B.2.5 for
beta_1 = 60 degrees"
                slope_2 =1.003 - 0.903*sigma - 0.696*sigma^2 + 1.02*sigma^3 - 0.289*sigma^4   "Figure B.2.5 for
beta_1 = 70 degrees"
                slope = Interpol(60,70,slope_1,slope_2,beta_1)
        ELSE
                IF (beta_1 <= 60) AND (beta_1 > 50) THEN
                        slope_1 =0.978- 1.955*sigma + 1.490*sigma^2 - 0.475*sigma^3 + 0.046*sigma^4 "Figure
B.2.5 for beta_1 = 50 degrees"
                        slope_2 = 1.006 - 1.526*sigma + 0.475*sigma^2 + 0.276*sigma^3 - 0.132*sigma^4 "Figure
B.2.5 for beta_1 = 60 degrees"
                        slope = Interpol(50,60,slope_1,slope_2,beta_1)
                ELSE
                        slope_1 =0.972 - 2.563*sigma + 2.685*sigma^2 - 1.288*sigma^3 + 0.234*sigma^4
        "Figure B.2.5 for beta_1 = 0 degrees"
                        slope_2 =0.978- 1.955*sigma + 1.490*sigma^2 - 0.475*sigma^3 + 0.046*sigma^4 "Figure
B.2.5 for beta_1 = 50 degrees"
                        slope = Interpol(0,50,slope_1,slope_2,beta_1)
                ENDIF
        ENDIF
        delta = delta_min + (i-i_min)*slope                                                     "Equation 4.18"
END

"!Function to calculate stalling, thus maximum pressure rise coefficient - Koch(1981) and Casey(1987) "
FUNCTION StallPRC(L_div_g,Re_bar,tau_div_g,AS_div_s)                                            "Figure B.3.2"
        IF (10000 =< Re_bar) AND (Re_bar < 20000) THEN
                K_Re1=0.725 + 0.95*Re_bar*10^(-5)
        ELSE
                IF (20000 =< Re_bar) AND (Re_bar < 40000) THEN
                        K_Re1=0.87 + 0.225*Re_bar*10^(-5)
                ELSE
                        IF (40000 =< Re_bar) AND (Re_bar < 130000) THEN
                                K_Re1=0.942 + 0.044*Re_bar*10^(-5)
                        ELSE
                                K_Re1=0.994 + 0.00459*Re_bar*10^(-5)
                        ENDIF
                ENDIF
        ENDIF

        IF (K_Re1 < 1.05) THEN                  "Ensuring that maximum value is not more than correlation value"
```

```
            K_Re = K_Re1                    "due to assumption of straight lines for high Re values"
        ELSE
            K_Re = 1.05
        ENDIF

        K_tau=1.22436 - 8.18377*(tau_div_g) + 112.12121*(tau_div_g)^2 - 829.09091*(tau_div_g)^3 +
2230.30303*(tau_div_g)^4                    "Figure B.3.3"
        K_AS=1.1421 - 0.926*(AS_div_s) + 2.333*(AS_div_s)^2 - 2.753*(AS_div_s)^3 + 1.220*(AS_div_s)^4"Figure
B.3.4"

        StallPRC = (0.1636 + 0.2428*L_div_g - 0.0394*L_div_g^2)*K_Re*K_tau*K_AS"Figure B.3.1 and corrections"
END

"!Procedure to calculate operating range of cascade"
PROCEDURE Opp_Range(M,chi_1,sigma,theta_camber:delta_beta)
        IF (M < 0.2) THEN
            K_M = 1                                         "Equation 4.21"
        ELSE
            K_M = 10^(-2.5*(M-0.2)^4.4)                     "Equation 4.21"
        ENDIF
        K       =       0.001*(-40-7*(chi_1-45)+0.25*(chi_1-45)^2-0.02*(chi_1-45)^3)"Equation 4.20"
        delta_beta_i = 21 + K*(1+sqrt(sigma))/(sigma*theta_camber)
        delta_beta = delta_beta_i*K_M                       "Equation 4.19"
END

"!Procedure to determine if blade is stalled"
PROCEDURE Blade_Stall(stg,i,i_min,delta_beta:inop$)
        IF (ABS(i - i_min) > 0.8*(delta_beta/2)) THEN       "Equation 4.22"
            CALL {ERROR}WARNING('A bladerow in stage XXXA is outside the operating range',stg)
        ENDIF
        inop$ = 'In operating range'
END

"!PROFILE LOSS"
MODULE Profile_Loss_Lieblein(beta_1,beta_2,sigma,c:omega_bar_min,block)

        H_ex    =       1.08
        D_eq    =       cos(beta_2)/cos(beta_1)*(1.12+ 0.61*((cos(beta_1))^2/sigma)*(tan(beta_2) - tan(beta_1)))

        theta_ex/c=     0.0045/(1-0.95*ln(D_eq))            "Equation 3.2"

"Profile loss calculation"
{omega_bar_min          = 2*(theta_ex/c)*(sigma/cos(beta_2))*(cos(beta_1)/cos(beta_2))^2*(2/(3-(1/H_ex)))*(1-
((theta_ex/c)*((sigma*H_ex)/cos(beta_2))))^(-3) "Equation 3.1"}
omega_bar_min  = 2*(theta_ex/c)*(sigma/cos(beta_2))*(cos(beta_1)/cos(beta_2))^2     "Equation 3.4"

block = 0                                                   "Module needs to return blockage value"

END

MODULE
Profile_Loss_Koch_Smith(r_rms_1,r_rms_2,C_theta_1,C_theta_2,Re_c,mu,c,k_CLA,h_ratio,A_1,A_2,sigma,t_max,beta
_1,beta_2,W_1,W_2,M_1,M_z_1,rho_1:omega_bar_min,block)

        GAMMA =(r_rms_1*C_theta_1 - r_rms_2*C_theta_2)/(((r_rms_1+r_rms_2)/2)*sigma*W_1)  "Equation 3.13"
        A_p=(1-0.4458*sigma*(t_max/c)/(cos((beta_1+beta_2)/2)))*(1-(A_1-A_2)/(3*A_1))     "Equation 3.11"
        rho_p/rho_1 =   (1-(M_z_1^2/(1-M_z_1^2))*(1-A_p-0.2445*(tan(beta_1)/cos(beta_1))*sigma*GAMMA))
        "Equation 3.12"
        V_p/W_1=        (((sin(beta_1) - 0.2445*sigma*GAMMA)^2)+ (cos(beta_1)/(A_p*(rho_p/rho_1)))^2)^(1/2)
        "Equation 3.9"
        V_max  /V_p     =       1+0.7688*(t_max/c)+0.6024*GAMMA                             "Equation 3.10"

        D_eq            =       (W_1/W_2)*(V_max/V_p)*(V_p/W_1)                             "Equation 3.8"

"Apply corrections for conditions other than nominal"

        K_theta_1       =       KMM (M_1,D_eq)              "Correction factor for inlet Mach number effect"
        K_theta_2       =       KSTM (h_ratio)          "Correction factor for stream tube contraction effects"
        K_theta_3       =       KRSM (Re_c,k_CLA,c,W_1,rho_1,mu)"Correction factor for Reynolds numer and
surface finish effects"
```

```
        K_total_theta = K_theta_1*K_theta_2*K_theta_3"Calculation of total correction factor for Momentum thickness"

        K_H_1           =       KMH (M_1,D_eq)                  "Correction factor for Mach number effects"
        K_H_2           =       KSTH (h_ratio,D_eq)     "Correction factor for stream tube contraction effects"
        K_H_3           =       KRSH (Re_c,k_CLA,c,W_1,rho_1,mu)"Correction factor for Reynolds numer and
surface finish effects"

        K_total_H = K_H_1*K_H_2*K_H_3                   "Calculation of total correction factor for From factor"

        theta_te/c      =       (0.0025-0.352407 + 1.22974934*D_eq - 1.67813829*D_eq^2 + 1.13092129*D_eq^3
- 0.375468932*D_eq^4 + 0.0493289263*D_eq^5)*K_total_theta "Figure A.2.1 - 0.0025 adder included"
        H_te            =       (0.541309505 - 0.72941463*D_eq + 4.20572911*D_eq^2 - 3.8628472*D_eq^3 +
1.10677083*D_eq^4)*K_total_H                            "Figure A.2.2"

"Profile loss calculation"

omega_bar_min = 2*(theta_te/c)*(sigma/cos(beta_2))*(cos(beta_1)/cos(beta_2))^2*(2/(3-(1/H_te)))*(1-
((theta_te/c)*((sigma*H_te)/cos(beta_2))))^(-3)                 "Equation 3.1"

block           =       theta_te*H_te   "Calculation of boundary layer displacement thickness - blade blockage"

END

"!OFF - MINIMUM LOSS"
MODULE Off_Loss_Casey(omega_bar_min,i,i_min,delta_beta:omega_bar)
        CHI             =       (ABS(i - i_min))/(delta_beta/2)                 "Equation 3.47"
        omega_bar/omega_bar_min         =       1+ 0.1667*CHI + 0.8333*CHI^2    "Equation 3.46"
END

MODULE Off_Loss_Lieblein(beta_1,beta_2,sigma,c,i,i_min:omega_bar)
        k               =       0.0117
        D_eq_off        =       cos(beta_2)/cos(beta_1)*(1.12+k*(ABS(i-i_min))^1.43+
0.61*((cos(beta_1))^2/sigma)*(tan(beta_2) - tan(beta_1)))                       "Equation 3.48"

        H_ex            =       1.08
        theta_ex/c      =       0.0045/(1-0.95*ln(D_eq_off))                    "Equation 3.2"
        omega_bar       = 2*(theta_ex/c)*(sigma/cos(beta_2))*(cos(beta_1)/cos(beta_2))^2*(2/(3-(1/H_ex)))*(1-
((theta_ex/c)*((sigma*H_ex)/cos(beta_2))))^(-3)                                 "Equation 3.1"
END

"!ENDWALL LOSS"
MODULE Endwall_loss_Howell(beta_1,beta_2,s,h,sigma:omega_bar)
        tan(beta_m)     = 0.5*(tan(beta_1)+tan(beta_2))                         "Equation 3.17"
        C_D_A           = 0.02*s/h                                              "Equation 3.14"
        C_L             = (2/sigma)*(tan(beta_1)-tan(beta_2))*cos(beta_m)        "Equation 3.16"
        C_D_S           = 0.018*(C_L)^2                                         "Equation 3.15"
        omega_bar       = ((C_D_A+C_D_S)*sigma*(cos(beta_1))^2)/(cos(beta_m))^3 "Equation 3.18"
END

MODULE Endwall_loss_Hub_Fott(h,c,beta_1,beta_2,tau:omega_bar)
        omega_bar_t     = 0.165/(h/c)*((tan(beta_1-90))^(-2) - (tan(beta_2-90))^(-2))*(sin(beta_1-
90))^2*tanh(35*(tau/c))+0.0288                                                  "Equation 3.22"
        omega_bar_hb    = 2*(c/h)*(0.0505*((tan(beta_1-90))^(-2) - (tan(beta_2-90))^(-2))-0.01313)*(sin(beta_1-90))^2
"Equation 3.23"
        omega_bar       = (omega_bar_t+omega_bar_hb)/2                          "Equation 3.21"
END

FUNCTION V_jet(U_bar,theta_camber,V_njet_max,V_njet,sigma)
        IF ((U_bar*cos(theta_camber)) > V_njet_max) THEN
                V_jet = 1.05*V_njet+0.5*sigma*(U_bar*cos(theta_camber)-V_njet_max)  "Equation 3.35"
        ELSE
                V_jet = 1.05*V_njet                                             "Equation 3.36"
        ENDIF
END

MODULE
Endwall_loss_Roy_Kumar(beta_1,beta_2,sigma,h,c,rho_1,tau,C_P,W_1,U_bar,q_1,theta_camber:omega_bar)
        "Assume uniform tip gap - from Table 3.1"
        A                       =1
```

```
        B                       =-0.24
        C_d                     =0.84
        tan(beta_m)             = 0.5*(tan(beta_1)+tan(beta_2))
        C_L                     = (2/sigma)*(tan(beta_1)-tan(beta_2))*cos(beta_m)
        omega_bar_ew            = 0.04*C_L^2*(sigma*c*(cos(beta_1))^2)/(h*(cos(beta_m))^3)   "Equation 3.24"

        DELTA_P_total           = DELTA_P_gap+DELTA_P_mixing                                 "Equation 3.26"
        DELTA_P_gap             = 0.5*c*rho_1*tau*W_1^3*B*(ABS(C_P))^(1.5)                   "Equation 3.27"
        DELTA_P_mixing          = 0.5*c*rho_1*tau*V_jet^3                                    "Equation 3.28"
        V_njet/W_1              = C_d*sqrt(ABS(C_P))                                         "Equation 3.29"
        V_njet_max/W_1          = A*sqrt(ABS(C_P))                                           "Equation 3.30"

        V_jet           = V_jet(U_bar,theta_camber,V_njet_max,V_njet,sigma)      "Call function to return V_jet"
        omega_bar_tau           = DELTA_P_total/(q_1*1000)                                   "Equation 3.25"

        omega_bar               = omega_bar_ew+omega_bar_tau                                 "Equation 3.33"
END

PROCEDURE
Endwall_loss_Koch_Smith(DELTA_s_fs,h_stg,DELTA_h_0,T_0_3,eta_fs,K_1,K_2,stg,C_P_eff,C_P_max,tau_wtd,AS_w
td,g_stg:delta_bar,DELTA_s_ks_rtr,DELTA_s_ks_str)

        X       =       C_P_eff/C_P_max

        IF (X > 0.7) AND (X <=1) THEN
                Y =-74.0578 + 493.6841*(X) - 1306.4354*(X)^2 + 1719.0773*(X)^3 - 1125.3951*(X)^4 + 93.4619*(X)^5
"Polinomial fit of correlation for tau/g = 0 - Figure A.4.1"
        ELSE
                IF (X > 1) THEN
                        CALL {ERROR}WARNING('Stage XXXA is stalled',stg)"Error procedure to halt calculations if
C_P > C_P_max"
                        Y = 0.126
                ELSE
                        Y = 0.126                                                            "For X <= 0.7"
                ENDIF
        ENDIF

        delta_initial = ((Y+2*(tau_wtd)*X)*g_stg)/2     "Relation for lines with other tau/g values - Equation A.4.1"

        IF (AS_wtd < 0.7) THEN
                AGP = 0.8301 + 1.50438*(AS_wtd) - 6.51982*(AS_wtd)^2 + 16.1595*(AS_wtd)^3 -
20.05944*(AS_wtd)^4 + 9.55128*(AS_wtd)^5        "Only applicable for gap/pitch ratios < 0.7 - Figure A.4.2"
        ELSE
                AGP = 1.02
        ENDIF

        delta_bar = delta_initial*AGP                   "Corrected boundary layer displacement thickness"

        IF (X > 0.7) THEN
                nu_bar = (2.9464 - 9.29627*X + 11.8667*X^2 - 5.11111*X^3)*delta_bar  "Polinomial fit of correlation
for tangential force thickness - Figure A.4.3"
        ELSE
                nu_bar = 0.5*delta_bar                                               "For X <= 0.7"
        ENDIF
        "Rewrite 3.19 to give entropy increase rather than new efficiency"
        DELTA_s =(((1-(eta_fs*(1-((2*delta_bar)/g_stg)*(g_stg/h_stg))/(1-
((2*nu_bar)/(2*delta_bar))*((2*delta_bar)/g_stg)*(g_stg/h_stg))))*DELTA_h_0)/T_0_3 - DELTA_s_fs)
        DELTA_s_ks_rtr  =       DELTA_s*K_1             "Assign entropy change for rotor according to row factor"
        DELTA_s_ks_str  =       DELTA_s*K_2             "Assign entropy change for stator according to row factor"
END

"!PART SPAN SHROUD LOSS"
MODULE Pss_loss(beta_1,beta_2,C_z,a,r_sh,N_b,c_sh,t_sh,A_bar,R,gamma:DELTA_s)
        tan(beta_m)     =       (tan(beta_1)+tan(beta_2))/2
        W_m             =       C_z*(1/(cos(beta_m)))
        M_m             =       W_m/a                                                    "Equation 3.39"
        P_M             =       (1-M_m^2*(cos(beta_m))^2)^(-1/2)                         "Equation 3.37"
        b               =       (2*pi*r_sh)/N_b                                          "Equation 3.38"
        C_D_sh =1.8*(0.012*((c_sh/t_sh)/cos(beta_m)+2+60*P_M^3*(t_sh/c_sh)^2)+3*P_M^3*(t_sh/b)*(t_sh/c_sh))
        "Equation 3.36"
```

```
        A_sh            =       2*pi*r_sh*t_sh                                  "Equation 3.35"
        DELTA_s         =       C_D_sh*(gamma/2)*M_m^2*(A_sh/A_bar)*R           "Equation 3.40"
END

"!WINDAGE LOSS"
MODULE Windage_loss(C_z,U,r_hb_1,r_hb_2,Re,DELTA_h_0,h_bar,T_0_2:DELTA_s)
        psi             =       C_z/U                                           "Equation 3.42"
        phi             =       DELTA_h_0/U^2                                   "Equation 3.43"
        D_hb            =       r_hb_1+r_hb_2
        C_m     =       0.12654*Re^(-0.222)"Power fit for Reynolds numbers between 10^5 and 10^11 - Figure 3.4"
        C_f             =       0.398*C_m                                       "Equation 3.44"
        DELTA_W_windage/DELTA_h_0 = 0.1*(C_f/(phi*psi))*(D_hb/h_bar)*(1/(1+(4*h_bar)/D_hb)) "Equation 3.41"
        DELTA_s  = DELTA_W_windage/(T_0_2*m_dot)                                "Entropy increase due to windage"
END

"!ROTOR"
MODULE
Rotor(delta_ks,DELTA_s_ks_rtr,m_dot_c,ABF_in,stg,T_0_1,P_0_1,alpha_1,P_1,T_1,r_rms_2,alpha_2,M_2a,P_2,T_2,P
_0_2,T_0_2,C_2,A_2,M_z_2,C_theta_2,C_z_2,C_1,U_1,U_2,beta_1,q_1,q_1_eff,ABF,DELTA_h_0,DELTA_s,Re,L,g,DE
LTA_s_fs,omega_bar)
$COMMON fluid$,N

"Inputs from lookup table"
tau_rtr         =       LOOKUP('Stage inputs',stg,3)            "Tip clearance"
xi_rtr          =       LOOKUP('Stage inputs',stg,4)            "Blade stagger angle"
chi_1_rtr       =       ABS(LOOKUP('Stage inputs',stg,5))       "Blade inlet angle"
chi_2_rtr       =       ABS(LOOKUP('Stage inputs',stg,6))       "Blade outlet angle"
r_t_1           =       LOOKUP('Stage inputs',stg,7)            "Tip radius at inlet of blade row "
r_t_2           =       LOOKUP('Stage inputs',stg,8)            "Tip radius at outlet of blade row"
r_hb_1          =       LOOKUP('Stage inputs',stg,9)            "Hub radius at inlet of blade row"
r_hb_2          =       LOOKUP('Stage inputs',stg,10)           "Hub radius at outlet of blade row"
t_max_rtr       =       LOOKUP('Stage inputs',stg,11)           "Midspan maximum thickness"
c_rtr           =       LOOKUP('Stage inputs',stg,12)           "Blade chord at midspan"
s_rtr           =       LOOKUP('Stage inputs',stg,13)           "Blade pitch at mid span"
k_CLA_rtr       =       LOOKUP('Stage inputs',stg,14)           "Blade roughness - arithmetical avarage
deviation normal to the centre line"
m_dot           =       m_dot_c - LOOKUP('Stage inputs',stg,1)  "Flow rate, compressor inlet flow rate minus
bleed flow"
r_sh            =       LOOKUP('Stage inputs',stg,15)           "Part span shroud radius"
t_sh            =       LOOKUP('Stage inputs',stg,16)           "Part span shroud thickness"
c_sh            =       LOOKUP('Stage inputs',stg,17)           "Part span shroud chord"

"Calculate other geometrical rotor parameters"
sigma           =       c_rtr/s_rtr                             "Solidity"
N_b             =       ROUND((2*pi*((r_rms_1+r_rms_2)/2))/s_rtr)  "Number of blades if trailing edge is assumed
infinitly small"
h_ratio         =       (r_t_1-r_hb_1)/(r_t_2-r_hb_2)           "Blade heigth ratio"
h_bar           =       ((r_t_1-r_hb_1)+(r_t_2-r_hb_2))/2       "Average blade height"
theta_camber    =       chi_1_rtr - chi_2_rtr                   "Blade camber angle"
g               =       s_rtr*cos(xi_rtr)                       "Rotor staggerd spacing"
L               =       (c_rtr*pi*theta_camber)/(360*sin(theta_camber/2))   "Meanline length of circular arc airfoil"

"Thermodynamic fluid properties assumed constant throughout bladerow"
C_p             =       CP(fluid$,T=(T_1+T_2)/2,P=(P_1+P_2)/2)  "Bladerow specific heat at constant pressure"
C_v             =       CV(fluid$,T=(T_1+T_2)/2,P=(P_1+P_2)/2)  "Bladerow specific heat at constant volume"
R               =       C_p-C_v                                 "Gas constant"
gamma           =       C_p/C_v                                 "Relation of C_p to C_v"

"!ROTOR INLET CALCULTIONS"
"Rotor inlet pressure and temperature calculations"
T_1             =       T_0_1- C_1^2/(2*C_p)                    "Calculation for T - static temperature"
P_1             =       P_0_1/(T_0_1/T_1)^(gamma/(gamma-1))     "Calculation for P - static pressure"
T_0_1r          =       T_0_1 + (W_1^2-C_1^2)/(2*C_p)           "Calculates relative stagnation temperature"
P_0_1r          =       P_0_1*((T_0_1r/T_0_1)^((gamma)/((gamma)-1)))    "Calculates relative stagnation
pressure"
h_T             =       C_p*T_0_1r - 0.5*U_1^2          "Rothalpy at rotor inlet, equal to rothalpy at rotor outlet"
P_T_1           =       P_1*(((h_T/C_p)/T_1)^((gamma)/((gamma)-1)))     "Calculates pressure based on
rothalpy at rotor inlet"
"Rotor inlet thermodynamical property calculations from built in EES functions"
rho_1           =       DENSITY(fluid$,T=T_1,P=P_1)             "Density of fluid at bladerow inlet"
```

```
a1              =       sqrt(gamma*R*T_1)                       "Velocity of sound, m/s at bladerow inlet"
mu_1            =       VISCOSITY(fluid$,T=T_1,P=P_1)           "Viscosity of fluid at bladerow inlet"
"Inlet velocity triangle equations"
A_1             =       ((pi*r_t_1^2)-(pi*r_hb_1^2))*ABF        "Inlet annulus area with ABF taken into account"
r_rms_1         =       sqrt((r_t_1^2 + r_hb_1^2)/2)            "Rms diameter at inlet of blade row"
U_1             =       ((2*pi*N)/60)*r_rms_1                   "Blade pheripheral speed at rms_1"
C_z_1           =       m_dot/(rho_1*A_1)                       "Inlet axial velocity, calculated from the
continuity"
W_1             =       sqrt((U_1-C_theta_1)^2 + (C_z_1)^2)     "Inlet relative velocity"
C_1             =       C_z_1/cos(alpha_1)                      "Inlet Absolute velocity"
C_theta_1       =       C_z_1*tan(alpha_1)              "Tangential component of absolute inlet velocity"
beta_1          =       -arccos(C_z_1/W_1)                      "Calculates angle relative to rotor at inlet"
"Other required inlet variables"
i               =       -chi_1_rtr - beta_1                     "Incidence"
M_z_1           =       C_z_1/a1                                "Inlet axial Mach number, based on axial
velocity"
M_1             =       W_1/a1                                  "Relative inlet Mach number"
q_1             =       (P_0_1r - P_1)                          "Inlet dynamic head to rotor"
q_1_eff         =       q_1*((1+2.5*(C_1*sin(alpha_1+beta_1))^2+0.5*U_1^2)/(4*C_1^2))"Effective inlet dynamic
head for rotor"

"!ROTOR OUTLET CALCULATIONS"
"Rotor outlet pressure and temperature calculations"
T_0_2r          =       (h_T+ 0.5*U_2^2)/C_p                    "Outlet relative temperature, rothalpy at rotor
outlet = rothalpy at rotor inlet"
P_T_2           =       P_T_1 - (omega_bar*q_1*P_T_1)/P_0_1r    "Outlet pressure based on rothalpy
incorporating pressure losses"
P_2             =       P_T_2/(((h_T/C_p)/T_2)^((gamma)/((gamma)-1)))   "Static pressure at outlet"
T_0_2           =       T_0_2r - (W_2^2-C_2^2)/(2*C_p)          "Stagnation temperature at outlet"
P_0_2           =       P_2*(T_0_2/T_2)^(gamma/(gamma-1))       "Stagnation pressure at outlet"
P_0_2r          =       P_0_2*((T_0_2r/T_0_2)^((gamma)/((gamma)-1)))"Relative outlet stagnation pressure"
T_2             =       T_0_2-C_2^2/(2*C_p)                     "Calculation for static temperature at outlet"
"Rotor outlet thermodynamical property calculations from built in EES functions"
rho_2           =       DENSITY(fluid$,T=T_2,P=P_2)             "Density of fluid at bladerow outlet"
a2              =       sqrt(gamma*R*T_2)                       "Velocity of sound, m/s at bladerow outlet"
mu_2            =       VISCOSITY(fluid$,T=T_2,P=P_2)           "Viscosity of fluid at bladerow outlet"
"Outlet velocity triangle equations"
A_2             =       ((pi*r_t_2^2)-(pi*r_hb_2^2))*ABF        "Outlet annulus area with ABF taken in account"
r_rms_2         =       sqrt((r_t_2^2 + r_hb_2^2)/2)            "Mean diameter at exit of blade row"
U_2             =       ((2*pi*N)/60)*r_rms_2                   "Blade pheripheral speed at r_rms_2"
C_z_2           =       m_dot/(rho_2*A_2)                       "Outlet axial velocity - calculated from
continuity"
W_2             =       (sqrt((U_2-C_theta_2)^2 + (C_z_2)^2))   "Outlet relative velocity"
C_2             =       C_z_2/cos(alpha_2)                      "Outlet absolute velocity"
C_theta_2       =       C_z_2*tan(alpha_2)              "Tangential component of absolute outlet velocity"
beta_2          =       -arccos(C_z_2/W_2)                      "Calculates angle relative to rotor at outlet"

CALL Deviation(i,i_min,ABS(beta_1),t_max_rtr,c_rtr,theta_camber,sigma:delta_min,delta) "Call sub-section for deviation
at min loss and off-min loss"

beta_2          =       -chi_2_rtr - delta                      "Definition of deviation"
"Other required outlet variables"
M_z_2           =       C_z_2/a2                        "Outlet axial Mach number, based on axial velocity"
M_2             =       W_2/a2                          "Outlet Mach number, based on relative exit velocity"
M_2a            =       C_2/a2                          "Outlet Mach number, based on absolute exit velocity"
BBF             =       1-(2*block)/(g+t_max_rtr)       "Blade blackage factor - block is value returned from
profile loss module"
W_2_fs          =       W_2/BBF                         "Freestream outlet velocity due to BBF - blade blockage
factor from and to profile loss"
ABF             =       ABF(ABF_in,delta_bar,h_bar)     "Annulus blockage factor - from Function ABF"

"Other variables needed for calculations"
DELTA_h_0       =       C_p*(T_0_2 - T_0_1)                     "Stagnation enthalpy change accross bladerow"
DELTA_h         =       C_p*(T_2-T_1)                   "Static enthalpy change accross bladerow"
Re_c            =       ((rho_1+rho_2)/2*((W_1+W_2)/2)*c_rtr)/((mu_1+mu_2)/2)   "Chord Reynolds number"
Re              =       ((rho_1+rho_2)/2*(C_z_1+C_z_2)/2*sqrt((4*(A_1+A_2)/2)/pi))/((mu_1+mu_2)/2)  "Reynolds
number based in equivalent diameter"
CALL Blade_stall(stg,i,i_min,delta_beta:inop$)  "Test if blade is in stall and halt calculations with error message"
CALL Min_inc(ABS(beta_1),sigma,t_max_rtr,c_rtr,theta_camber:i_min)  "Minimum loss or reference incidence from sub-
section Min_inc"
```

```
CALL Opp_Range(M_1,chi_1_rtr,sigma,theta_camber:delta_beta)      "Operating range of cascade from sub-section Opp-Range"

delta_bar      =      delta_ks                    "Sets endwall boundary layer displacement thickness parameter equal to Koch and Smith value calculated in calling module"

"!CALLS TO LOSS MODEL SUB-SECTIONS"
CALL
Profile_Loss_Koch_Smith(r_rms_1,r_rms_2,C_theta_1,C_theta_2,Re_c,mu_1,c_rtr,k_CLA_rtr,h_ratio,A_1,A_2,sigma,t_max_rtr,ABS(beta_1),ABS(beta_2),W_1,W_2_fs,M_1,M_z_1,rho_1:omega_bar_min,block)
{CALL Profile_Loss_Lieblein(ABS(beta_1),ABS(beta_2),sigma,c_rtr:omega_bar_min,block)}

CALL Off_Loss_Casey(omega_bar_min,i,i_min,delta_beta:omega_bar_p)
{CALL Off_Loss_Lieblein(ABS(beta_1),ABS(beta_2),sigma,c_rtr,i,i_min:omega_bar_p)}

CALL Pss_loss(beta_1,beta_2,(C_z_1+C_z_2)/2,(a1+a2)/2,r_sh,N_b,c_sh,t_sh,(A_1+A_2)/2,R,gamma:DELTA_s_pss)

DELTA_s_ew     =      DELTA_s_ks_rtr  "Koch and Smith endwall loss model"
{CALL Endwall_loss_Howell(ABS(beta_1),ABS(beta_2),s_rtr,h_bar,sigma:omega_bar_ew)}
{CALL Endwall_loss_Hub_Fott(h_bar,c_rtr,ABS(beta_1),ABS(beta_2),tau_rtr:omega_bar_ew)}
{CALL Endwall_loss_Roy_Kumar(ABS(beta_1),ABS(beta_2),sigma,h_bar,c_rtr,rho_1,tau_rtr,(P_2-P_1)/q_1,W_1,U_1,q_1,theta_camber:omega_bar_ew)}

CALL Windage_loss((C_z_1+C_z_2)/2,(U_1+U_2)/2,r_hb_1,r_hb_2,Re,DELTA_h_0,h_bar,T_0_2:DELTA_s_windage)

"Equations nessacary to obtain both pressure loss and entropy increase for losses"
DELTA_s        = C_p*ln(T_2/T_1)-R*ln(P_2/P_1)                    "Total entropy change through rotor"
DELTA_s_fs     = DELTA_s_p + DELTA_s_pss                          "Freestream entropy change through rotor"
DELTA_s        = DELTA_s_fs+DELTA_s_ew+DELTA_s_windage            "Windage loss only influence efficiency, not pressure loss"
DELTA_s_ew     = -R*ln((P_T_1 - (omega_bar_ew*q_1*P_T_1)/P_0_1r)/P_T_1) "Calculates pressure loss coefficient from endwall loss"
DELTA_s_pss    = -R*ln((P_T_1 - (omega_bar_pss*q_1*P_T_1)/P_0_1r)/P_T_1)"Calculates pressure loss coefficient from part span shroud loss"
omega_bar = omega_bar_ew+omega_bar_p+omega_bar_pss+omega_bar_windage"Sum of pressure loss coefficients for use in pressure loss equations"

END


"!STATOR"
MODULE
Stator(delta_ks,DELTA_s_ks_str,m_dot_c,ABF_in,alpha_1,stg,r_rms_2,alpha_2,M_2a,P_2,T_2,P_0_2,T_0_2,C_2,A_2,M_z_2,C_theta_2,C_z_2,C_1,U_1,U_2,beta_1,P_3,T_3,T_0_3,P_0_3,alpha_3,ABF,DELTA_s,Re,L,g,q_2,q_2_eff,DELTA_s_fs,omega_bar)
$COMMON fluid$,N

"Inputs from lookup table"
tau_str        =      LOOKUP('Stage inputs',stg,18)              "Tip clearance"
xi_str         =      LOOKUP('Stage inputs',stg,19)              "Blade stagger angle"
chi_2_str      =      LOOKUP('Stage inputs',stg,20)              "Blade inlet angle"
chi_3_str      =      LOOKUP('Stage inputs',stg,21)              "Blade outlet angle"
r_t_2          =      LOOKUP('Stage inputs',stg,8)               "Tip radius at inlet of blade row"
r_t_3          =      LOOKUP('Stage inputs',stg,22)              "Tip radius at outlet of blade row"
r_hb_2         =      LOOKUP('Stage inputs',stg,10)              "Hub radius at inlet of blade row"
r_hb_3         =      LOOKUP('Stage inputs',stg,23)              "Hub radius at outlet of blade row"
t_max_str      =      LOOKUP('Stage inputs',stg,24)              "Midspan maximum thickness"
c_str          =      LOOKUP('Stage inputs',stg,25)              "Blade chord at midspan"
s_str          =      LOOKUP('Stage inputs',stg,26)              "Blade pitch at mid span"
k_CLA_str      =      LOOKUP('Stage inputs',stg,27)              "Blade roughness - arithmetical avarage deviation normal to the centre line"
m_dot          =      m_dot_c - LOOKUP('Stage inputs',stg,1)     "Stage flow rate"
r_sh           =      LOOKUP('Stage inputs',stg,28)              "Part span shroud radius"
t_sh           =      LOOKUP('Stage inputs',stg,29)              "Part span shroud thickness"
c_sh           =      LOOKUP('Stage inputs',stg,30)              "Part span shroud chord"

"Calculate other geometrical stator parameters"
sigma          =      c_str/s_str                                "Solidity"
N_b            =      ROUND((2*pi*((r_rms_2+r_rms_3)/2))/s_str)  "Number of blades if trailing edge is assumed infinitely small"
```

```
h_ratio = (r_t_2-r_hb_2)/(r_t_3-r_hb_3) "Blade heigth ratio"
h_bar = ((r_t_2-r_hb_2)+(r_t_3-r_hb_3))/2 "Average blade height"
theta_camber = chi_2_str - chi_3_str "Blade camber angle"
g = s_str*cos(xi_str) "Stator staggerd spacing"
L = (c_str*pi*theta_camber)/(360*sin(theta_camber/2)) "Meanline length of circular arc airfoil"

"Thermodynamic fluid properties assumed constant throughout bladerow"
C_p = CP(fluid$,T=(T_2+T_3)/2,P=(P_2+P_3)/2) "Bladerow specific heat at constant pressure"
C_v = CV(fluid$,T=(T_2+T_3)/2,P=(P_2+P_3)/2) "Bladerow specific heat at constant volume"
R = C_p-C_v "Gas constant"
gamma = C_p/C_v "Relation of C_p to C_v"

"!STATOR INLET CALCULATIONS"
"Mostly done in Rotor sub-section"
q_2 = (P_0_2 - P_2) "Inlet dynamic head to stator"
q_2_eff = q_2*((1+2.5*U_2^2+0.5*U_2^2)/(4*C_2^2)) "Effective inlet dynamic head for stator"
"Stator inlet thermodynamical property calculations from built in EES functions"
rho_2 = DENSITY(fluid$,T=T_2,P=P_2) "Density of fluid at bladerow inlet"
a2 = sqrt(gamma*R*T_2) "Velocity of sound at bladerow inlet"
mu_2 = VISCOSITY(fluid$,T=T_2,P=P_2) "Viscosity of fluid at bladerow inlet"
i = alpha_2 - chi_2_str "Incidence"

"!STATOR OUTLET CALCULATIONS"
"Rotor outlet pressure and temperature calculations"
T_0_3 = T_0_2 "Constant h_0 over stator"
P_0_3 = P_0_2- omega_bar*q_2 "Calculation for P_0 at outlet of stator"
T_3 = T_0_3-C_3^2/(2*C_p) "Calculation for T - static at outlet"
P_3 = P_0_3/(T_0_3/T_3)^(gamma/(gamma-1)) "Calculation for P - static at outlet"
"Stator outlet thermodynamical property calculations from built in EES functions"
rho_3 = DENSITY(fluid$,T=T_3,P=P_3) "Density of fluid at bladerow outlet"
a3 = sqrt(gamma*R*T_3) "Velocity of sound at bladerow outlet"
mu_3 = VISCOSITY(fluid$,T=T_3,P=P_3) "Viscosity of fluid at bladerow outlet"
"Outlet velocity triangle equations"
A_3 = ((pi*r_t_3^2)-(pi*r_hb_3^2))*ABF "Calculates outlet annulus area, ABF_out is due
to the endwall boundary layer of this stage"
r_rms_3 = sqrt((r_t_3^2 + r_hb_3^2)/2) "Rms diameter at outlet of blade row"
U_3 = 0 "Blade pheripheral speed at r_rms_3"
C_z_3 = m_dot/(rho_3*A_3) "Outlet axial velocity - calculated from continuity"
W_3 = sqrt((U_3-C_theta_3)^2 + (C_z_3)^2) "Outlet relative velocity"
C_3 = C_z_3/cos(alpha_3) "Outlet absolute velocity"
C_theta_3 = C_3*sin(alpha_3) "Tangential component of absolute outlet velocity"
beta_3 = arccos(C_z_3/W_3) "Calculates angle relative to stator at outlet"

CALL Deviation(i,i_min,alpha_2,t_max_str,c_str,theta_camber,sigma:delta_min,delta) "Call sub-section for deviation at
min loss and off-min loss"

alpha_3 = chi_3_str + delta "Definition of deviation"
"Other required outlet variables"
M_z_3 = C_z_3/a3 "Outlet axial Mach number, based on axial velocity"
M_3 = C_3/a3 "Outlet Mach number, based on absolute velocity"
BBF = (1-2*block/(g-t_max_str)) "Blade blackage factor - block is value returned from
profile loss boundary layer equations"
C_3_fs = C_3/BBF "Freestream outlet velocity due to BBF - blade
blockage factor from and to profile loss"
ABF = ABF(ABF_in,delta_bar,h_bar) "Annulus blockage factor, from function ABF "

"Other variables needed for calculations"
DELTA_h = C_p*(T_3-T_2) "Static enthalpy rise across stator"
Re_c = ((rho_2+rho_3)/2*((C_2+C_3)/2)*c_str)/((mu_2+mu_3)/2) "Chord Reynolds number"
Re = ((rho_2+rho_3)/2*(C_z_2+C_z_3)/2*sqrt((4*(A_2+A_3)/2)/pi))/((mu_2+mu_3)/2) "Reynolds
number based on equivalent diameter"
CALL Blade_Stall(stg,i,i_min,delta_beta:inop$) "Test if blade is in stall and halt calculations with
error message"
CALL Min_inc(alpha_2,sigma,t_max_str,c_str,theta_camber:i_min) "Minimum loss or reference incidence from sub-
section Min_inc"
CALL Opp_Range(M_2a,chi_2_str,sigma,theta_camber:delta_beta) "Calcualtion of operating range of cascade from
sub-section Opp-Range"

delta_bar = delta_ks "Sets endwall boundary layer displacement thickness
parameter equal to Koch and Smith value calculated in calling module"
```

```
"!CALLS TO LOSS MODEL SUB-SECTIONS"
CALL
Profile_Loss_Koch_Smith(r_rms_2,r_rms_3,C_theta_2,C_theta_3,Re_c,mu_2,c_str,k_CLA_str,h_ratio,A_2,A_3,sigma,t_
max_str,alpha_2,alpha_3,C_2,C_3_fs,M_2a,M_z_2,rho_2:omega_bar_min,block)
{CALL Profile_Loss_Lieblein(alpha_2,alpha_3,sigma,c_str:omega_bar_min,block)}

CALL Off_Loss_Casey(omega_bar_min,i,i_min,delta_beta:omega_bar_p)
{CALL Off_Loss_Lieblein(alpha_2,alpha_3,sigma,c_str,i,i_min:omega_bar_p)}

CALL
Pss_loss(alpha_2,alpha_3,(C_z_2+C_z_3)/2,(a2+a3)/2,r_sh,N_b,c_sh,t_sh,(A_2+A_3)/2,R,gamma:DELTA_s_pss)

DELTA_s_ew    =    DELTA_s_ks_str    "Koch and Smith endwall loss model selected"
{CALL Endwall_loss_Howell(alpha_2,alpha_3,s_str,h_bar,sigma:omega_bar_ew)}
{CALL Endwall_loss_Hub_Fott(h_bar,c_str,alpha_2,alpha_3,tau_str:omega_bar_ew)}
{CALL Endwall_loss_Roy_Kumar(alpha_2,alpha_3,sigma,h_bar,c_str,rho_2,tau_str,(P_3-
P_2)/q_2,C_1,U_2,q_2,theta_camber:omega_bar_ew)}

"Equations nessacary to obtain both pressure loss and entropy increase for losses"
DELTA_s          = C_p*ln(T_3/T_2)-R*ln(P_3/P_2)   "Total entropy change through rotor"
DELTA_s_fs       = DELTA_s_p + DELTA_s_pss          "Freestream entropy change through rotor"
DELTA_s          = DELTA_s_fs+DELTA_s_ew
DELTA_s_ew   = -R*ln((P_0_2 - (omega_bar_ew*q_2))/P_0_2)"Calculates pressure loss coefficient from endwall loss"
DELTA_s_pss  = -R*ln((P_0_2 - (omega_bar_pss*q_2))/P_0_2)"Calculates pressure loss coefficient from part span
shroud loss"
omega_bar        = omega_bar_ew+omega_bar_p+omega_bar_pss"Sum of pressure loss coefficients for use
in pressure loss equations"

END

"STAGE – Main Program"
"!Assigns user inputs from Lookup table"
fluid$      =    LOOKUP$('Inlet comp',1,1)          "Defines working fluid for use in fluid property
calculations"
N           =    LOOKUP('Inlet comp',1,2)           "Rotational speed"
T_0_1       =    LOOKUP('Inlet comp',1,3)           "Inlet stagnation temperature"
P_0_1       =    LOOKUP('Inlet comp',1,4)           "Inlet stagnation pressure"
alpha_1     =    LOOKUP('Inlet comp',1,5)  "Absolute flow inlet angle measured from axial direction"
ABF_in      =    LOOKUP('Inlet comp',1,6)           "Inlet blade blockage factor"
m_dot       =    LOOKUP('Inlet comp',1,7)           "Flow rate in kg/s"
stg         =    1

"Call rotor and stator sub-codes"
CALL
Rotor(delta_ks,DELTA_s_ks_rtr,m_dot,ABF_in,stg,T_0_1,P_0_1,alpha_1,P_1,T_1,r_rms_2,alpha_2,M_2a,P_2,T_2,P_0
_2,T_0_2,C_2,A_2,M_z_2,C_theta_2,C_z_2,C_1,U_1,U_2,beta_1,q_1,q_1_eff,ABF_rtr,DELTA_h_0,DELTA_s_rtr,Re_rt
r,L_rtr,g_rtr,DELTA_s_fs_rtr,omega_rtr)
CALL
Stator(delta_ks,DELTA_s_ks_str,m_dot,ABF_rtr,alpha_1,stg,r_rms_2,alpha_2,M_2a,P_2,T_2,P_0_2,T_0_2,C_2,A_2,M_
z_2,C_theta_2,C_z_2,C_1,U_1,U_2,beta_1,P_3,T_3,T_0_3,P_0_3,alpha_3,ABF_str,DELTA_s_str,Re_str,L_str,g_str,q_
2,q_2_eff,DELTA_s_fs_str,omega_str)


h_stg       =    ((LOOKUP('Stage inputs',stg,7)-LOOKUP('Stage inputs',stg,9))+(LOOKUP('Stage
inputs',stg,22)-LOOKUP('Stage inputs',stg,23)))/2          "Average blade height"
L_wtd       =    (q_1/(q_1+q_2))*(L_rtr/g_rtr)+(q_2/(q_1+q_2))*(L_str/g_str)"Weighted average for L/g, where
L is the diffuser length needed to calculate stallPRC"
tau_wtd     =    (q_1/(q_1+q_2))*(LOOKUP('Stage inputs',stg,3)/g_rtr)+(q_2/(q_1+q_2))*(LOOKUP('Stage
inputs',stg,18)/g_str)                                     "Weighted average for tao/g"
g_stg       =    (q_1/(q_1+q_2))*g_rtr+(q_2/(q_1+q_2))*g_str"Weighted average for g"
AS_wtd      =    (q_1/(q_1+q_2))*(LOOKUP('Stage inputs',stg,2)/LOOKUP('Stage
inputs',stg,13))+(q_2/(q_1+q_2))*(LOOKUP('Stage inputs',stg,2)/LOOKUP('Stage inputs',stg,26))    "Weighted average
for AS/pitch"
C_P_max     =    StallPRC(L_wtd,(Re_rtr+Re_str)/2,tau_wtd,AS_wtd)   "Stalling static pressure rise coefficient
for stage from correlation"

C_P_stg     =    (P_3-P_1)/(q_1+ q_2)               "Static pressure rise coefficient of stage"

K_1    =(q_1_eff)/(q_2+q_1)                  "Row factor for use with Koch and Smith endwall loss model for rotor"
```

```
K_2    =(q_2_eff)/(q_2+q_1)                    "Row factor for use with Koch and Smith endwall loss model for stator"

DELTA_s_fs    =    DELTA_s_fs_rtr+DELTA_s_fs_str        "Freestream entropy change through stage"
eta_fs  =    1- ((T_0_3*(DELTA_s_fs))/(DELTA_h_0))    "Stage freestream total-to-total adiabatic efficiency"

CALL
Endwall_loss_Koch_Smith(DELTA_s_fs,h_stg,DELTA_h_0,T_0_3,eta_fs,K_1,K_2,stg,C_P_stg,C_P_max,tau_wtd,AS_w
td,g_stg:delta_ks,DELTA_s_ks_rtr,DELTA_s_ks_str)

DELTA_s      =    DELTA_s_rtr+DELTA_s_str      "Sum of the total rotor and stator entropy increases"
TR_tt        =    T_0_3/T_0_1                  "Stage total-to-total temperature ratio"
PR_tt        =    P_0_3/P_0_1                  "Stage total-to-total pressure ratio"
eta          =    1- ((T_0_3*(DELTA_s))/(DELTA_h_0))    "Stage total-to-total adiabatic efficiency"

"T_0_3,P_0_3,alpha_3,DELTA_h_0,DELTA_s,TR_tt,PR_tt,eta - - - - Export file format"

$Export /A 'C:\temp\Stage1.csv',T_0_3,P_0_3,alpha_3,DELTA_h_0,DELTA_s,TR_tt,PR_tt,eta
```

Appendix D

ADDITIONAL VERIFICATION AND EVALUATION INFORMATION

Appendix D.1

TEST COMPRESSOR SPECIFICATION

Chapter 6 deals with the verification of the EES code with a commercial software package called NREC. A four stage axial compressor is used in this chapter and Table D.1 presents the values of the input parameters used for implementing this test compressor.

Table D.1.1 Test compressor input values

General compressor user inputs					
Variable	**Value**				**Units**
N	9000				rpm
$Fluid$	Helium				-
T_{01}	299.3				K
P_{01}	4497				kPa
α_1	12				$°C$
ABF_{in}	1				-
$\dot{m}$	148				kg/s
Stage user inputs					
Variable	**Stage 1**	**Stage 2**	**Stage 3**	**Stage 4**	**Units**
$\dot{m}_{bleed}$	0	0	0	0	kg/s
AS	0.015	0.015	0.015	0.015	m
Rotor					
τ_{rtr}	0.0005	0.0005	0.0005	0.0005	m
ξ_{rtr}	50.9	50.9	50.9	50.9	°
$\chi_{1_{rtr}}$	-59.5	-55.5	-54.5	-53.5	°
$\chi_{2_{rtr}}$	-46	-46	-46	-46	°
r_{t_1}	0.392	0.39	0.388	0.386	m
r_{t_2}	0.391	0.389	0.387	0.385	m
r_{hb_1}	0.3335	0.3335	0.3335	0.3335	m

Variable	Stage 1	Stage 2	Stage 3	Stage 4	Units
r_{hb_2}	0.3335	0.3335	0.3335	0.3335	m
$t_{\max_{rtr}}$	0.002955	0.002955	0.002955	0.002955	m
c_{rtr}	0.0356	0.0356	0.0356	0.0356	m
s_{rtr}	0.0275	0.0275	0.0275	0.0275	m
$k_{CLA_{rtr}}$	5.000E-07	5.000E-07	5.000E-07	5.000E-07	m
$r_{sh_{rtr}}$	0.36	0.36	0.36	0.36	m
$t_{sh_{rtr}}$	0.002	0.002	0.002	0.002	m
$c_{sh_{rtr}}$	0.009	0.009	0.009	0.009	m
Stator					
τ_{str}	0.0005	0.0005	0.0005	0.0005	m
ξ_{str}	35	35	35	35	°
$\chi_{2_{str}}$	41	41	40	38	°
$\chi_{3_{str}}$	18	18	18	18	°
r_{t_3}	0.39	0.388	0.386	0.384	m
r_{hb_3}	0.3335	0.3335	0.3335	0.3335	m
$t_{\max_{str}}$	0.002955	0.002955	0.002955	0.002955	m
c_{str}	0.0356	0.0356	0.0356	0.0356	m
s_{str}	0.019	0.019	0.019	0.019	m
$k_{CLA_{str}}$	5.000E-07	5.000E-07	5.000E-07	5.000E-07	m
$r_{sh_{str}}$	0.355	0.355	0.355	0.355	m
$t_{sh_{str}}$	0.002	0.002	0.002	0.002	m
$c_{sh_{str}}$	0.009	0.009	0.009	0.009	m

Appendix D.2

ADDITIONAL NON-LOSS PARAMETER VERIFICATION

Chapter 6 deals with the verification of the EES code with a commercial software package called NREC. This appendix gives additional comparisons of the major non-loss parameters needed during stage performance prediction. In Chapter 6 the comparison is given for the design point mass flow for the first stage of the four stage compressor considered. Two more mass flows are considered, one lower and one higher than the design point value. Table D.1 and Table D.2 shows the comparison as well as the percentage difference between EES and NREC.

Table D.2.1: Ideal stage parameter verification at a reduced mass flow

Mass flow = 140 kg/s			
Variable	**NREC**	**EES**	**Difference %**
C_1	149.22	149.27	0.03
W_1	344.42	344.44	0.01
β_1	-64.93	-64.92	0.02
U_1	342.99	342.99	0.00
C_2	241.35	241.18	0.07
W_2	205.77	206.76	0.47
α_2	53.68	53.45	0.43
β_2	-64.00	-64.00	0.00
U_2	342.49	342.49	0.00
C_3	149.07	151.46	1.57
W_3	149.07	151.46	1.57
α_3	18.00	18.00	0.00
β_3	18.00	18.00	0.00
P_{03}	4915.12	4913.21	0.04
T_{03}	310.03	310.08	0.02

Table D.2.2: Ideal stage parameter verification at an increased mass flow

Mass flow = 160 kg/s			
Variable	**NREC**	**EES**	**Difference %**
C_1	171.12	171.15	0.02
W_1	350.03	350.04	0.00
β_1	-61.43	-61.43	0.00
U_1	342.99	342.99	0.00
C_2	238.09	238.05	0.02
W_2	236.88	238.16	0.53
α_2	46.28	45.97	0.67
β_2	-46.00	-46.00	0.00
U_2	342.49	342.49	0.00
C_3	172.84	175.18	1.34
W_3	172.84	175.18	1.34
α_3	18.00	18.00	0.00
β_3	18.00	18.00	0.00
P_{03}	4844.64	4842.20	0.05
T_{03}	308.30	308.24	0.02